

STAR Project
Conceptual Design Report
Update



January 1993

DISCLAIMER

This document was prepared as an account of work sponsored by the United States Government. While this document is believed to contain correct information, neither the United States Government nor any agency thereof, nor The Regents of the University of California, nor any of their employees, makes any warranty, express or implied, or assumes any legal responsibility for the accuracy, completeness, or usefulness of any information, apparatus, product, or process disclosed, or represents that its use would not infringe privately owned rights. Reference herein to any specific commercial product, process, or service by its trade name, trademark, manufacturer, or otherwise, does not necessarily constitute or imply its endorsement, recommendation, or favoring by the United States Government or any agency thereof, or The Regents of the University of California. The views and opinions of authors expressed herein do not necessarily state or reflect those of the United States Government or any agency thereof, or The Regents of the University of California.

This report has been reproduced directly from the best available copy.

Available to DOE and DOE Contractors
from the Office of Scientific and Technical Information
P.O. Box 62, Oak Ridge, TN 37831
Prices available from (615) 576-8401

Available to the public from the
National Technical Information Service
U.S. Department of Commerce
5285 Port Royal Road, Springfield, VA 22161

PUB-5347 Rev.

Please Note Name Change:

On June 16, 1995, the Regents approved the name change from Lawrence Berkeley Laboratory to Ernest Orlando Lawrence Berkeley National Laboratory.

Ernest Orlando Lawrence Berkeley National Laboratory
is an equal opportunity employer.



The STAR Collaboration

M.E. Beddo, J. W. Dawson, D.P. Grosnick, V.J. Guarino, W.N. Haberichter,
D.A. Hill, N. Hill, T. Kasprzyk, D.X. Lopiano, J. Nasiatka, E. Petereit,
H.M. Spinka, D.G. Underwood, and A. Yokosawa
Argonne National Laboratory, Argonne, Illinois 60439, U.S.A.

W.J. Braithwaite, A.A. Rollefson, and D.C. Wold
University of Arkansas, Little Rock, Arkansas 72204, U.S.A.

K. Kadija, A. Ljubicic, **G. Paic**, and D. Vranic
Rudjer Boskovic Institute, 41001 Zagreb, Croatia

S.E. Eiseman, A. Etkin, **K.J. Foley**, R.W. Hackenburg, M.J. LeVine,
R.S. Longacre, W. A. Love, E.D. Platner, P. Rehak, A.C. Saulys, and J.H. Van Dijk
Brookhaven National Laboratory, Upton, New York, 11973, U.S.A.

H.J. Crawford, J.M. Engelage, I. Flores and L. Greiner
University of California, Berkeley, California 94720, U.S.A.

F.P. Brady, D. Cebra, J.E. Draper, and J.L. Romero
University of California, Davis, California 95616, U.S.A.

J.B. Carroll, V. Ghazikhanian, T. Hallman, **G.J. Igo**,
S. Trentalange, and C. Whitten, Jr.
University of California, Los Angeles, California 90024, U.S.A.

P.A. DeYoung, **M. Kaplan**, P.J. Karol, Z. Milosevich, and E. Vardaci
Carnegie Mellon University, Pittsburgh, Pennsylvania 15213, U.S.A.

M. Cherney, T.S. McShane, and J. Seger
Creighton University, Omaha, Nebraska 68178, U.S.A.

D. Ferenc, M. Gazdzicki, R.E. Renfordt, D. Röhrich, **R. Stock**, H. Ströbele, and S. Wenig
University of Frankfurt, D-6000 Frankfurt am Main 90, Germany

L. Madansky and R. Welsh
The Johns Hopkins University, Baltimore, Maryland 21218, U.S.A.

B. Anderson, A. Baldwin, M. L. Justice, **D. Keane**, Y. Shao, and J. Watson
Kent State University, Kent, Ohio 44242, U.S.A.

J. Berkovitz, F. Bieser, M.A. Bloomer, S.I. Chase, W. Christie, W.R. Edwards, E. Friedlander
W. Gong, M. Green, D. Greiner, J.W. Harris, W. Hearn, H. Huang, P. Jacobs, P. Jones,
S. Kleinfelder, R. LaPierre, P. Lindstrom, S. Margetis, J. Marx, H.S. Matis, C. McParland,
J. Mitchell, R. Morse, C. Naudet, T. Noggle, G. Odyniec, D. Olson, **A.M. Poskanzer**,
G. Rai, J. Rasson, H.-G. Ritter, I. Sakrejda, J. Schambach, L.S. Schroeder, D. Shuman,
A. Sobel, J. Sopher, R. Stone, T.J.M. Symons, H. Wieman, and W.K. Wilson
Lawrence Berkeley Laboratory, Berkeley, California 94720, U.S.A.

C.S. Chan, M.A. Kramer, **S.J. Lindenbaum**, K.H. Zhao, and Y. Zhu
City College of New York, New York, New York 10031, U.S.A.

A. Aprahamian, N.N. Biswas, **U. Garg**, V.P. Kenney, and J. Piekarz
University of Notre Dame, Notre Dame, Indiana 46556, U.S.A.

T. Humanic, R. Jayanti, G. Vilkelis
Ohio State University, Columbus, Ohio 43210, U.S.A.

S.A. Akimenko, Y.I. Arestov, N.I. Belikov, A.M. Davidenko, A.A. Dereschikov,
V. Erin, A. Grachov, Y. Matulenko, A.P. Meschanin, A. Mysnick, **S.B. Nurushev**,
A.I. Ronjin, V.L. Rykov, V. Sidorov, L. Soloviev, A. Ufimtsev, and A.N. Vasiliev
Institute of High Energy Physics, Protvino, Russia

A. Hirsch, E. Hjort, N. Porile, **R.P. Scharenberg**,
B. Srivastava, and M.L. Tincknell
Purdue University, West Lafayette, Indiana 47907, U.S.A.

D.L. Adams, S. Ahmad, **B.E. Bonner**, J.A. Buchanan, C.N. Chiou,
J.M. Clement, M.D. Corcoran, T. Empl, H.E. Miettinen, G.S. Mutchler,
J.B. Roberts, J. Skeens, and I. Stancu
Rice University, Houston, Texas 77251, U.S.A.

A. D. Chacon, R.K. Choudhury, and **K. L. Wolf**
Texas A & M University, College Station, Texas 77843, U.S.A.

G. Glass, **J. Hoffmann**, F.C. Moore, L. Ray, D. Read, P.J. Riley
University of Texas, Austin, Texas 78712, U.S.A.

W. Dominik and J. Grebiezkow
Warsaw University, Warsaw, Poland

T. Pawlak, W. Peryt, and J. Pluta
Warsaw University of Technology, Warsaw, Poland

J.G. Cramer, D. Prindle, D. Seymour, T.A. Trainor, and X.-Z. Zhu
University of Washington, Seattle, Washington 98195, U.S.A.

R. Bellwied, S. Bennett, J. Bielecki, **T.M. Cormier**, A. French, F. Gang, J. Hall,
Q. Li, A. Lukaszew, R. Matheus, C. Pruneau, and G. Roger
Wayne State University, Detroit, Michigan 48201, U.S.A.

Z. Fraenkel and **I. Tserruya**
Weizmann Institute of Science, Rehovot 76100, Israel

Spokesperson: **J.W. Harris**
Deputy Spokespersons: **T. Hallman, E.D. Platner**

Technical Director: **J. Marx**

STAR Conceptual Design Report Update

Introduction

This document is meant to update the Conceptual Design Report (CDR) for the Solenoidal Tracker at RHIC (STAR) detector. The CDR was submitted to the RHIC management on June 15, 1992. Since that submittal, a major change in the detector solenoidal magnet design has taken place and this CDR Update documents that change and its impact on the overall detector design, integration and installation, cost, schedule and funding. In addition, several smaller design changes in detector subsystems are described.

The major change that has taken place in the solenoidal magnet system has been to adopt a warm coil approach rather than the superconducting approach documented in the CDR. This change was driven by the recognition that the relatively low magnetic field (0.5 T) required for the detector permitted a choice of coil approach and that a warm coil would improve the physics capability of the detector by permitting the barrel electromagnetic calorimeter to be placed radially inside of a warm coil. This results in a significant reduction (by about a factor of three) of the material between the collision vertex and the calorimeter, resulting in improved performance, especially for the low energy particles that are typical of the kind of heavy ion collisions that are the primary focus of RHIC. A warm coil also requires less capital cost and could be fabricated more rapidly than a cryogenic coil. In addition, the technical risk inherent in a thin, cryogenic coil is greater than that for a warm coil with no special constraints on the coil thickness. On the other hand, a warm coil requires a significant increase in the supporting utilities that must be provided by RHIC to support operations of the STAR detector. The RHIC management has agreed that BNL/RHIC would provide the additional installed capabilities required (e.g. power, cooling tower, heat exchangers, etc.) and that the additional power load of a warm coil would be accommodated within the power allocation and the operating budget for RHIC.

The change of magnet coil approach has a major impact on the magnet system itself, on the barrel electromagnetic calorimeter, on support facility requirements, and to a lesser extent on those components of the trigger system in the central rapidity region, on the detector integration and installation planning, and on the cost, schedule and funding profile. Updated CDR sections are included in this document for these systems. In addition, updates for the Time Projection Chamber, trigger and Silicon Vertex Tracker are included to represent the additional work that has taken place since the CDR was submitted.

The cost estimate provided in Chapter 9 of this update is for the Phase 1

STAR scope consisting of the TPC, solenoid magnet, electronics, data acquisition, trigger systems, controls, on-line computing, detector conventional systems, detector installation and testing, project management and systems integration including EDIA and an average contingency of 26.5% is \$40.1M in FY'92 dollars. At present an estimate of STAR Collaboration resources which can be credited towards specific costs of the detectors amounts to approximately \$4.3M. A portion of the effort associated with installation, testing and other pre-operational activities that are expected to be supported by operating funds for the build-up and training of a core STAR operations group and by RHIC project support for experimental operations. This provides for an additional credit of \$1.4M against the overall estimate including \$0.4M as part of RHIC project support for experimental operations. An additional reduction of \$1M of STAR's contingency budget is taken by assuming that a portion of the \$2 M RHIC management reserve fund set up for the RHIC experimental program will be available to STAR. Therefore, the amount of capital funding required from RHIC and other sources for the Phase 1 scope of the detector (i.e. excluding SVT, EMC, XTPC, TOF and associated electronics system and installation) is \$33.4M in FY'92 dollars. Funding for the EMC, TOF, and XTPC will be sought from sources outside RHIC detector construction funds. Initially, the SVT will be designated an R&D project, supported from R&D funds. Upon successful R&D and prototyping, support for SVT construction will be sought from supplemental funds. An R&D budget of approximately 4.0 M in FY'93-95 is anticipated from RHIC R&D funds.

In addition to the detector systems that will be constructed by the STAR collaboration and the associated R&D program, STAR requires a number of modifications and additions to the Wide Angle Hall at RHIC and the provision for utilities to support detector testing and operations. These utilities include those required for the warm solenoid magnet for STAR. These needs have been documented for the RHIC management and appear in the STAR CDR Update. The RHIC Management has agreed that these needs will be provided for STAR by RHIC and BNL. For this reason their cost is not included in any of the estimates presented in this plan.

4.B. Solenoid Magnet Update

4.B.1. Specialized Physics Issues

The decision has been made to proceed with a conventional (warm) coil design, largely because of capital costs and to reduce material ahead of the Electromagnetic Calorimeter (EMCAL). This leads to a different configuration since the EMCAL will now be placed inside the coil, leading to better calorimeter performance but a larger coil ID. The field uniformity required for good TPC operation remains as before. The location of the EMCAL means that radial gaps must be left through the magnet for fibers to bring the light beyond the magnetic field, since very long paths for fibers parallel to the coil would seriously degrade calorimeter performance. Thus the design chosen has "pancake" coils so that gaps can be left, and employs trim coils for final field shaping. Studies with "Poisson" have shown that the required field uniformity can be achieved with the new magnet configuration. The yoke end poles have holes to permit particles produced at $\eta > 2.0$ to reach external detectors.

4.B.2 Description of Subsystem

The STAR magnet includes the following subsystems: 1) a copper room temperature main coil 5.24 meter ID. 2) An iron return yoke and end poles with some field shaping. 3) Trim coils attached to the end poles for precise field shaping. 4) A cooling system and associated utilities provided by RHIC in the facility to remove heat from the coils to help satisfy the temperature requirements of the TPC and calorimeter. 5) A power supply with low ripple and good stability. 6) A monitoring system to ensure stable, safe operations.

4.B.5 Engineering

4.B.5.a Brief Technical Description

A quadrant of the magnet is shown in Figure 4B-1. The coil is built with 9 gaps needed for calorimeter fibers and two needed near the ends for field shaping. The copper coil uses 2 MW at 0.5 Tesla. The return yoke has 30 longitudinal iron bars each supporting two of the 60 azimuthal calorimeter sections. Trim coils are located on the end poles.

4.B.5.b Description and Specifications of Major Components

The solenoid coil is 5.24 m ID, 5.94 m OD and 6.2 m long. Nine gaps are left between pancakes to accommodate the aluminum rings supporting the calorimeter and to allow paths for the calorimeter fibers to exit radially. Two additional gaps are left near the ends to help in field-shaping. At 0.5 Tesla the DC power use is ~2 MW. As shown in fig 4B-1 the trim coils are located near the pole tips. The iron return yoke is designed for a maximum magnet field of 0.5 Tesla.

The iron return yoke consists of 30 bars, supported by end rings. The return yoke is used to support the rest of the apparatus, transferring the gravitational forces to the hall floor via a multi-legged support cradle. The maximum flux in the return yoke is ~15 Tesla, which leads to satisfactory field uniformity at 0.5 and 0.25 Tesla. The endcaps can be rolled back to allow access to the ends of the TPC.

The cooling system is shown in Figure 4B-2. In order to control the temperature of the apparatus a chiller will be used to keep the average temperature of the coil at the Hall ambient. The chiller will be needed only on the hottest days, and is thus a large factor in determining only peak, not average, power.

The power supply will supply 2 MW DC to the coil at full field. A 12 phase supply is planned, with external filters to reduce voltage ripple. Current ripple is handled effectively by the time constant of the magnet. Since the solenoid field is coupled to the collider lattice and indeed collider magnets will be used to compensate for small effects on the optics, the magnet excitation will be controlled as part of RHIC. It is expected that the solenoid will not have to be turned off during injection, because of the small size of its perturbation of the lattice.

4.B.5.c Initial Fabrication, Testing and Shipping

The coils will be built and tested by industry without the iron return yoke. They will be shipped to BNL by the vendor, with shipping included in the cost estimate. The magnet iron will be built in industry, pre-assembled under BNL supervision, and shipped to BNL with all relevant fixturing.

4.B.5.d Assembly and Testing at RHIC

After inspection and further testing at BNL the coil will be assembled with the magnet iron the wide angle hall assembly building. The magnet will then be measured at full and at half fields to provide field maps for use in correcting the data for field non-uniformity. After satisfactory field maps have been achieved, the TPC and other detectors will be installed in the magnet .

Figure 4B-1

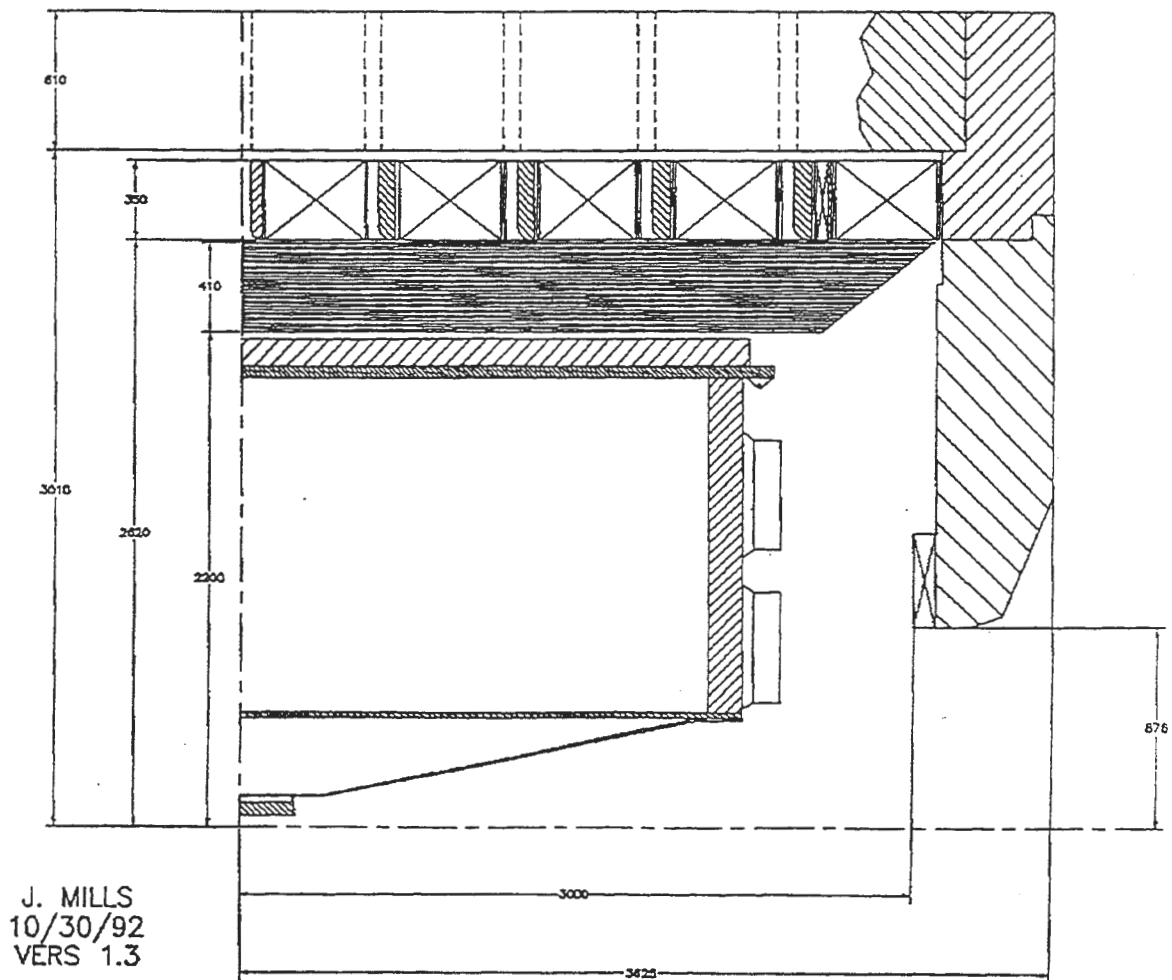
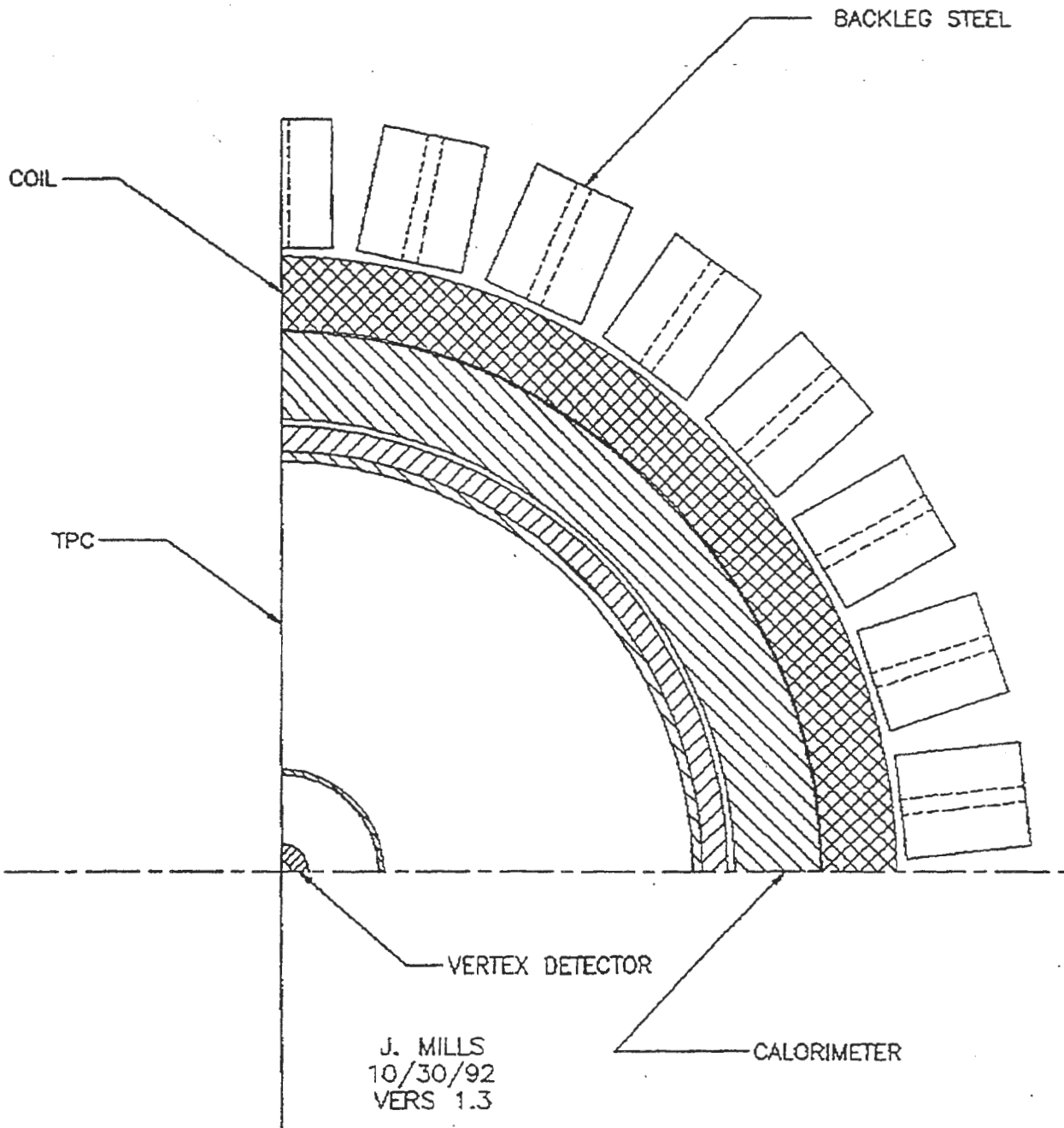


Figure 4B-2



4.C. Time Projection Chamber Update

4.C.2. Description of Subsystem

4.C.2.a. General Description

The pad plane design has been modified to use straight pad rows instead of circular pad rows. The primary reason for rejecting the circular design (even though it improves resolution for high p_t tracks) was to solve several construction difficulties. Uniform coupling of the wires to the pads is another argument in favor of the straight pad row design since this may provide better dE/dx performance. The momentum resolution for the low p_t tracks (the vast majority) is dominated by multiple scattering and is therefore not affected by the pad-row geometry. Momentum resolution for the high p_t tracks degrades, but that loss will be compensated by including an accurate tracking point at the inner radius from either the SVT or the reconstructed primary vertex.

The new pad plane design is illustrated in Figure 4C-1 and 4C-2. Details of recent simulations that have led to this choice are given below.

The STAR Conceptual Design Report (CDR) [1] envisioned two sizes of pad readout for the main TPC. Small pads ($2.85 \times 11.5 \text{ mm}^2$) were to be adopted on the inner half of each sector where the track density was shown to be highest and larger pads ($6.2 \times 19.5 \text{ mm}^2$) were to be adopted on the outer half of the sector. This design was driven by simulations of a TPC pad plane composed solely of the larger pad size which showed that as many as 64% of the hits on the innermost pad row may be lost to hit merging.

In this document, further consideration is given to the optimization of the TPC pad plane design. Three different pad designs have been considered.

- low resolution straight pad rows (66 pad rows)
- high resolution straight pad rows (48 pad rows, small pads on rows 1-18)
- high resolution circular pad rows (50 pad rows, small pads on rows 1-18)

Results of simulations with the smaller pad size employed on the inner half of the sectors are presented. The implications of this design for two track resolution, track reconstruction efficiency and momentum resolution are explored. In addition, the effect of the pad geometry on the momentum resolution (straight versus circular pad row designs) are discussed.

Pad Response and Two Track Resolution

As previously described in section 4.C.2.r of the CDR, the characteristic width of the induced charged distribution on the pad plane may be parametrized by the pad response function,

$$\sigma_{\text{prf}}^2 = \sigma_0^2 + \sigma_D^2 \lambda (1 + \tan^2 \alpha) + \sigma_\alpha^2 \tan^2 \alpha \quad (4C-1)$$

where,

λ - is the drift length (in meters)

α - is the track crossing angle relative to the direction normal to the wires

and

$$\sigma_\alpha^2 = D^2 \left(\frac{1}{12} + S_2 \right) \quad (4C-2)$$

where,

D - is the sense wire pitch (4 mm)

$S_2 = \sum_i i^2 \omega_i$ - is the sum over wire weights ω_i (where $\sum_i \omega_i = 1$)[†]

The three coefficients appearing in equation 4C-1 correspond to an intrinsic pad response σ_0^2 , a diffusion term σ_D^2 , and a term related to the track crossing angle relative to the pads σ_α^2 . In keeping with this parametrization, values for the coefficients have been calculated according to the procedure presented in the CDR.

The intrinsic pad response is determined by the wire-pad geometry. In order to obtain the optimal signal sharing for the smaller pad size, the anode-to-cathode spacing must be reduced to 2 mm on the inner half of the sector, to be compared with 4 mm for the larger pads. A value for intrinsic pad response has been deduced from measurements reported from a highly segmented cathode pad MWPC [2] and NA35 prototype results. The values of the coefficients calculated for both the $2.85 \times 11.5 \text{ mm}^2$ and $6.2 \times 19.5 \text{ mm}^2$ pads, are given in table 4C-1.

Table 4C-1 Summary of the coefficients of the pad response function for two pad sizes.

[†] This term corrected for the power of two missing in the CDR.

	$2.85 \times 11.5 \text{ mm}^2$	$6.2 \times 19.5 \text{ mm}^2$
σ_o (cm)	0.200	0.362
σ_D (cm/ \sqrt{m})	0.233*	0.233*
σ_α (cm)	0.349	0.637

* This term is larger than the $0.185 \text{ cm}/\sqrt{m}$ reported in the CDR due to the larger value of the single electron diffusion which has been used in the simulation.

To enable the study of the different pad plane designs, central (small impact parameter) Au+Au events have been generated according to the Lund-FRITIOF model at $\sqrt{s_{NN}} = 200 \text{ GeV}$. These have been processed by a GEANT simulation of the detector set-up, creating a list of TPC pad crossings for all produced particles and secondary particles arising from decays and secondary interactions in surrounding material. The individual pad crossings from GEANT are then subject to a parametrization of the TPC pad response as outlined above. In this final step, individual pad crossings may be merged depending upon their separation and the calculated spatial width of the charge distribution in the pad and drift directions. (In the drift direction, the spatial width is calculated according to the projected track length over each pad, the longitudinal diffusion and the electronics shaping time). Hits in the same pad row are merged if their separation Δ is given by,

$$\Delta_{\text{pad}} < \sigma_{\text{prf}}^1 + \sigma_{\text{prf}}^2 + \text{one pad width} \quad (4C-3)$$

and

$$\Delta z < \sigma_z^1 + \sigma_z^2 + \text{two time bins} \quad (4C-4)$$

In this way, the simulation models the performance of the hit finder. The merging criterion have been chosen after consideration of current hit finders employed by the ALEPH, EOS and NA35 collaborations [3].

The advantage of adopting the smaller pad size on the inner sector is shown in Figure 4C-3, where the total hit multiplicity for a central Au+Au event is plotted as a function of TPC row number. The three distributions on each plot show the number of GEANT crossings, the number of reconstructed hits from the simulation (FST[†]), and the number of those FST hits which are the result of merged pad crossings. Merged hits have been discarded if their combined spatial width is larger than 10 pad widths (3 or 6 cm) and 20 time bins (11 cm). Figure 4C-3a shows the number of reconstructed hits for the original TPC pad plane design incorporating the single pad size ($6.2 \times 19.5 \text{ mm}^2$). Here, only 36%

[†] The FaSt TPC simulation program [4].

of the GEANT pad crossings are reconstructed as hits in the innermost pad row and of these 25% are the result of merging two or more pad crossings. This is to be compared with the Figure 4C-3b, where the first 18 rows have been equipped with the high resolution $2.85 \times 11.5 \text{ mm}^2$ pads. In this case, 55% of the GEANT pad crossings are reconstructed on the innermost pad row and of these hits only 12.5% are the result of merging. Thus a clear improvement in two track resolution is obtained with the high resolution (small) pads on the innermost rows.

Spatial Resolution

As described in section 4.C.3.d in the CDR, the spatial resolution for isolated tracks is given by,

$$\sigma^2 = \sigma_A^2 + \sigma_B^2 \lambda e^{\gamma\lambda} \sec \alpha + \sigma_C^2 e^{\gamma\lambda} \cos \alpha \tan^2 \alpha \quad (4C-5)$$

where,

λ - is the drift length (in meters)

α - is the wire crossing angle

$e^{\gamma\lambda} \rightarrow 1$ - is the inverse of an attenuation factor due to electron capture

This has a similar functional form to that of the pad response function (which determines the spatial width of the signal) given by equation 4C-1. The three terms in the resolution function are an intrinsic resolution σ_A determined by the expected signal-to-noise ratio, a diffusion term σ_B , and a term which accounts for the crossing angle of the track relative to the pads (perpendicular to the wires) σ_C . The values of the three coefficients appearing in equation 4C-5 have been evaluated for the two pad sizes now under consideration, following the procedure described in section 4.C.3.d of the CDR. The results are shown in Table 4C-2.

Table 4C-2 Summary of the coefficients of the pad resolution function for two pad sizes.

	$2.85 \times 11.5 \text{ mm}^2$	$6.2 \times 19.5 \text{ mm}^2$
σ_A (μm)	135 [†]	303 [†]
σ_B (μm)	213	166
σ_C (μm)	1000	1665

[†] Average value

Track Reconstruction Efficiency

In order to determine the effect of the high resolution pads on track reconstruction efficiency and momentum resolution, 5 simulated Au+Au events have been analyzed using the pattern recognition algorithm described in section 4.C.3.c of the CDR. Figure 4C-4, shows the available number of reconstructed (FST) hits per generated track and the actual number of hits found on reconstructed tracks, for both the low resolution (one pad size) and high resolution (2 pad sizes) straight pad row designs. Only tracks generated within ± 1 units of pseudo rapidity and with a transverse momentum $p_T > 160$ MeV/c have been considered. These cuts select tracks which in principle traverse the full radius of the TPC. In practice, hit merging results in shifting the distribution of generated hits-per-track to lower values. Furthermore, particle decays and high p_T (large curvature) tracks emitted close to a sector boundary may leave very few hits in the detector and produce the long tail in the distribution. Superimposed on each plot is the distribution of the number of hits found on reconstructed tracks. In the low resolution design, clear evidence of track fragmentation is seen from the peak at around 5 hits per track in the reconstructed distribution. This is the minimum number of hits that are currently required for track formation by the pattern recognition algorithm. Comparison with the high resolution design clearly shows a marked improvement in the reconstructed track length and results in fewer ghost tracks by reducing track fragmentation in the reconstruction process.

The ratio of the two distributions in Figure 4C-4 provides a more quantitative assessment of the improvement in track reconstruction. Here, an additional cut must be imposed on the number of hits per track, in order to avoid double-counting those tracks which were fragmented in the reconstruction process. In detail, those tracks in both the generated and reconstructed distributions with more than half the maximum possible number of hits were selected (*i.e.* tracks with hits $> 0.5 \times$ total number of rows). The efficiency for track reconstruction in this case is an average of 80% for the high resolution design, compared to 60% for the low resolution design. This is shown in Figure 4C-5, where the ratio of reconstructed to generated tracks is plotted as a function of the transverse momentum. In each case, there is no obvious p_T dependence.

It should be stressed that the development of the pattern recognition algorithm is still in its early stages and that significant improvements are foreseen. However, Figures 4C-4 and 4C-5 are representative of the fact that hit merging at the inner radius is a major source of fragmentation in the track reconstruction process. This is due to the fact that the centroid of merged hits is typically displaced outside the tolerances consistent with unmerged portions of the parent track. The problem is greatly reduced by adopting the high resolution (small) pads on the inner sector. The quoted efficiencies are therefore representative of the relative improvement in the tracking efficiency as a function

of the two pad plane designs and the current development of the pattern recognition algorithm. Improvements, especially concerning the matching of track fragments will help to realize the 93% tracking efficiency (for producing one or more track fragments) reported in section 4.C.3.c of the CDR.

Momentum Resolution

The above cut on the number of reconstructed hits (greater than half the total number of pad rows) translates into a cut on track length which is approximately equal for each design. Furthermore, it is the projected track length on the pad plane that is the dominant factor in determining the momentum resolution [5]. This is evident in Figure 4C-6, where the momentum resolution $\Delta p_T/p_T$ is plotted as a function of $p_T \geq 2$ GeV/c for both the low resolution and high resolution pad row designs. The cut on the reconstructed track length results in a similar momentum resolution function for the two straight pad row designs, albeit the track reconstruction efficiency (Figure 4C-5) is very different. Also shown is the improvement that may be obtained by adopting a high resolution circular pad row design (*i.e.* circular pad rows with smaller pads on the first 18 rows). The circular pad row design helps to minimize the track crossing angle relative to the pads for high p_T tracks. For the case of tracks with $p_T = 10$ GeV/c the improvement in the momentum resolution is found to be an average 15%.

Another consideration for improving momentum resolution of primary tracks, is the inclusion of a known primary interaction point or hits from the Silicon Vertex Tracker (SVT). This increases the projected track length and aids a better determination of the radius of curvature. The result is shown in Figure 4C-7, where the momentum resolution $\Delta p_T/p_T$ is plotted as a function of p_T for tracks in the high resolution straight pad design, with and without the addition of SVT hits[†]. This shows a potential improvement in the momentum resolution on the order of 80% for primary tracks with $p_T = 10$ GeV/c. This is to be compared with the 15% improvement to be gained from radial pad geometry alone. Similar results for the momentum resolution are found when adding SVT hits to tracks in the radial pad geometry. For this reason and due to the ease of fabricating straight rather than circular pad rows, the decision has been made to construct a prototype sector consisting of the two pad sizes in a straight pad row geometry.

[†] An ideal matching scenario has been employed for the adding SVT hits to reconstructed tracks.

References

- [1] STAR Conceptual Design Report, PUB-5347 (1992).
- [2] R. Debbe et al., NIM A283 (1989) 772.
- [3] J. Knobloch and P. Norton (Eds.), Reconstruction Algorithms for ALEPH, ALEPH-NOTE (1991).
EOS (private communication).
NA35 (private communication).
- [4] P.G. Jones and I.M. Sakrejda, STAR note #56.
- [5] R.K. Bock et al., Data Analysis Techniques for High Energy Physics Experiments, Cambridge University Press (1990) pp 310-313.

4.C.5. Engineering

4.C.5.b. Description of Major Components.

Endcap

The new end cap design is illustrated in Figure 4C-1.

Technical details of the inner and outer sector assembly are shown in Figure 4C-2.

Inner Field Cage

The baseline design configuration of the inner field cage (IFC) has been changed to a Rohacell core with aluminum/Kapton skins. The change made to minimize the amount of material between the TPC tracking volume and the SVT. The new lay-up is shown on Figure 4C-8. This design reduces the radiation length for the IFC down to about 0.22% (0.5% in the CDR configuration). The maximum stress in the Kapton due to gravitational loading is calculated to be very low, however, it has been observed that this type of design may creep over time. Several means of minimizing this potential problem exist. The IFC can be supported at $z=0$, the core Rohacell foam or the Kapton thickness may be increased to provide more stiffness and strength. Since the major contribution to the radiation length of the IFC is the aluminum stripes, an R&D task is planned to determine if thinner aluminum can be used with a resulting radiation length reduction.

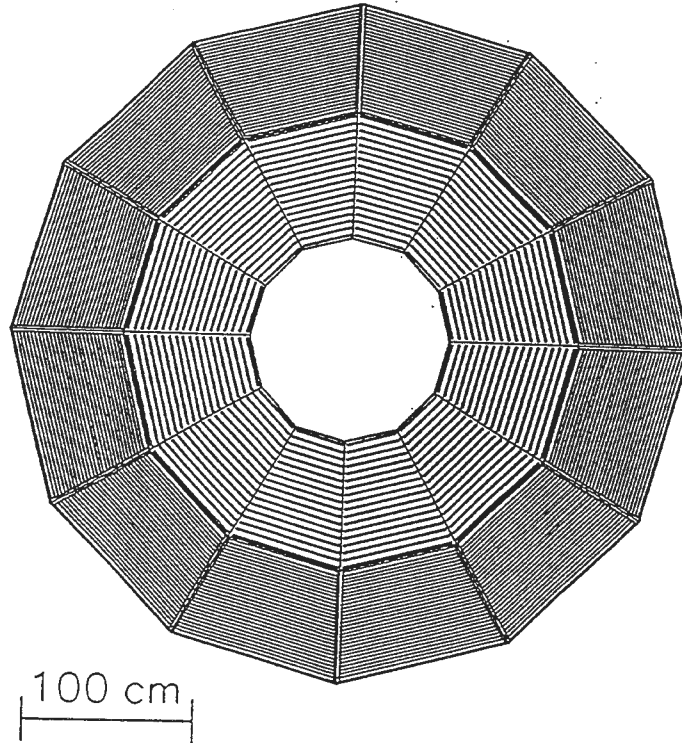


Figure 4C-1 A diagram of the TPC end-cap indicating the locations of the pad-plane sectors and the pad rows.

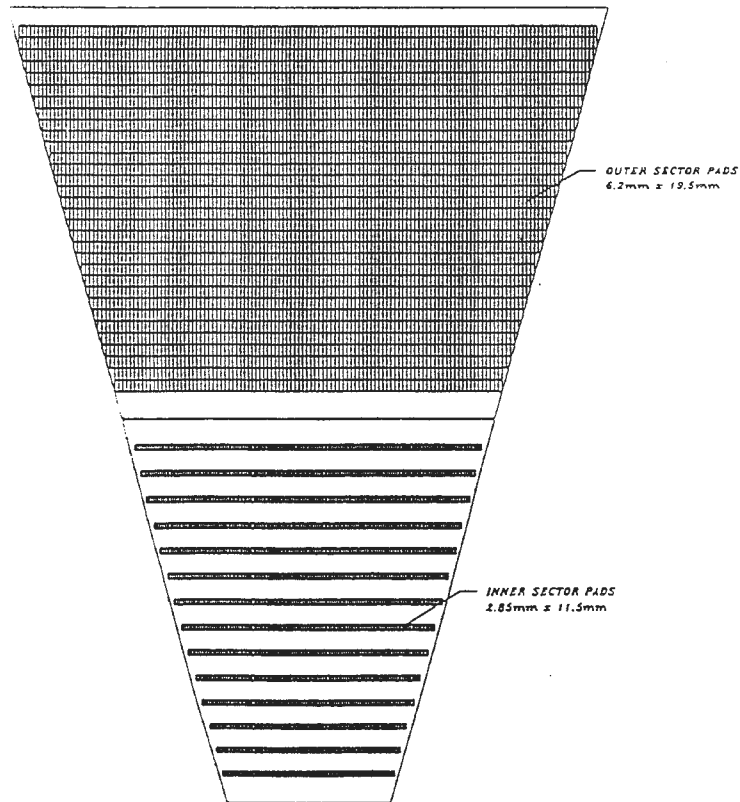


Figure 4C-2 The pad layout for the inner and outer pad plane sector.

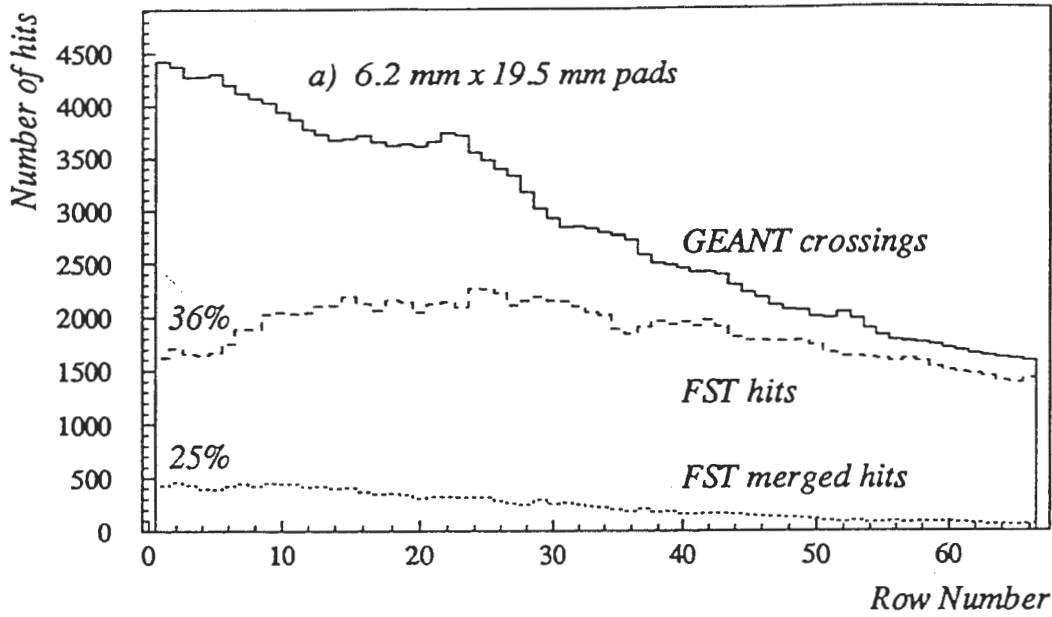


Figure 4C-3a The total hit multiplicity as a function of pad row for a central Au+Au event for a) low resolution pads ($6.2 \times 19.5 \text{ mm}^2$) throughout and b) high resolution pads ($3.85 \times 11.5 \text{ mm}^2$) equipped on rows 1-18.

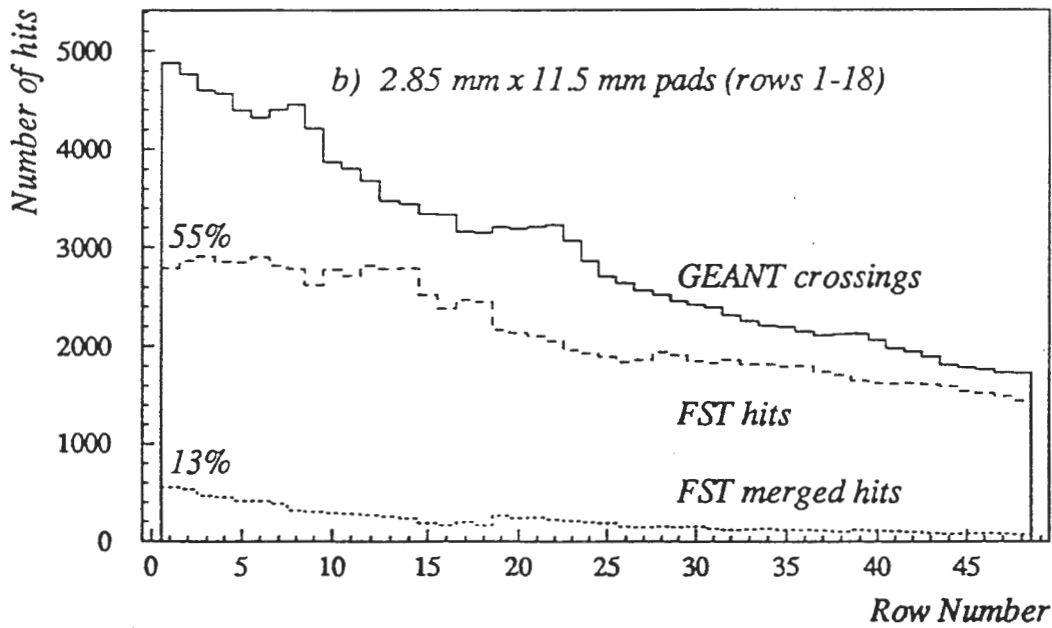
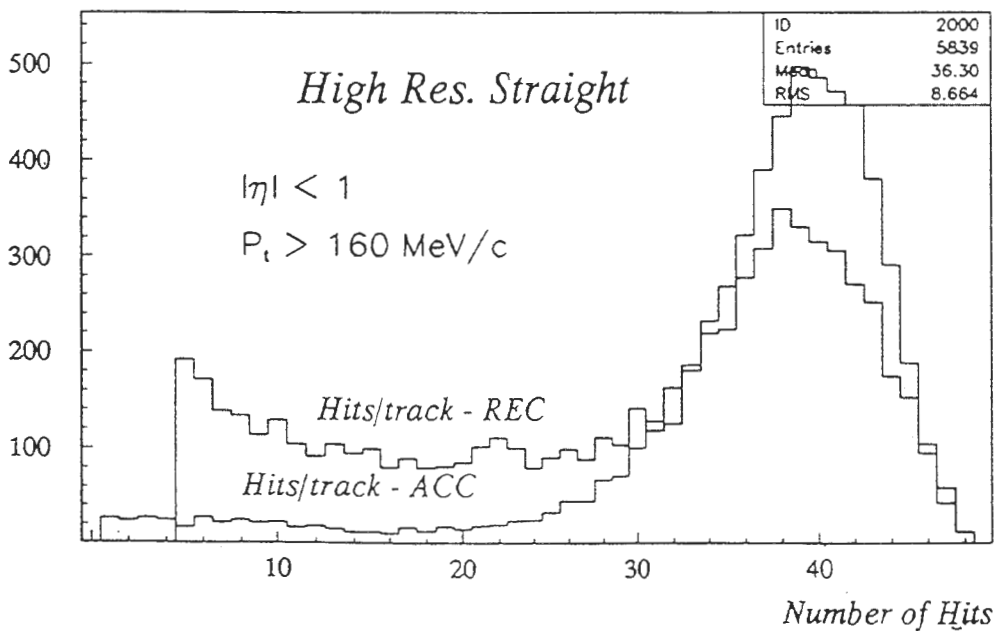
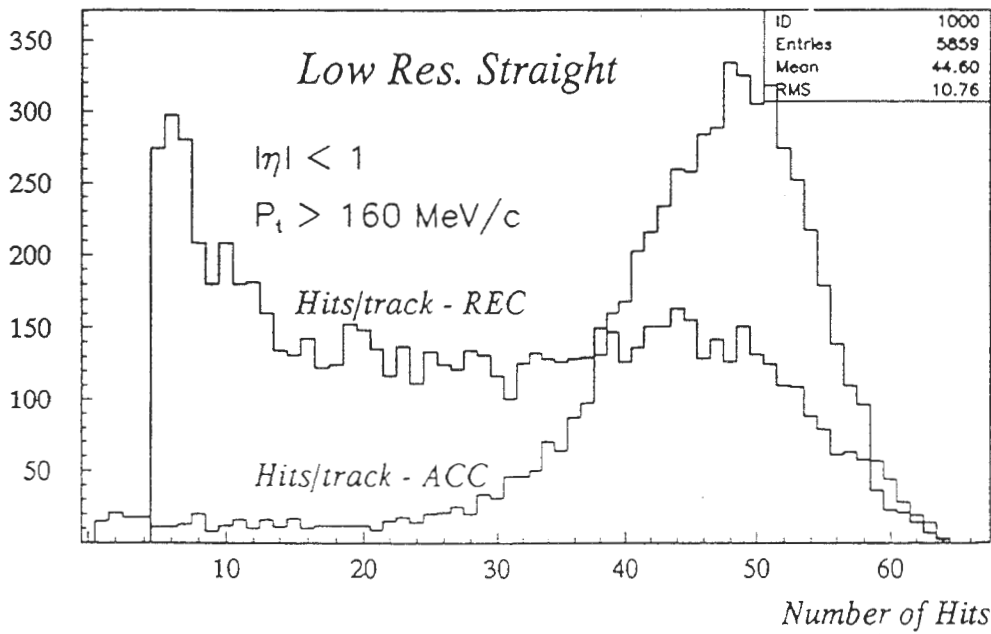


Figure 4C-3b Distributions of generated (solid) and reconstructed (dashed) hits per track for a) low resolution pads ($6.2 \times 19.5 \text{ mm}^2$) throughout and b) high resolution pads ($3.85 \times 11.5 \text{ mm}^2$) equipped on rows 1-18.

Figure 4C-4 Distribution of the number of hits on a track. The histograms labeled Hits/track — REC shows the distribution of tracks as a function of the number of hits on the track that survive the FST filter, ie hits that can be expected to give good position and dE/dx information. The histograms labeled Hits/track — ACC shows the distribution of tracks as a function of the number of hits on the track that get used in the helix curve fit. There are two cases shown: the original large pad configuration (Low Res. Straight) and the new design with large pads on the outer radius and small pads on the inner radius (High Res. Straight).

STAR TPC: Distribution of hits/track - Au+Au



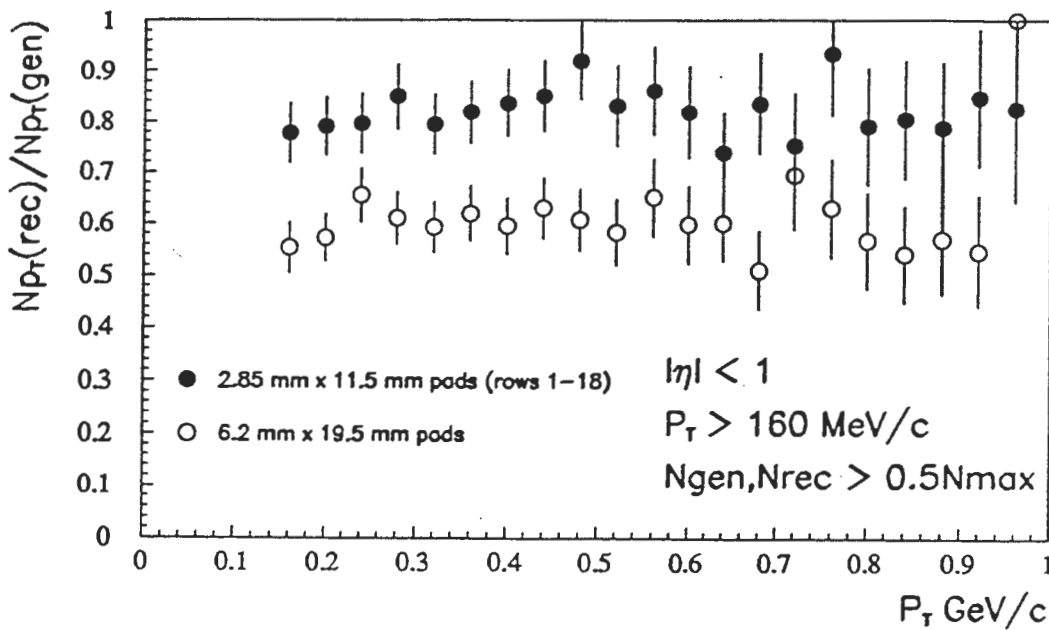
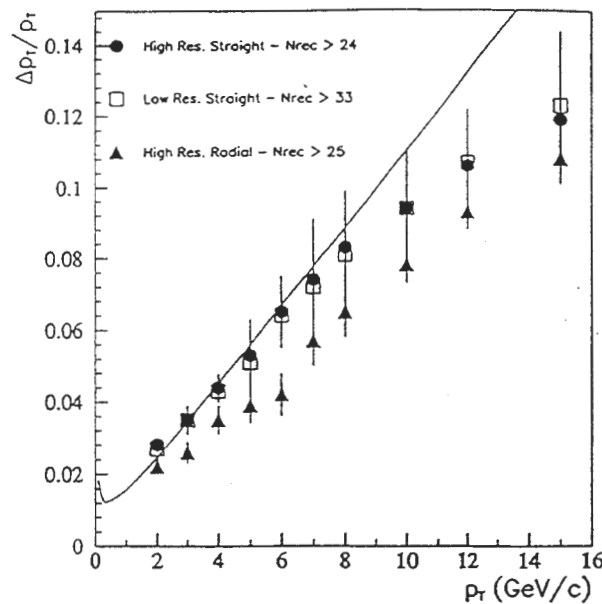
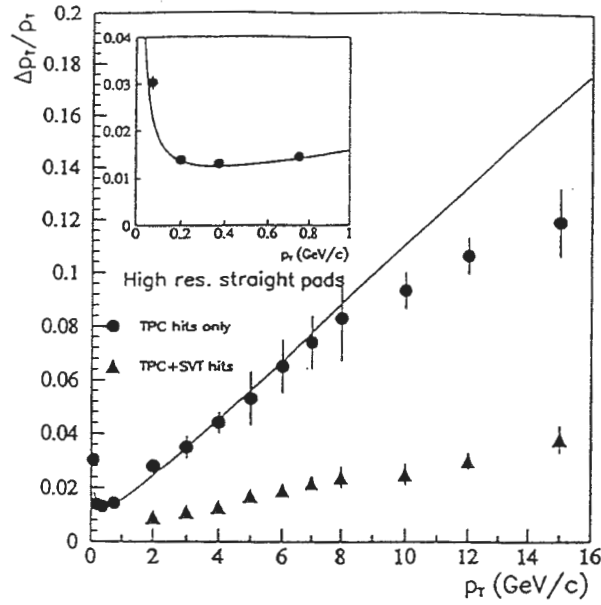


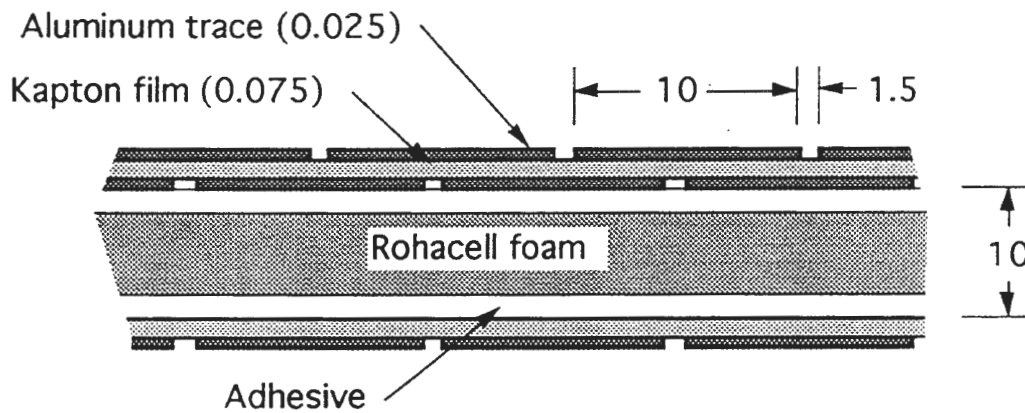
Figure 4C-5 Track reconstruction efficiency as a function of p_T for both high and low resolution designs. Only tracks with a generated (reconstructed) number of hits greater than half the total number of pad rows were considered. (See text for details).



4C-6 The reconstructed momentum resolution $\Delta p_T/p_T$ for primary tracks as a function of p_T for high and low resolution straight pad designs and the high resolution circular pad row design. A cut on the number of reconstructed hits (N_{rec}) greater than half the total number of pad rows has been applied in each case. The function plotted is an analytic formula for the p_T resolution [5] and corresponds to the values presented in the CDR.



4C-7 A comparison of the p_T momentum resolution for primary tracks in the high resolution straight pad row design, with and without the addition of SVT hits.



Not to scale. Dim. in mm.

Fig. 4C-8 Layout of the inner field cage design.

4.E. Trigger Update

This note is meant to supplement the STAR CDR trigger description by providing a more detailed description of the digital trigger system to be employed.

4.E.1 Introduction

A high energy nucleus-nucleus (AA) collision differs from a proton-proton (pp) collision in that there can be many nearly simultaneous nucleon-nucleon interactions within a volume significantly smaller than that of either original nucleus. This leads to the idea that new states of matter may be formed in AA collisions that cannot be made in collisions of smaller systems. Presumably these new states are formed preferentially in events involving the largest number of directly interacting nucleons, the central collisions. The large particle multiplicities of such events coupled with STAR's nearly 4π coverage provide a unique opportunity for detailed study of global variables and particle distributions on an event by event basis. Early in the STAR program trigger criteria will be based on interaction geometry. A variety of triggers including minimum bias will be applied and prescaled for continuous recording in the data stream. The STAR trigger system is designed to be programmable to incorporate new information as it is learned and flexible to incorporate new detectors as they are added.

All trigger decisions are made digitally, preserving the information available from each detector and presenting this information to various trigger algorithms for event selection or rejection. Algorithms are applied in sequence to match the natural timing characteristics of RHIC and the central STAR detector, the TPC. Fast trigger decisions based on simple multiplicity information are made in a \sim few \cdot 110ns, the RHIC crossing time. Slow trigger decisions based on track information are made in a few \cdot 10ms, the TPC readout time. When STAR is first turned on, event selection will be based on overall multiplicity. As STAR operates it will provide information on particle distributions that can then be programmed into the trigger algorithms as selection or rejection criteria for event recording.

4.E.2 Interaction Description

As a brief description of the interaction process, colliding nuclei are

considered to be composed of A individual nucleons. As the projectiles move toward each other they can be on paths leading to grazing incidence which result in peripheral collisions in which only one or a few nucleons from each projectile actually undergo strong interactions. Or, the projectiles can be on direct collision paths, leading to head-on or central interactions, in which a large fraction of the individual nucleons participate. The number of nucleons participating in direct interactions is a statistical function of the impact parameter in any interaction. The outcome can be viewed, in the simplest model, as a superposition of the appropriate number of nucleon-nucleon (nn) interactions. The produced particle multiplicity as a function of number of participating nucleons is shown in Figure 4E-1 for 1000 minimum bias Monte Carlo AuAu interactions. The particles from a typical central AuAu collision are distributed in pseudo-rapidity (η) as shown in Figure 4E-2. The TPC covers the range $-2 < \eta < 2$. The detectors used to trigger the TPC are shown in Figure 4E-3 and cover the η range shown in the Figure 4E-2.

The fast STAR trigger is designed to select events based on vertex location, multiplicity and structure in the multiplicity distribution $d^2N/d\eta d\phi$ ($-2 < \eta < 2$; $0 < \phi < 2\pi$). Information on these quantities is presented to the trigger system from the central trigger barrel (CTB), the endcap multi-wire proportional chambers (MWPC), the vertex position detector (VPD) and the veto calorimeter (VC). These are described briefly below. The addition of the electromagnetic calorimeter (EMC) will allow us to select on $d^2E/d\eta d\phi$. With a shingle time-of-flight (TOF) system and EMC we can trigger on mean energy per particle, $\langle E_i \rangle$, by comparing EMC tower energy with TOF shingle hits. Additional information from the time-projection-chamber (TPC) and the silicon vertex tracker (SVT) is available for a slow trigger once these are digitized. Slow trigger selection can be based on track clusters indicating jets or on percentage of stiff tracks indicating high temperature in the collision. The trigger scheme described in this note assumes that only the CTB, MWPC, VPD, and VC will be available, although the architecture of the trigger is designed to allow easy addition of the much more powerful EMC and TOF detector systems. Triggers can be made up within a few RHIC crossings for simple quantities; more time is needed for complex decisions based on tracking information.

Each crossing is examined to see if an interesting event occurred. The taping speed of the data acquisition (DAQ) system limits the recording rate to a few events per second. Since the interactions are occurring at rates from 1kHz to 1MHz depending on projectile masses (see Table 1), some acceptance criteria or trigger conditions must be applied to reduce the data rate from the interaction rate down to the recording rate.

Table 4E-1: Interaction Rates

projectiles	luminosity	cross section	int/ sec
pp	1.4×10^{31}	0.04×10^{-24}	6×10^5
OO	9.8×10^{28}	1.0	10^5
SiSi	4.4×10^{28}	1.7	70,000
CuCu	9.5×10^{27}	3.4	30,000
AuAu	1.1×10^{27}	7.8	8600
AuAu	2×10^{26}	7.8	1500

A simple detector system and trigger architecture has been designed to achieve the required rejection factors within the constraints of available resources. Fast rejection is based on centrality and structure in particle density, and must account for reductions of 10-100 or more. Slow rejection is based on clustering and stiffness obtained from the tracking information, and must account for reductions of similar magnitude.

4.E.3 Detector Descriptions

The detectors of the trigger system are shown in Figure 4E-3. The properties of each detector are summarized in Table 4E-2.

Table 4E-2 : Trigger Detectors

Detector	Position	Description	Purpose
Vertex Detector	VPD	48 Ck radiators in 2 small cylinders	locate interaction vertex eliminate beam-gas events provide min-bias trigger
Veto Calorimeter	VC	2 small hadron calorimeters +/- 15 m from diamond	detect spectator fragments provide min-bias trigger verify central collisions
Central Trigger Barrel	CTB	240 slats in 2 cylinders on either side of $\eta=0$	Detect charged particle multiplicity from $-1 < \eta < 1$
Endcap MWPC	MWPC	TPC anode wires	Detect charged particle multiplicity from $1 < \eta < 2$

The VPDs are designed to locate the interaction vertex and to reject beam-

gas interactions. The VPD locates the interaction vertex to within a few cm based on the arrival times of particles and photons. It consists of two small cylindrically symmetric groups of 24 photomultiplier tubes viewing individual Cherenkov radiators. These are located on the beamline 3m from the center of the interaction diamond. Beam-gas rejection is achieved by requiring hits on both detectors. A simple requirement of hits in both VPD1 and VPD2 provides an approximation to a minimum bias trigger, especially for AuAu interactions.

The VCs are designed to detect spectator fragments from the projectiles, that is, to detect those portions of each incident nucleus that did not participate directly in the collision. Each VC is placed downstream of the first RHIC dipole to view the region on either side of the beam pipe. Projectile fragments, having nearly the same velocity as the beam but a different charge/mass ratio, are not bent into the beam pipe and so can be detected with little interference from uninteracted beam nuclei. The signal in the VC is anti-correlated with interaction multiplicity. Truly central events will produce only a few nucleons scattered into the VC's, rather than the large fragments that may survive a less central interaction. A simple requirement on energy deposit in both VCs provides another approximation to a minimum bias trigger.

The CTB and MWPC are designed to detect charged particle multiplicity in the central η region. To determine the multiplicity distribution there will be 240 detectors (photomultiplier tubes or PMTs) in the CTB, covering the central 2 units of pseudorapidity, and 96 detectors (collections of wires) in the MWPC, covering the units from $1 < |\eta| < 2$. The CTB consists of two cylinders joined at pseudorapidity $\eta=0$, with 60 slats in each "barrel". Each slat is 2m long subtending one η unit and viewed at both ends by a 2" diameter Hamamatsu mesh-anode photomultiplier tube. The 12 sectors of each TPC endcap multi-wire proportional counter are divided into 4 segments covering η from 1-2. This gives 48 segments per end or 96 segments total. Total multiplicity in each segment is deduced from the total charge in each segment, just as for the CTB multiplicity is deduced from the charge at each PMT anode. Eventually, the EMC will include 1200 towers and 2400 PMT's while the TOF system will have a fine granulation requiring 8000 PMTs. The architecture discussed here is designed to accommodate these upgrades, with digital information from each PMT available to the trigger. The TPC has 70000 pads on each end, or 140,000 total. The schematic trigger diagram is shown in Figure 4E-4.

4.E.4 Trigger conditions as filters

The least restrictive trigger condition is simply to take an event for each crossing for which the system is "alive", that is, to trigger on the 9 MHz RHIC clock. This leads to nearly 100% dead time or 0% livetime. We prefer to run at large livetime to catch more interesting events when they occur. Although we

will take a heavily prescaled set of "minimum bias" events, we expect most of our triggers to be aimed at selecting events which optimize the "interesting" physics we record. In the absence of a well defined QGP signature, the STAR trigger is designed to be easily programmed for different selection criteria, prescale, and priority. Many different trigger conditions will be sampled continuously with individual prescale values.

Each set of trigger conditions represents a different filter applied to the incoming data stream. Some filters will be very coarse, passing many events and requiring a prescale to avoid swamping the acquisition system. Triggers based on overall multiplicity are coarse, primarily because of statistical fluctuations in particle generation. Triggers based on local particle or energy density extremes, such as expected from multijet events, represent much finer filters which may require no prescaling for DAQ. Application of fine-grained filters will require study, however, to avoid selecting on statistical fluctuations. It is our goal to develop a trigger system that allows filter algorithms to use all of the information taken in an event to decide whether to record the event.

In general, the amount of time required to apply a filter depends on its information content or granularity. The minimum amount of time required is set by detector response and electronic propagation time. Some detectors such as phototubes and narrow gap wire chambers can respond fast enough to allow decisions based on their information to be made in less than a RHIC crossing time of 110ns. A timeline for a fast detector, a PMT of the CTB, is shown in Figure 4E-5. Others such as the TPC require 50 μ s to complete a drift cycle and, in the present scheme, 10ms to complete a digitization cycle.

Until the TPC is triggered it simply records the passage of each charged particle in a local ionization track which drifts toward the anode pads but does not reach them because of a blocking grid. Once triggered, the blocking grid is turned off and the ionization is amplified and stored in 100ns time bites in a 512 deep switched-capacitor-array (SCA) analog pipeline. The grid must be turned off as fast as possible and certainly within 1 μ s of the time of the interaction, although it should not be switched at a rate >10kHz. A 10 μ s penalty is paid to reset the system once the grid is turned off. The signal to begin a digitization cycle must be available within 100 μ s. An abort issued after this requires a 100 μ s penalty. The general STAR timing diagram is shown in Figure 4E-6.

If a second interaction occurs during the TPC drift time associated with the original trigger, then tracks from the second interaction are drifted over to the SCA's and stored for digitization. This "pileup" is a serious concern for the proton program and leads to the natural idea that we would like to keep pipelined response for all detectors for a time equal to the storage time of the TPC. In the AuAu case the mean time between interactions is 1ms, so all triggers

that had another interaction within $\pm 50\mu\text{s}$ could be rejected and not much data would be lost. However, luminosities for light nuclei suggest that there may often be multiple interactions within the $50\mu\text{s}$ response time. Fully piped detector information for off-line data correction would be useful for these ions as well.

The CTB and the MWPC measure multiplicity through total charge collected in each element. Both types of detector are susceptible to fluctuation in the collected charge that reflect the statistical nature of the energy loss and amplification processes. The charge output for the whole CTB has been shown to be a well correlated measure of charged particle multiplicity. However, for most of the beam combinations the total multiplicity is too coarse a filter to provide the trigger rejection required to reduce the event rate to where the event is fully digitized (100 Hz or 10ms) and available for tracking analysis.

For the case of AuAu collisions, it would be reasonable to select central events based on, at best, the top 3% of the multiplicity distribution. This would provide a rejection factor of 30 and reduce the rate to ≈ 30 Hz, near the maximum TPC digitizing rate. A further reduction of a factor of 30 is needed to match the DAQ taping speed. This is a total rejection of 300-1000 for the AuAu case. The required reduction factor is larger for lower A beams. With the SCA scheme for the TPC, at most 100 events/second can be analyzed for track content at the trigger level, and this only if the analysis takes 0 time. Realistically, it requires some 25ms to locate most of the tracks in the outer region of the TPC, limiting the reduction factor using tracking information to less than 40/sec. This means that any greater reduction factor must be achieved without tracking information. Note that the tracking information can achieve much greater reduction factors but only if they lead to a lower recording rate.

4.E.5 Pixel space

A schematic diagram of how the trigger detectors are used in the trigger is shown in Figure 4E-7. The 120 slats of the CTB can be mapped into the central region of $\eta\phi$ space as shown. Each slat subtends 1 unit in η and 6° in ϕ . Further segmentation in η can be achieved by splitting slats in half or by timing hits on each PMT. The sectors of the endcap MWPC can be mapped into $\eta\phi$ space also. Each sector covers 1 unit in η and 22.5° in ϕ . Further segmentation in η is achieved by using subsets of the wires in each sector. The mapping for these detectors is shown in the figure. The level 0 trigger processing will group these individual pixels into a coarser grid as shown. Level 0 and 1 decisions will be based on analysis of this coarser grid containing 32 cells in $\eta\phi$ space. Levels 2 and 3 will use the full pixel $\eta\phi$ space. The slow trigger, level 3, will have tracking information from the TPC available as well.

Achieving the required reduction appears to provide a compelling

argument to look a bit harder at the information that is potentially available much faster than the TPC information. In 100ns not much real computer processing can be done, although quite sophisticated logic array analysis is possible. Rough multiplicity cuts can be made using a combination of programmed logic arrays. The mean multiplicity can be extracted within a few (3) crossing times. This information is used in the 0th level trigger to determine whether something worth a further look has occurred.

Each trigger detector is digitized for each RHIC crossing. This information is strobed into a 1000 deep random-access-memory (RAM), for automatic history archiving, and into a FPGA (field-programmable-gate-array) simultaneously. Each FPGA takes 16 detector inputs at step 1 and creates the sum and passes this information to another FPGA, step 2, which compresses by another factor of 16 and so on until all detectors are exhausted, returning just a few numbers to a final FPGA after N steps to provide the 0th level trigger. For 256 trigger detectors this decision can be made in two crossings, or steps, or less. For 3000 trigger detectors this process takes an additional crossing or 3 steps total. This process is diagrammed in Figure 4E-8. Decisions and architecture such as this are truly dead-timeless, since the decision at each step is reached in less than one crossing time, or 1 time unit, and passed to another process thereby making way for the information from the next crossing. The result of this level 0 processing is stored in RAM as a trigger tag just like the data words. This is also done for the results of steps 1 and 2 above.

4.E.6 General Timing

If the trigger tag for this event is of interest to the experimenters, then the trigger signal is sent to the other detectors. During the 50 μ s TPC drift time, the level 1 processors will be looking at the information from the first step and second step FPGA words, that is, an array in $\eta\phi$ space consisting of some 32 cells (16 from the CTB and 16 from the MWPC). This granular information may prove useful as more is learned about the RHIC interaction topology. Certainly it would be more powerful to have pixels containing energy information such as is available from the EMC, rather than just the multiplicity information from the first generation trigger detectors.

Once a level 0 trigger is asserted the TPC gate is opened and the level 1 trigger processing begins. A busy circuit for TPC events is asserted at this time also. If the event is aborted in level 1 processing, the busy is cleared and the system reset from within the trigger electronics. Algorithms applied at this point are not dead-timeless, however, since the analysis may take many crossing time units. This analysis may be viewed as asynchronous, as opposed to the synchronous operation of level 0.

When a level 1 trigger is asserted some 100 μ s after the level 0 assertion, the TPC digitization process begins. The busy circuit is now put under control of the DAQ system, and is not cleared until DAQ is ready to accept another event. At this point, level 2 analysis can begin on the single detector information. This is also assumed to be an asynchronous analysis, following on the heels of level 1 to take advantage of the 10ms digitization time. This time would not exist if the full experiment could be digitized each crossing, and then the TPC information would be available for finer grained filtering after just 50 μ s. The analysis performed during this 10ms time period will depend on what we learn of event topologies during the early STAR operations. The main idea is that all of the trigger detector information is available digitally at this time.

Once the TPC hits are available, level 3 analysis begins and transform analysis can be performed in a \sim 25ms on the data in the outer radius area where tracks are well separated to give track number. A few ms later the cluster distributions in both space and momentum could be calculated. This information is then available for trigger selection as well. Level 2 and 3 both require that the trigger CPUs have access to a larger portion of each event than level 1, which operated on a set of sums, not individual hits. Algorithms applied at Level 3 will include topology, ionization and jet analysis on the track information.

Since each trigger detector is digitized for each crossing, there is no need for an additional ADC for DAQ. The trigger will have a separate DAQ CPU whose task it is to gather the relevant data from each detector RAM and make this data block available to the event builder. This gathering will begin at the time at which TPC digitization begins.

4.E.7 Special triggers

During tune-up and debugging, it will be necessary to trigger the system for specific detectors only. For instance, it may be desirable to trigger the EMC without any TPC interaction while checking tower operations. Or it may be desirable to record laser events in the CTB to test individual PMT operations. Such triggers are shown in the diagram as "special" triggers. These would be passed to DAQ without waiting for the TPC drift cycle and could presumably be taped at much greater rates than full events just because of their smaller size. The "busy" operations would be taken care of within this architecture in the same way that DAQ controls the busy for full events.

With the architecture and the simple trigger detectors envisioned, the STAR system should be able to optimize physics data recording from the very beginning of the experimental program.

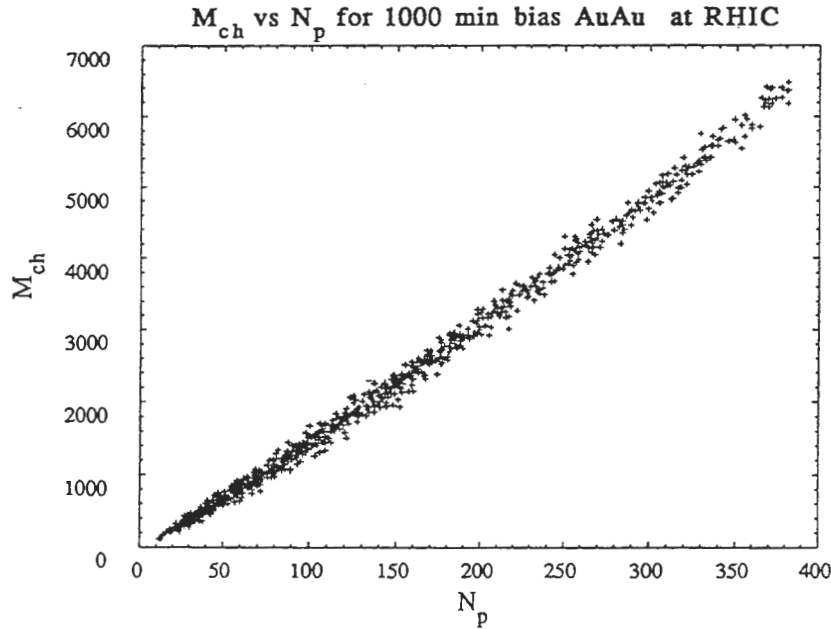


Figure 4E-1 Correlation between number of participant nucleons and the overall charged particle multiplicity as calculated in Fritiof code for 1000 minimum bias AuAu interactions at RHIC energies. Measurement of charged particle multiplicity is used to select "central" collision events, those having the largest number of participating nucleons.

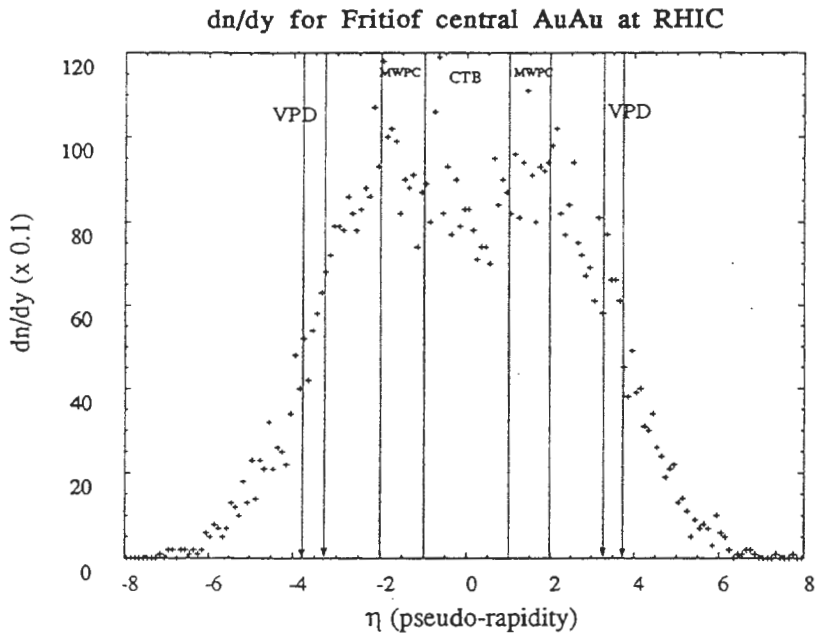
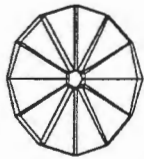
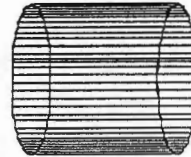


Figure 4E-2 The pseudorapidity (η) distribution of charged particles in a single central AuAu collision as calculated in Fritiof. The regions in η covered by the major detectors of the trigger system are shown as bands in the figure. Addition of the PbG1 array would allow coverage in the holes from $2 < |\eta| < 5$.

Figure 4E-3 Schematic representation of the trigger detectors. The TPC is inside the central trigger barrel (CTB). The MWPC's are the TPC endcap multi-wire-proportional-chambers. The CTB and MWPC are the main multiplicity detectors for the trigger system. The vertex-position-detectors (VPD's) are located at +/- 3m from the center of the interaction diamond and serve to locate the interactions within the diamond and to eliminate background. The veto-calorimeters (VC) are located at +/- 15m from the center.



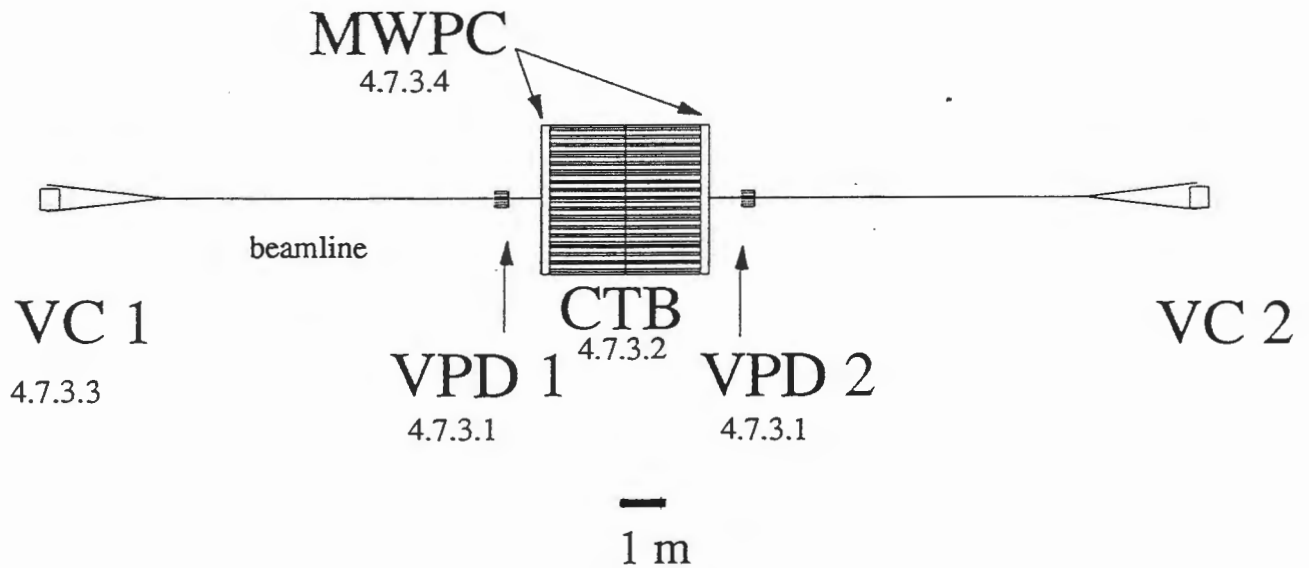
MWPC :
12 sectors/end
4 segments/sector
96 total signals



CTB:
120 scintillator slats
2 PMT each
240 total signals

STAR Trigger Detectors

4.7.3



VPD :
24 PMT each
48 total signals

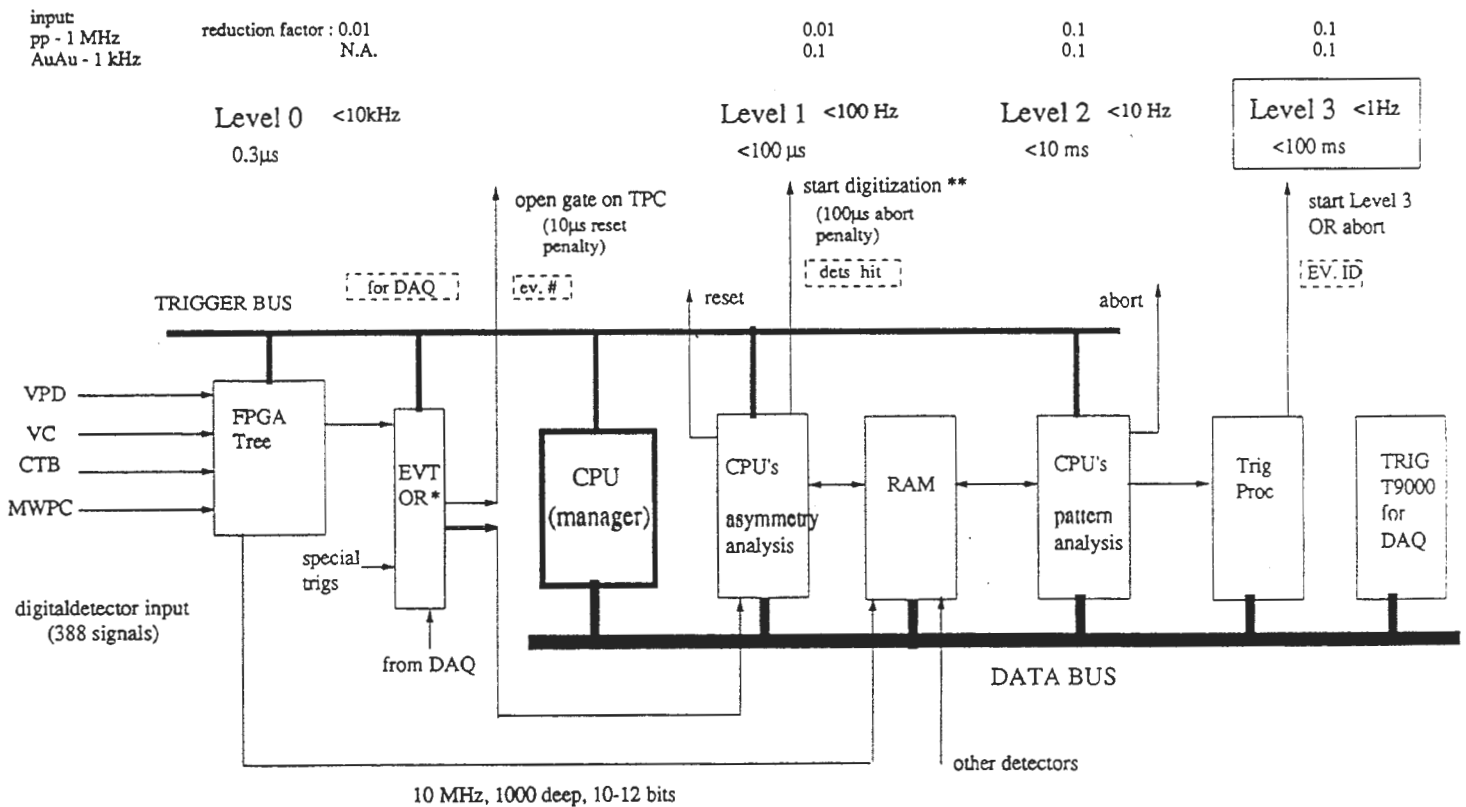


VC:
2 PMT each
4 total signals

Figure 4E-4 Overall scheme of the trigger system. The 4 trigger levels are established to coincide with the timing requirements of the TPC: Level 0 opens the gate within 1 μ s of the interaction; Level 1 begins TPC digitization within 100 μ s; Level 2 begins event build after end of digitization at 10 ms; Level 3 begins event write. Data from the trigger detectors enters the system digitally and is stored in RAM for at least 1000 crossings to provide event history.

STAR Triggers

10 Dec 1992

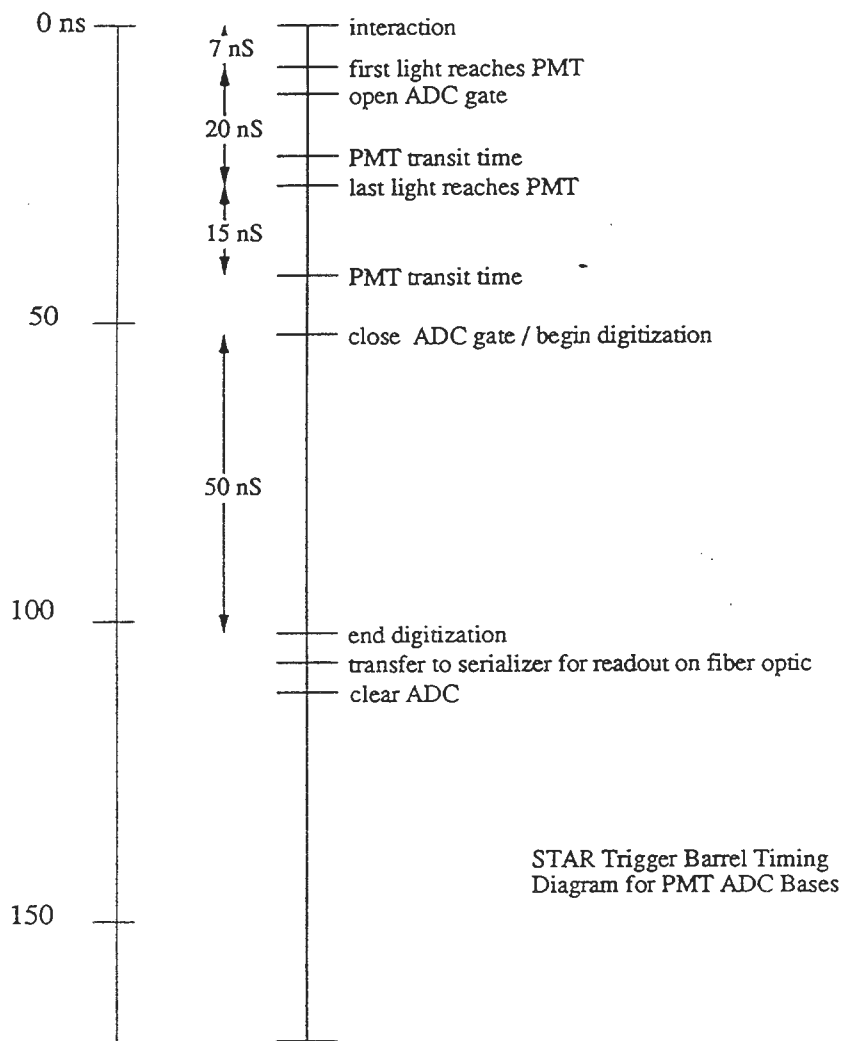


* this unit will have prescale and busy capability to keep output rate below 10k
 ** must be fixed Δt after opening gate

note : TPC has natural 50 μ s pipe. The 100 μ s decision time is chosen to minimize the number of digitization aborts issued. This concept works best if all analysed detectors have 100 μ s pipe to store for digitization.

Figure 4E-5 The timing response of a typical photomultiplier (PMT) in the STAR trigger system. Signals are digitized on the PMT base within a single RHIC crossing time of 110 ns and sent to the electronics carriage via 250 MHz optical fiber.

STAR trigger detector timing response



STAR Trigger Barrel Timing Diagram for PMT ADC Bases

Leo Greiner
November 3, 1992

Figure 4E-6 Timing diagram for trigger actions. Level 0 is deadtimeless so it does not generate any busy.

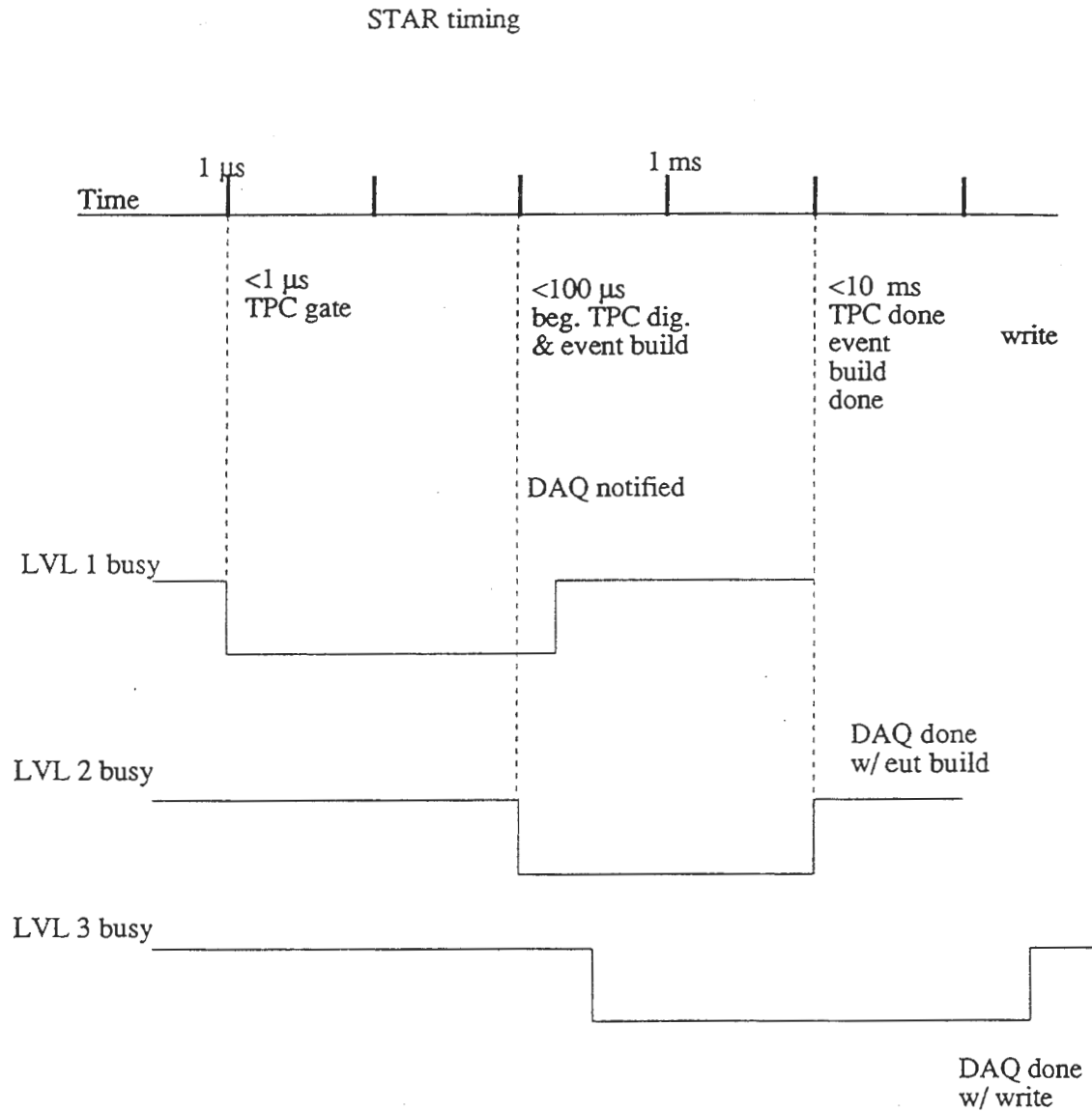


Figure 4E-7 Mapping of the CTB and MWPC on to $\eta\phi$ space is shown. Each detector (slat or segment) covers a small range in η (pseudorapidity) and ϕ (cylindrical angle) as shown. The detectors are taken in groups of 16 for input to the first step of field-programmable-gate-array (FPGA) analysis, effectively providing a larger bite in both η and ϕ for further analysis. Individual detector signals from the fine pixel array, with FPGA output forming the coarse pixel array.

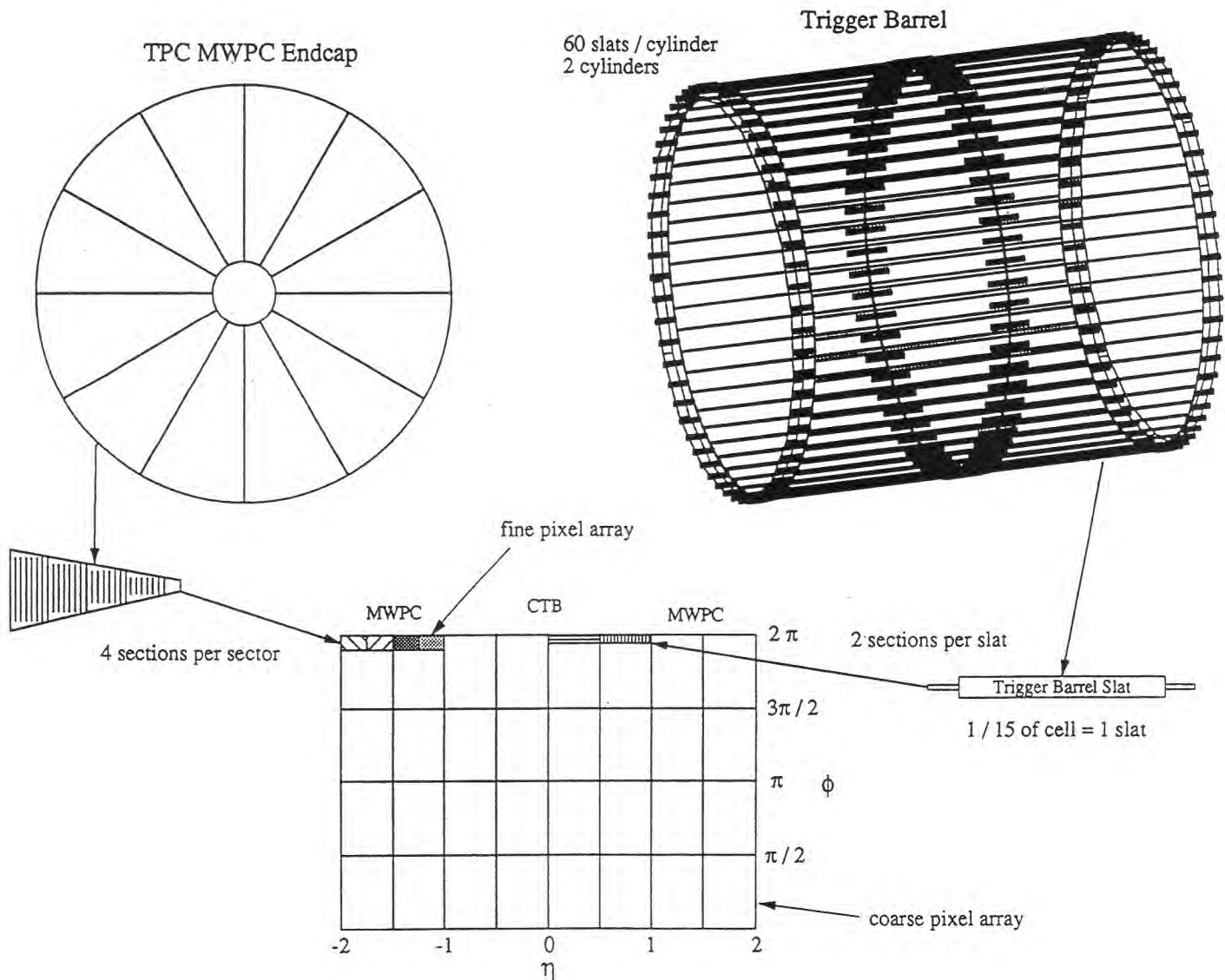
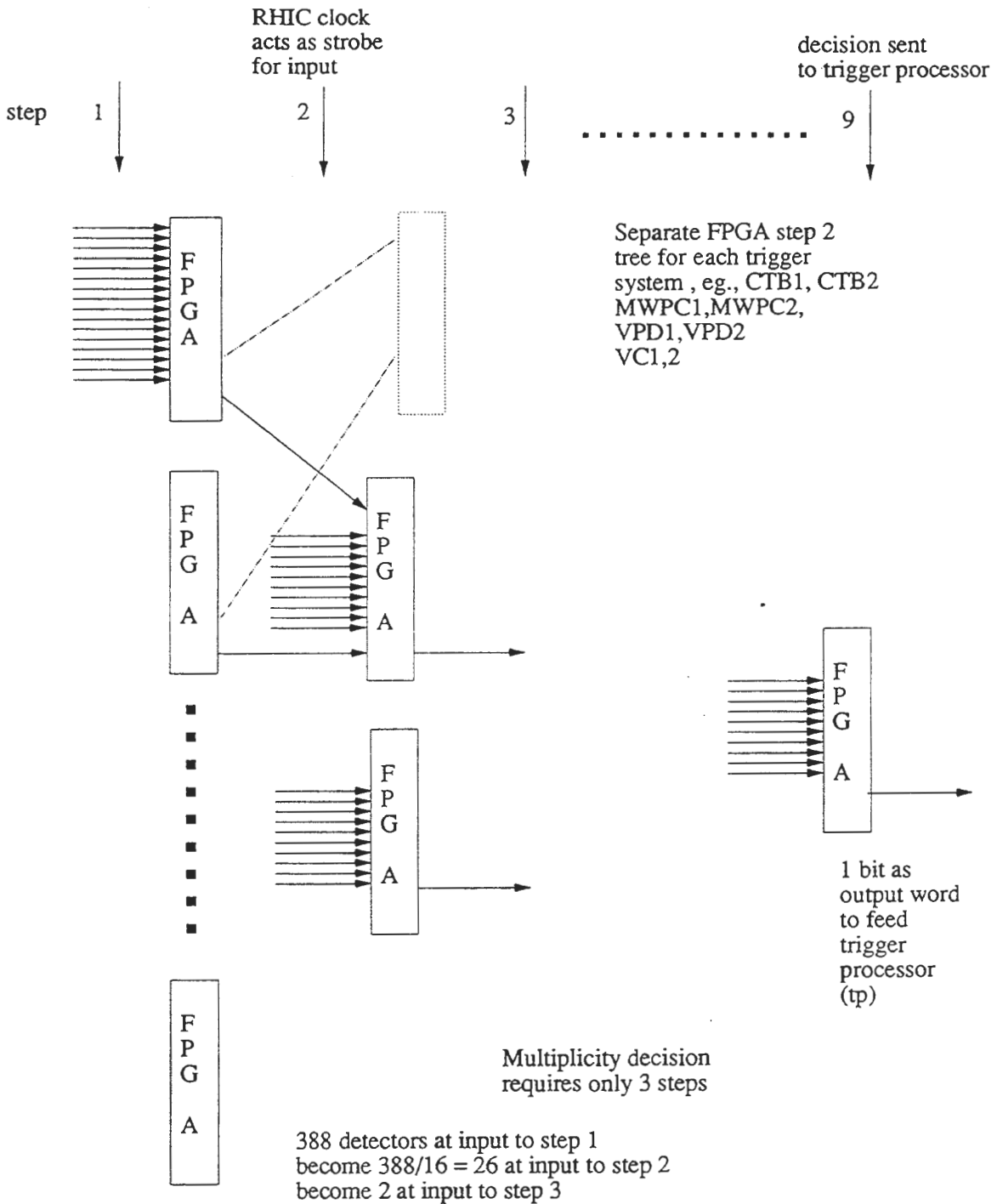


Figure 4E-8 Diagram showing the timing of FPGA steps. Each FPGA receives input from either the detectors (step 1) or from preceding FPGAs (step 2-9). Many independent FPGA trees may run simultaneously using copies of input words. Note that decisions on overall multiplicity can be completed within 3 crossings from the time of the interaction, although such decision need not be made in less than 9 crossing times.



4.H. Silicon Vertex Tracker

4.H.1 Mechanical Aspects

The updated version of the SVT still foresees a 3 barrel design for the basic version of the Silicon Tracker. Within the last months the distances between the layers as well as the coverage were further optimized. The present design assumes a three barrel version with 6,10,16 ladders, respectively. This approach is based on an even number of ladders in each of the layers, which would allow use of a tiling scheme as proposed in the original CDR. The distances from the vertex to the point of closest approach for each layer are 4.58, 8.14 and 13.29 cm respectively, instead of 4.96, 7.89, 10.92 cm as shown on original Figure 4H-23. These distances were chosen to improve the matching capabilities as well as the position resolution of the device. Details of the calculations can be found in STAR note 69.

The bigger outer radius of the modified SVT leads to a considerable increase in the number of channels compared to the original CDR. We therefore decided to optimize the pseudorapidity coverage of the device by proposing a 'butterfly design' for the active area. That means that the number of SDD's per ladder increases from the innermost layer to the outermost layer from 4 to 7 Silicon Drift Detectors (SDD). The resulting number of channel is 83328 for the whole device.

This geometry covers the pseudorapidity range of ± 1 with a ± 6 cm uncertainty in the 9th order vertex definition. The ± 6 cm originates from a conservative estimate of the beam-beam trigger detector capabilities. The support structure for this design will not resemble the butterfly shape of the active area. That means all the layers have ladders of the same length (49.35 cm) that will be mounted to the support endcaps on each side of the ladder, as described in the original CDR. This also allows to upgrade to a non butterfly geometry, and therefore enhanced partial eta-coverage, if additional funds become available.

A further option under consideration is an upgrade of the endcaps to accommodate a fourth, inner layer with 4 ladders to enhance the secondary reconstruction capabilities at lower momentum. Presently, the structures of the two detectors, a basic 3 barrel design and a 4 barrel upgrade, are proposed as a clam shell design that can be opened so that the detector is removable without breaking the beam vacuum.

4.H.2 Electronics Aspects

A basic block diagram for the SVT readout chain was designed over the last months. In this scheme the anodes would be wire bonded to a FEE board that hosts a pre-amp/shaper/driver-IC. The signals will then be cabled out to a readout board which hosts the SCA/ADC-IC's. This board will be located at the TPC endcaps, close to the TPC-FEE. From there the signals will be processed via transputer board to the DAQ. Each transputer board serves two readout boards. Each readout board has 14 SCA/ADC-IC's on it with 224 channels each. So two readout boards serve one SDD.

Up to the transputer board the signals are not multiplexed. This causes a difficult integration environment due to the number of signal cables. First prototypes of Kapton/Al cables were produced and seem a viable option.

Besides the signal readout, the low voltage for the electronics as well as the high voltage bias levels for the detectors have to be supplied externally. The present scheme utilizes the internal resistor chain, so that each wafer only needs two bias levels (0 V, and -3000 V). One R+D project is to work out an integrated Kapton cable, that serves as a signal cable and a power cable for the high and low voltage. First prototypes of such a highly segmented cable seem promising.

The cooling system has to be decided after the final design of the FEE and detailed measurements of the heat dissipation on the detector. IR imaging techniques are used to map the temperature on the STAR1 prototypes. Presently, several integrated cooling schemes are being simulated to meet the cooling requirements for the SDD's. Gas as well as liquid cooling is considered. If the final electronics design calls for a liquid cooling scheme, evaporative cooling is preferred over simple water cooling because of its considerably reduced radiation length.

4.H.3 Simulation Update

4.H.3.a Stand-alone tracking in the SVT

The stand-alone tracking code, first mentioned in the original CDR, was optimized to allow a TPC independent reconstruction of all tracks. In the present scheme the simulation runs through all the identified space points in the SVT to determine the primary vertex and exclude 'stiff' tracks ($P_t > 200$ meV/c) from the data sample by applying a very restrictive cut on the sagitta of the track in the field. In a second path through the same subroutines one then relaxes the search area definition from layer to layer to allow the identification of low momentum

tracks between 40 and 200 MeV/c. The superior position resolution in the SVT (σ around 25 micron) allows almost complete 'ghost-track' elimination in the two paths through this tracking procedure. This running mode does not rely at all on any TPC information.

The track efficiency for the second path down to 40 MeV/c is shown in Figure 4H-1. The 'all track' curve shows a comparison with the efficiency assuming no first path, so that all space points contribute to the efficiency. The other lines show the efficiency for the second iteration in a tiled and non-tiled design. In this application tiling causes a major improvement by avoiding any loss in space points, due to dead area on the detector.

In Figure 4H-2 we show the track efficiencies for a 4 barrel upgrade. The 4-layer design foresees a fourth layer very close to the beam pipe ($R = 3$ cm). Around 10% of all secondaries decay in the SVT (the secondaries are dominated by pion decays). 8% of all secondaries would decay before an inner fourth layer. This subset contains the majority of the multiple strange particles. The simulations show that the upgrade enhances the track efficiency to 97% for all particles including secondaries. The SVT tracking is crucial for the reconstruction of especially the multistrange particles (ω , cascade), because around half of the decays contain a decay product with low momentum. Most of these decays can be properly reconstructed by an integrated tracking algorithm (SVT+TPC).

Besides the sizable decrease in background in the invariant mass reconstruction, which was demonstrated in the original CDR, most of the decay products with low momentum would be lost in a TPC stand-alone version, because of tracks that do not reach the TPC. Together with its good momentum resolution that was shown in the CDR, the SVT alone provides a powerful tool for measuring the low p_t part of all particle spectra at RHIC. These simulations demonstrate that low p_t tracking can be addressed with the SVT down to 40 MeV/c. Further work to include a realistic detector response simulation is in progress.

4.H.3.b Matching between TPC and SVT

Since the CDR, there have been a number of modifications to the TPC-to-SVT matching program. We have used an updated, more realistic simulation for the TPC and we extended the tree search among the SVT hits to allow for missing hits, which are due to dead electronic channels or inactive SVT regions. We ran simulations with three different options for the TPC track input:

- a) raw GEANT points where the tracks cross the TPC pad planes
- b) raw GEANT points that have been smeared by the TPC resolution (the TPC space point resolution is predicted to be about 600 micron).

c) points resulting from the TPC tracking

The first case represents the multiple scattering limit. The second case represents ideal tracking in the TPC. The third case represents the status of the present TPC tracking algorithm.

The resulting matching efficiencies for the first two cases are remarkably close to each other and to the results in the CDR. Using a TPC space point for tracks with $p_t > 200$ MeV/c in Au-Au events.

Using the tracks reconstructed in the TPC as input the matching efficiency decreases down to 85%. This is due to some GEANT tracks that split into multiple segments during the TPC tracking and are not merged in subsequent steps. With improvement in the TPC tracking and merging of TPC track segments as well as utilizing the dE/dx information in the tracking code, we believe the TPC to SVT matching efficiency for tracks above $p_t=200$ MeV/c will remain higher than 95%. First concepts to match the track segments of lower momentum particles were applied by matching from the SVT to the TPC. Further work, based on the matching of the output vectors of the SVT stand-alone tracking and the TPC tracking, is in progress.

4.H.3.c Inner field cage modification

The SVT group suggested to change the material of the inner field cage from an aluminum/kapton composite to a ROHACELL structure. In the original CDR a breakdown of the composite structure (*Appendix 4, page A-12) showed the IFC accounts for 0.57% radiation length. The new ROHACELL structure decreases this value by 60% to 0.22% radiation length.

Simulations show a resulting decrease in multiple Coulomb scattering between the SVT and TPC by 20% on average. This also takes the effect of the SVT cone support structure into account. Multiple Coulomb scattering between the SVT and the TPC is the main uncertainty in the track matching between the two detectors. The overall matching efficiency gets improved by 3% if a ROHACELL structure is chosen. The effect is largest for the low momentum tracks (up to 20% at 450 MeV/c).

Figure 4H-1: track efficiency for a stand-alone SVT tracking algorithm assuming a 3 barrel design as described in the text.all tracks': one path track reconstruction for all particlesother lines: two path track reconstruction for particles between $p_t=40-200$ MeV/c. The curves represent an un-tiled and a tiled version of a 3 barrel design.

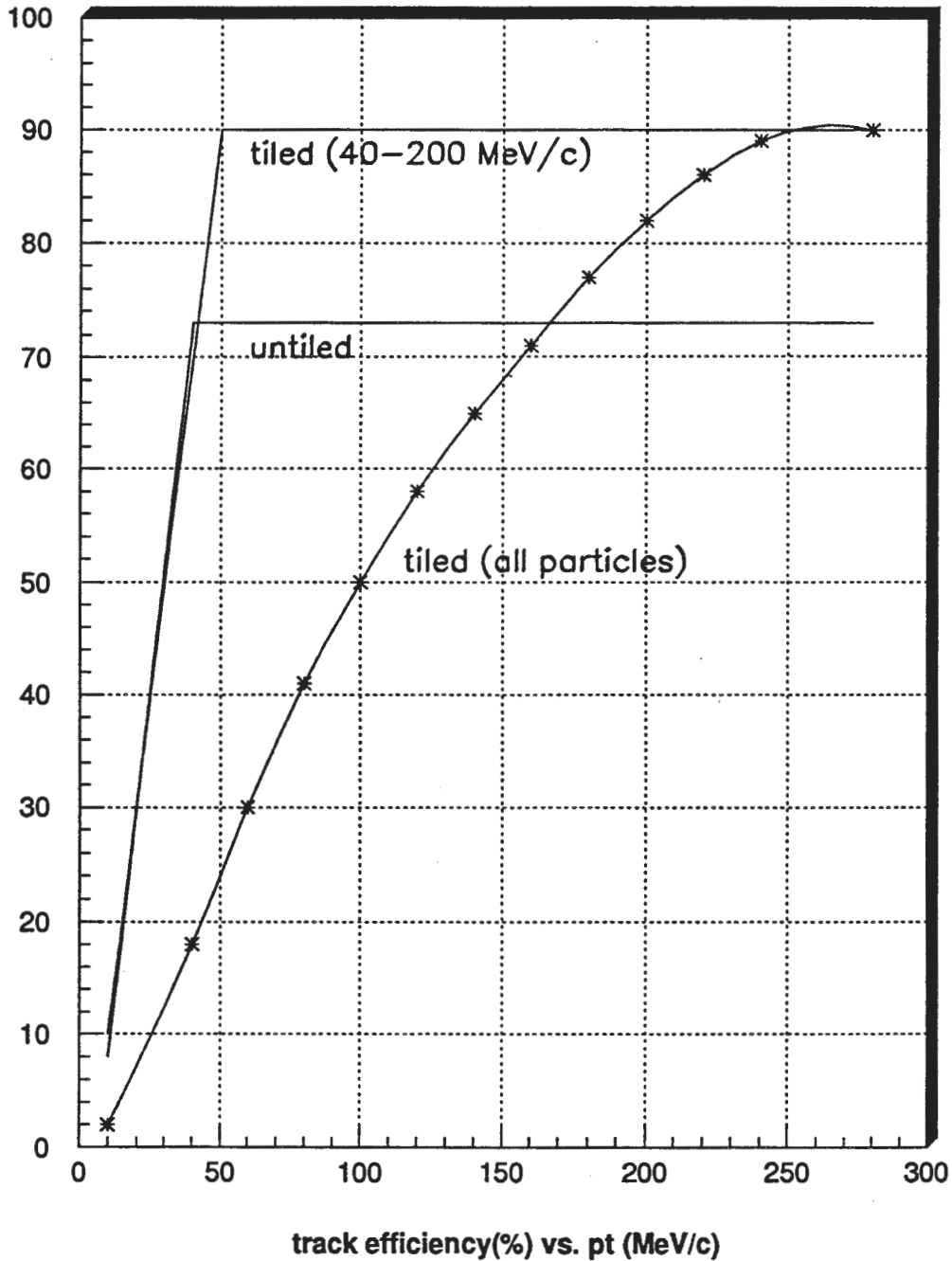
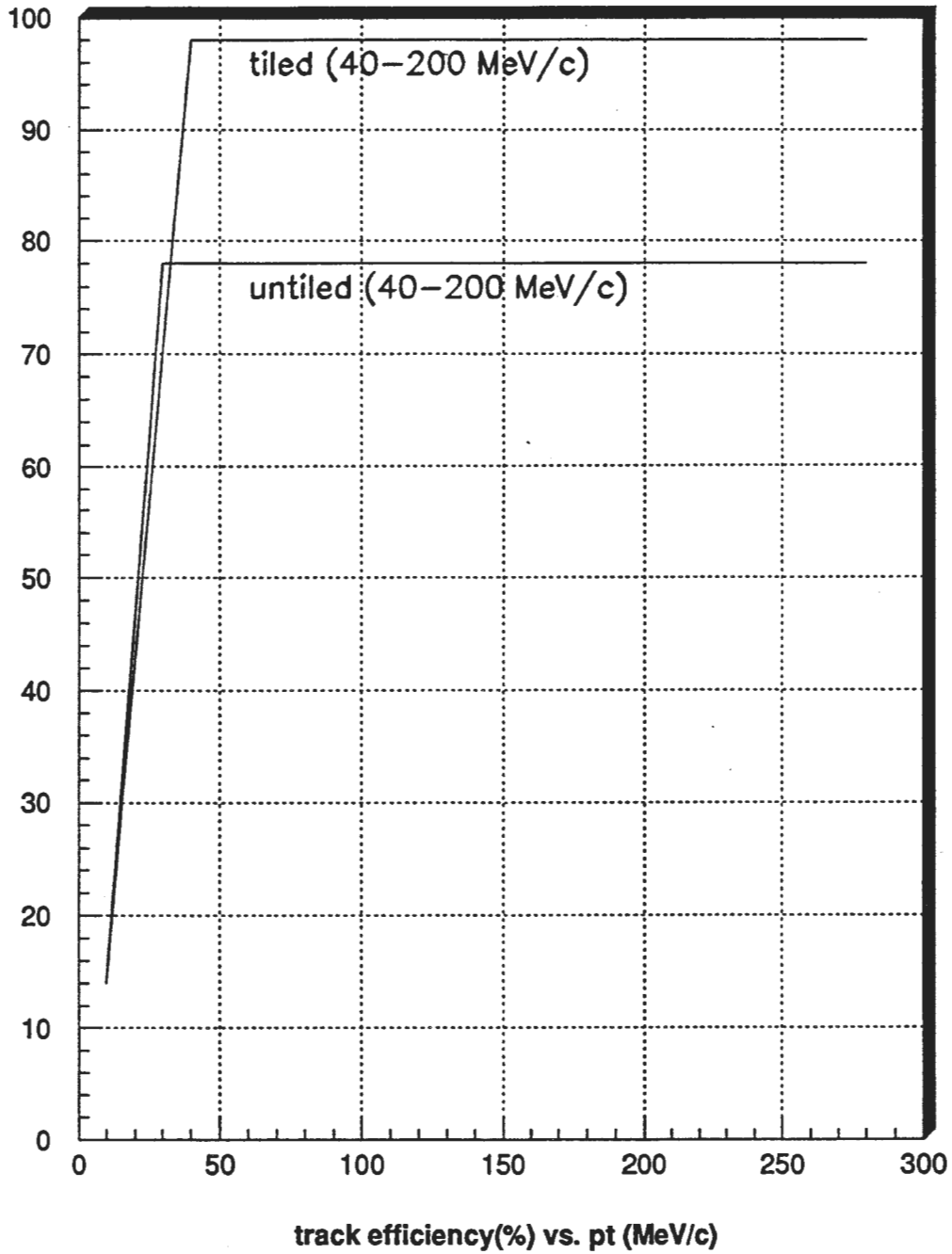


Figure 4H-2: track efficiency for a stand-alone tracking algorithm assuming a 4 barrel design. The curves show a tiled and a non-tiled version.



4.I Electromagnetic Calorimeter

4.I.1 Specialized Physics Issues

For the purposes of making a neutral energy trigger and measurement for heavy ion physics, a Monte-Carlo study is in progress on the low energy response for π^0 vs π^\pm . It will take into account the reduced intervening mass as a result of the selection of a warm coil with a radius larger than the barrel EM calorimeter.

4.I.2 Description of Subsystem.

The barrel part of the EM calorimeter is now located inside the warm coil magnet. The space allotted is from radius 2200mm to 2620 mm. The length available is approximately 6250 mm. The baseline design Lead-scintillator sampling calorimeter with spacers between lead plates and minimal strongback for support fits within this space. The baseline design is 60 segments in ϕ and 20 in η for the barrel calorimeter. Physically, the calorimeter is subdivided in 60 wedges in ϕ by two in η . The size of the projective towers in η is approximately 0.100, but this will be increased slightly, depending on the details of the design for routing the TPC cables and other cables out of the magnetic volume near the magnet pole piece, and also on the details of mounting the calorimeter.

The phototubes are mounted on the outside of the return iron bars inside iron boxes because they do not work well in a magnetic field. Clear optical fibers are spliced to the waveshifter fibers. This is because the shortest path through the magnet coils from the scintillator to the phototube is at least 3 meters. The attenuation length of green light in the shifter fiber is between 1.8 and 2.1 meters. The attenuation length in the clear fiber is about 7.0 meters allowing adequate signal to reach the phototubes.

The calorimeter modules are supported on 9 aluminum rings of approximately the same inner and outer diameter as the magnet coils. These rings are interspersed in the coils at intervals of approximately 60 cm. A finite-element study of the deflections of all the structure of the STAR detector indicates that the rings must be attached to the iron magnetic flux return bars at several positions around the magnet. The weight of each of the 120 calorimeter wedges is 1.5 tons. The rings are 7.5 cm in thickness in the z direction. Spaces of 5 cm in the z direction next to each ring will provide space for the optical fibers to exit radially from the magnet volume between the magnet coils. The center ring at $z=0$ may be split in thickness and the gap between magnet coils may be of slightly different dimension from the others so that the fibers can be threaded as the calorimeter modules are installed by sliding them in the axial, z , direction.

The number of phototubes is 1200 for the barrel calorimeter initially, plus 10000 for the shower max detector. The calorimeter can be upgraded by a factor of 2 in eta and a factor of 2 in depth segmentation at a later date so that 4800 tubes will then be needed for the calorimeter. The phototubes for the barrel calorimeter will occupy about four cubic meters on the outside of the detector. This will be spread over the circumference in 30 segments in phi, about 50 cm in width, 5.8 meters long and 20 cm deep. Roughly 25 % of these, or 3000 tubes, must be removed from the top of the detector in order to fit it through the door to the experimental hall.

The endcap calorimeter is a proposed upgrade. The mechanical design is still in the conceptual stage. The endcap calorimeter will cover the rapidity range from 2.0 to about 1.0. The exact coverage again depends on the routing of the cables from the TPC, SVT, and TOF systems, as well as the TPC mechanical support. The face will be roughly at $z=0$ and the back will be mounted directly to the inner face of the pole piece. The segmentation of the active scintillator will be 60 in phi and 12 in eta, with non uniform segmentation in eta. The end cap calorimeter will consist of 25 layers, about 20 radiation lengths, instead of 20 layers as in the barrel, because of the higher energy of particles in the forward direction. The thickness is determined by the resolution due to fluctuations in shower leakage out the back. About half the fibers would exit through the $\eta=2$ hole in the pole piece and about half through the crack between the pole piece and the iron ring that holds the flux return bars. The Phototubes for the endcap calorimeter and shower max must move with the pole piece when it is pulled to service the TPC. There will be roughly 720 calorimeter phototubes and 3000 to 6000 shower max tubes. These will cover the pole piece about 3 layers deep.

4.I.4 R&D Issues and Technology Choices

The immediate R&D activity related to the calorimeter focuses on integration issues. We are doing finite element studies to optimize the design of the calorimeter support. The possibility of interference with the warm coil depends on the fiber bend radius and attenuation length. The space required between TPC and coil depends on the spacer required to separate the lead plates, on the cladding required to prevent bending of the lead plates, and on the strongback thickness and on the installation procedure for the calorimeter.

The next set of R&D issues are the technology choices for the calorimeter, the shower max detector, and the readout. We will resume mechanical tests on the feasibility of stacked lead with spacers. The issues are the coining of hard lead with stainless cladding, and the creep with a bending moment. We will continue to investigate the sensitivity, construction cost, and electronics cost for scintillator shower max vs wire chamber shower max. We are getting samples of

Russian phototubes. We will test the suitability of one type for the calorimeter and another type for the shower max detector. We are also building models of the calorimeter to optimize the fiber routing.

A small, 4 tower, prototype calorimeter is being built to be used in a test beam. The physics issue is the relative response of very low energy charged pions vs pi-zeros.

4.1.5 Engineering

4.1.5.a Technical Description & Specifications

The barrel EM calorimeter is now located inside the STAR conventional magnet coils. The available space at inner radius is 2200 mm and the outer radius, including strong back support, at 2610 mm. The barrel calorimeter is divided in 60 wedges in phi and in two pieces in z. Each of the 120 pieces weighs approximately 1.5 tons. The calorimeter is supported at 9 locations in z by aluminum rings interleaved with the magnet coils. These rings are 7.5 cm thick and 50 cm between inner and outer radius. A space of 5 cm is provided next to each ring for the optical fibers to exit the magnet.

In the baseline design each barrel calorimeter wedge is held together by friction and the clamping force is about 5 times the weight of the module. The clamping is done with steel straps at intervals on the side of the wedge.

Two designs are being considered for the endcap calorimeter. One would use individual boxes for each of 60 segments on the face of the magnet polepiece. The other design would be in two halves with the back plates attached to the pole piece.

4.1.5.b Description of Major Components

Optical system

Each of the 1200 towers in the barrel will have 84 optical fibers. There are 100,800 calorimeter fibers as in the previous design. These fibers must be approximately 3 to 3.5 meters long even with the shortest path through the coil to the phototubes outside the field return iron. The shifter fibers must be spliced to 3 meters of clear fiber approximately 5 cm from the calorimeter. The splices involve thermal fusion and a reinforcing sleeve.

The attenuation length of green light in the shifter fiber is between 1.8 and

2.1 meters. The attenuation length in the clear fiber is about 7.0 meters. The light output of our scintillator-shifter optical system is about 2. photoelectrons per minimum ionizing particle with less than 1 meter of shifter fiber. In the baseline design, the fibers from two sub-towers are all routed to one phototube.

The optical design of the endcap calorimeter is similar.

Shower Maximum Detector

The baseline design places the shower max between the 5th and 6th layers in the calorimeter at about 5 radiation lengths depth. The radial space is 25 mm. Each module is 24 cm by 300 cm and has 250 fibers from the phi detector scintillator strips and 500 fibers from the eta detector strips. The total is 90,000 fibers. These will be multiplexed to 10,000 phototubes. The multiplexing will make effective scintillator strip lengths of approximately .5 in eta and approximately 4 radians in phi. The pressure on the shower max detector in a wedge will be about 5 times the weight of a wedge, or 8 tons for a 3 meter long unit. This is because the wedges are held together by friction and the clamping force is large.

Phototubes

Initially there are 1200 phototubes for the Barrel calorimeter and 10,000 phototubes for the barrel shower max. The area on the face of a calorimeter phototube must be the 82 mm^2 for the fibers and additional space for light mixing, so the tube radius must be over 1 cm.

These tubes with bases and associated fiber routing and cabling cover almost the entire outside of the STAR detector to a depth of 3 layers. The phototubes are in boxes 50 cm wide by 18 cm high by 5.8 meters long on each of the 30 return iron bars.

The phototubes will be existing tubes provided by the Serpukhov group.

Support System

The calorimeter modules will be supported on 9 aluminum rings of approximately the same inner and outer diameter as the magnet coils. These rings are interspersed in the coils at intervals of approximately 60 cm. A finite-element study of the deflections of all the structure of the STAR detector indicates that the rings must be attached to the iron magnetic flux return bars at

several positions around the magnet. The weight of each of the 120 calorimeter wedges is 1.5 tons. The rings are 7.5 cm in thickness in the z direction. Spaces of 5 cm in the z direction next to each ring will provide space for the optical fibers to exit radially from the magnet volume between the magnet coils. The center ring at $z=0$ may be split in thickness and the gap between magnet coils may be of slightly different dimension from the others so that the fibers can be threaded as the calorimeter modules are installed by sliding them in the axial, z, direction.

Front End Electronics

The bases of the calorimeter phototubes will contain charge-integration/shaper electronics, flash ADC's, and Cockroft-Walton high voltage generation. A precise timing signal referenced to beam crossing is used for the integration reset and the ADC strobe. An analog signal is available for a very fast analog trigger compatible with the TPC gate.

The shower max detector phototubes are read out with switched capacitor pipelines similar to the TPC, with the electronics located over the back of the return iron.

4.I.5.e Transportation, Reassembly, Installation and Alignment

The calorimeter support system uses axial rails at the inside of the magnet coils so that calorimeter wedges can be slid into place axially. This is to allow the installation of barrel EM modules after the TPC is installed and operating. The center ring at $z=0$ may be split in thickness and the gap between magnet coils may be of slightly different dimension from the others so that the fibers can be threaded as the calorimeter modules are installed by sliding them in the axial, z, direction.

The phototubes are in boxes 50 cm wide by 18 cm high by 5.8 meters long on each of the return iron bars. In order to fit the STAR detector through the door of the experimental hall, the phototubes from the top 14 wedges, or about 25% of the total number must be removed. This involves disconnecting approximately 50,000 optical fibers, half from the calorimeter towers and half from shower max. The fibers from shower max may go to special connectors which can connect 250 fibers at once. The fibers to the phototubes may be in bundles of 21 to 84 glued into phototube cookies.

4.I.6 Testing and Calibration Issues

4.I.6.1 Calibration

With the calorimeter inside the magnet coil, the stainless steel tubes which carry radioactive sources must exit through the gap between the magnet pole piece and the iron ring along with the TPC cables. These tubes are .06 inch in diameter and constrain the source and aircraft cable which moves the source. There are two per module, or 240 total. The minimum allowable bend radius for these tubes is about 5 inches. The tubes run on the surface of the shower max, detector inside the calorimeter within grooved plastic to protect them from the 8 ton compressive force.

There are 60 small lead houses on each of the iron end rings. These contain the radioactive sources and their drive motors for the calibration. There will be a similar system for the end cap calorimeter.

5. Integration of Experiment

5.A. Subsystems Integration

Subsystems Integration tasks include the following:

- Subsystem dimension control including subsystem upgrades
- Routing of cables, pipes, ducts
- Assembly and service scenario modeling
- Structure support paths for subsystems
- Determination of conventional facilities needs, which include assembly hall requirements and modifications and utility needs (power, HVAC, water, etc.)
- Provide the necessary AC power to run the instrumentation for the various detectors and sub-systems of the STAR experiments. This includes the requirements for future upgrades.
- Provide a system for carrying signal and DC power cables between the detector and the electronic instrumentation.
- Identify and support electrical issues that are common to the various sub-systems.
- Interface with RHIC/BNL on issues common to facilities

5.A.1 Subsystem Dimension Control

Engineering and design effort is being devoted to ensure that subsystems fit together, can be assembled and serviced, and have minimum negative impact on other subsystem's performance. Subsystem overall dimensions have been defined along with assembly clearances. Allowance is made for future subsystem upgrades. Figure 5-1 shows a cross-section of the STAR detector with some basic dimensions. Figure 5-2 shows an end view of the detector. The subsystem overall dimensions are shown in Table 5-1.

It is important to note that these dimensions represent simple geometrical volumes and maximum subsystem dimensions. A subsystem's nominal dimensions will likely be different due to manufacturing and alignment tolerances. More detailed geometries will be defined as systems evolve. Three-D CAD solid modeling will be used to model these geometries in an unambiguous manner.

5.A.2. Assembly

Initial assembly and subsequent servicing of the detector has been modeled on both 2-D and 3-D CAD in order to determine the dimensions for the new assembly building and to insure adequate fit in the existing Wide Angle

Hall. The detector will be assembled, fully cabled, and tested in the assembly building. Figure 5-3 shows the assembled detector with its electronics trolley in the proposed assembly building. The detector with its electronics trolley will then be rolled into place on the beamline, then the beampipe will be installed, and the shielding wall/room erected around the electronics trolley. At this point, the detector is ready for testing and operation on the beamline. Figure 5-3 also shows the detector in its operating position.

Table 5-1 STAR subsystem basic dimensions.

SVT		
	Inner Radius	50 mm
	Outer Radius	107 mm
	Half length	211 mm
TPC		
	Inner Radius	500 mm
	Outer Radius	2060 mm
	Half length, Tracking Volume	2100 mm
Trigger Barrel (CTB)		
	Inner Radius	2060 mm
	Outer Radius	2170 mm
	Half length	2280 mm
EMC		
	Inner Radius	2200 mm
	Outer Radius	2610 mm
	Maximum Half Length	3100 mm
Solenoid Magnet		
	Inner Radius	2620 mm
	Outer Radius	2970 mm
	Max. Coil Half Length	3100 mm
	Max. Return Iron Half Length	3625 mm

Assembly of the detector begins with erection of the detector supports onto the steel floor plates as shown in Figure 5-4. The lower barrel return iron (BRI) segments are placed on the support system. The end iron rings are then mounted and bolted onto these segments. Temporary auxiliary supports are used to hold the rings in place, then they are surveyed and aligned into proper position.

The aluminum spacer rings to hold the coils' sub assembly are installed and aligned using temporary lateral supports. The magnet coils are then inserted and aligned using hydraulic jacks as shown in Figure 5-5. After alignment, the coils are mounted to the aluminum rings by coil locking screws. The remaining iron segments are brought in from the side, then picked up using special lifting fixtures by cranes and bolted to the end return rings. The mounting nuts are tightened evenly to pull the segments up into final position on the end return iron rings.

After the iron and coil are assembled, the detector is ready for field mapping, which must be done without the TPC in place. Field measurement equipment is installed in the magnetic volume, and the poletips are then installed. The poletips have their own rolling supports. The supports may be left on when the detector is in the operating position or in the testing position in the assembly hall. They must be removed before the detector can be moved through the door of the wide angle hall, because of the limited WAH door width. After field mapping is complete, the poletips are removed while on their supports, and a TPC installation beam is installed through the detector. This beam is more than twice as long as the detector to allow three possible supporting points. Twin double-arm TPC supports roll along this beam. This allows the TPC, without Central Trigger Barrel (CTB) modules, to be installed onto the beam. The TPC can then (by removing the central beam support) be rolled along the beam into place inside the magnet, where it is mounted. The beam is then withdrawn from the detector. This sequence is shown in Figures 5-6 and 5-8.

After the TPC is installed and roughly aligned, the CTB and SVT modules are installed. After installation, the SVT, TPC, and CTB cables are connected and routed through the cableways. After cabling to the electronics trolley is completed, pole tips are replaced and the complete detector is then ready for testing.

After testing of the assembled detector, the detector together with its electronics trolley can be rolled into the experimental hall, as noted above. This is accomplished by installing anchor blocks into the holes in the steel floor plates and jacks between the blocks and detector supports. The detector is then moved with the jacks, the jacks are retracted and the anchor blocks moved to the next set of holes, similar to the method used by the SLD, and D0 detectors.

5.B. Plumbing & Cabling Plans and Issues

Cable and pipe routing, provision for electronics power and cooling and ventilation needs are being developed. Three-D CAD solid modeling will be used to both visualize and check for interferences. A general concept has been developed for the routing of cables and pipes from the various subsystems to their respective electronics and service connections. Cables and pipes which service the SVT, TPC, and CTB will be routed between the end return ring and

the pole tip, as shown in Figure 5-9. Thirty cableways 10 x 15 cm each are located at each end. EMC PMT cables are routed between the coils to the outside surface of the barrel return iron and routed directly to the electronics. The cooling water and the power connections to the solenoid are external to the detector

The slots between the end return ring (ERR) and the pole tip (for the SVT, TPC, and CTB cables and pipes) result in a loss of about 30% of the iron circumferential flux return path at this radius. With improved pole tip design, the remaining 70% iron area carries both higher overall field and a small amount of localized magnetic saturation which is not thought to adversely affect the operating field in the TPC. The CTB modules are removed by sliding them axially outward after removing the poletip. Some CTB modules will be blocked by cables and pipes as well. These pipes and cables will have to be made flexible enough to move laterally to the side.

5.C. Access and Maintenance Requirements.

There are three service scenarios which may occur. Table 5-2 summarizes the STAR detector's expected service and repair time estimates.

The first scenario requires the removal of the detector from the wide angle hall. This would be required in the case where a subsystem needs major service, such as a coil failure, or for a time consuming upgrade. The beampipe is removed, the necessary shielding disassembled, and the detector rolled into the assembly building. As soon as the detector is off the beamline, the beampipe is replaced and the shielding rebuilt. It is estimated that the accelerator could be operational in 2-3 weeks.

The second type of service scenario is where quick access is needed to service SVT, TPC, and CTB electronics, or for replacement of a TPC sector and/or CTB module(s).

Table 5-2

Service	Frequency	Repair Time
1. TPC electronics	biweekly	hours
2. EMC phototubes	bimonthly	hours-day
3. CTB /TOF phototubes	bimonthly	days
4. TPC pad planes	annually	days-week
5. SVT Electronics	bimonthly	hours-day

In this second scenario, the poletip(s) are retracted while the beampipe is left undisturbed. The XTPC's (if present) would first roll back on their own

supports.

The third scenario is for removal and replacement of a (non-clamshell) SVT. For this non-baseline case, the intermediate beampipe sections would be removed and then the XTPC's and poletips would be moved off the beamline out of the way. The SVT can then be removed and replaced. The center beampipe section remains mounted within the SVT during these handling operations. The baseline SVT design is clamshell, however, and does not require removal of any beampipe sections.

5.E. Detector Interface with Wide Angle Hall

5.E.1. Building Requirements

The Wide Angle hall has been selected by RHIC Management as the site for the STAR detector. Figures 5-10 and 5-11 show an "as is" layout of the hall and Table 5-3 lists the hall's major parameters. The beamline crosses the hall at approximately mid length, leaving little room on either end for assembly and service. The hall width is 53 ft, which limits the space needed to retract the pole tips for quick detector subsystem access. This constraint may impact the design of the XTPC and the fixture required to remove TPC sectors. Other hall constraints that may impact the detector operation are the limited crane capacity, the floor loading capacity, the size of the entry door and the clearance between the crane hook and the top of the detector. Because the south wing of the hall is too small for assembly/disassembly of the detector while the RHIC machine is operating, the detector will be assembled and cabled in a new assembly building which will be constructed adjoining the wide angle hall. After the detector is completely assembled, cabled, and tested, it will be rolled into position in the hall.

Table 5-3 Wide angle hall parameters.

Hall length and width	105 ft X 53 ft
Total area covered by crane	83 ft X 37 ft
Distance from floor to beamline	14 ft 2 in
Assumed distance from shield blocks to roll up door	47 ft
Roll up door dimension (when modified to max. size)	27 ft W X 27 ft H
Floor thickness/Load capacity	1.0 ft / 5000 psf
Crane capacity	20 ton

The southern end of the hall which is inaccessible during operation, can be used for storing STAR assembly and handling fixtures and shielding blocks.

The experiment requires power supplies and fast trigger electronics racks to be placed in the hall near the detector to minimize cable lengths. To facilitate assembly and testing of the detector in the assembly building, the electronics racks will be placed inside a special trolley which will move along with the

detector between the assembly building and the hall. Figure 5-3 shows a schematic layout of the detector and the electronics trolley. Figures 5-12 and 5-13 show elevation and side views of the electronics trolley in the WAH. It is a two stories enclosed structure designed to keep the electronics racks in a clean, conditioned space.

To allow access to the electronic crates during operation, a radiation shield will be built around the trolley. The details of this shield are discussed in Chapter 6.

The load capacity of the hall's floor must be assessed by RHIC's facility structural engineers. If required, the floor will be upgraded to handle the ≈ 1200 MT detector and shielding weight. Steel rails will have to be installed on the floor to facilitate detector movement between the assembly building and the hall. Other, more minor, modifications to the building will be discussed in a future document detailing the experimental facilities user requirement.

5.E.2. Hall Utilities Requirements

The Wide Angle hall is equipped with basic utilities such as tap water, 120 psi compressed air supply line and electric power for conventional systems, such as lights, crane and machine tools.

The STAR experiment is not expected to add much heat to the hall space since the magnet and most electronics will be cooled locally using modified chilled water. The maximum heat load added to the hall space from lights, pumps, motors and electric tools is about 200 kW. Since the STAR detector cannot tolerate ambient temperature swings of more than a few degrees Fahrenheit, the HVAC system will be required to handle the 200 kW plus any heat load added to the hall from the outside world. The building humidity control system should be upgraded to include temperature control capability as well.

The interfaces between utilities provided by RHIC and utility equipment provided by STAR is described in Chapter 6.

5.F. Interface with RHIC Accelerator Equipment

The only significant accelerator equipment located in the hall is the beampipe. Figure 5-14 shows a layout of the beam pipe and the vacuum equipment near the beam pipe. The interface between the RHIC accelerator and the STAR detector is basically limited to the beam pipe and space required to install the Veto Calorimeter. The details of the beampipe and its support structure within the detector have not yet been engineered. Preliminary layouts suggest a three piece beampipe, with the center narrow section being approximately 8 meters long and made of thin beryllium. None of the detector's subsystems require the removal of the beam pipe for routine service, with the exception of a (non-baseline) non-clamshell SVT. The impact on XTPC operation has not yet been determined.

Final engineering drawings of accelerator cryogenic bypass transfer lines and power cables are not available at this time. However, it is expected that this equipment will be located outside the hall to avoid any potential interference with the detector.

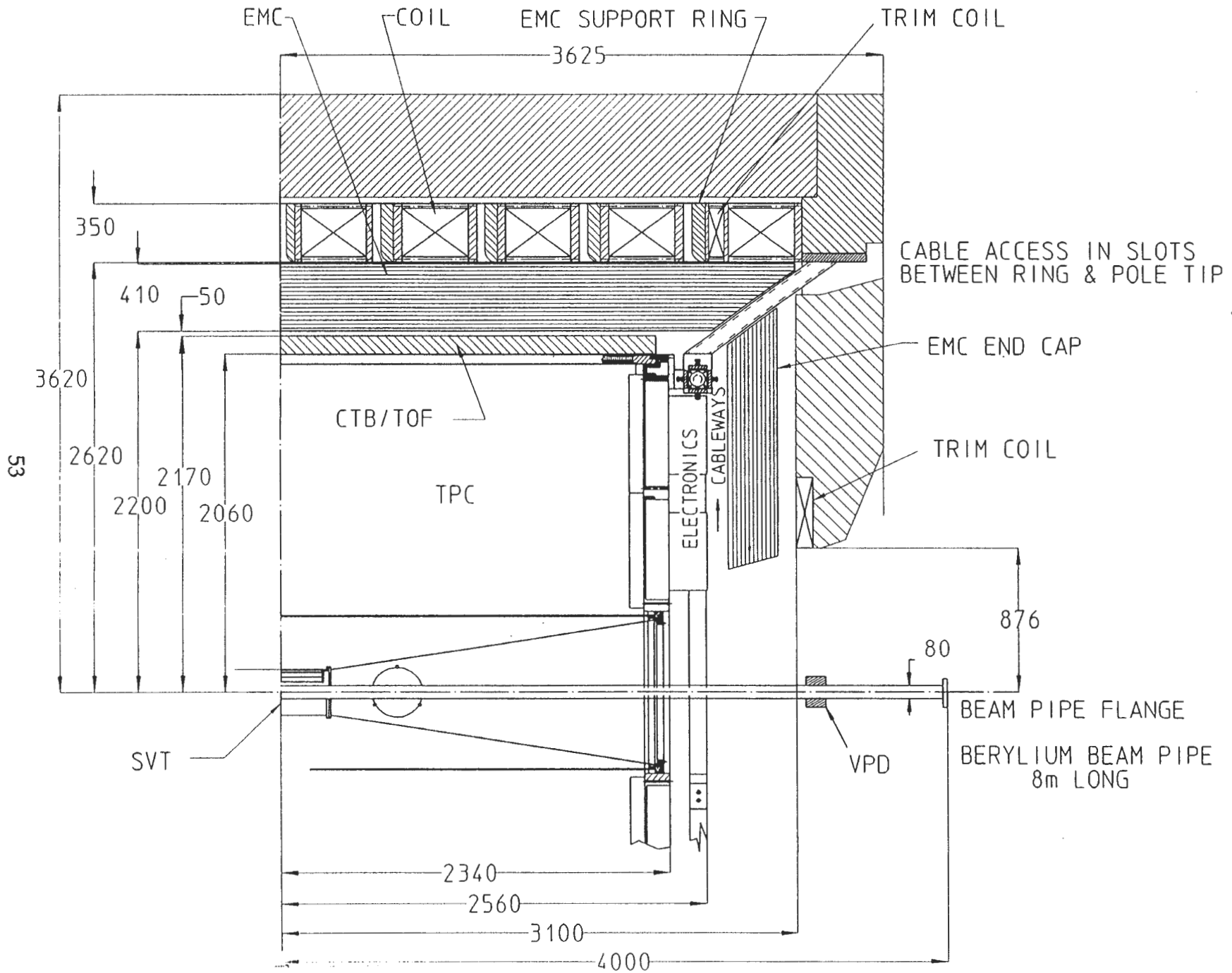


Figure 5-1 Cross Section of STAR Detector

Figure 5-2 STAR Detector: End View

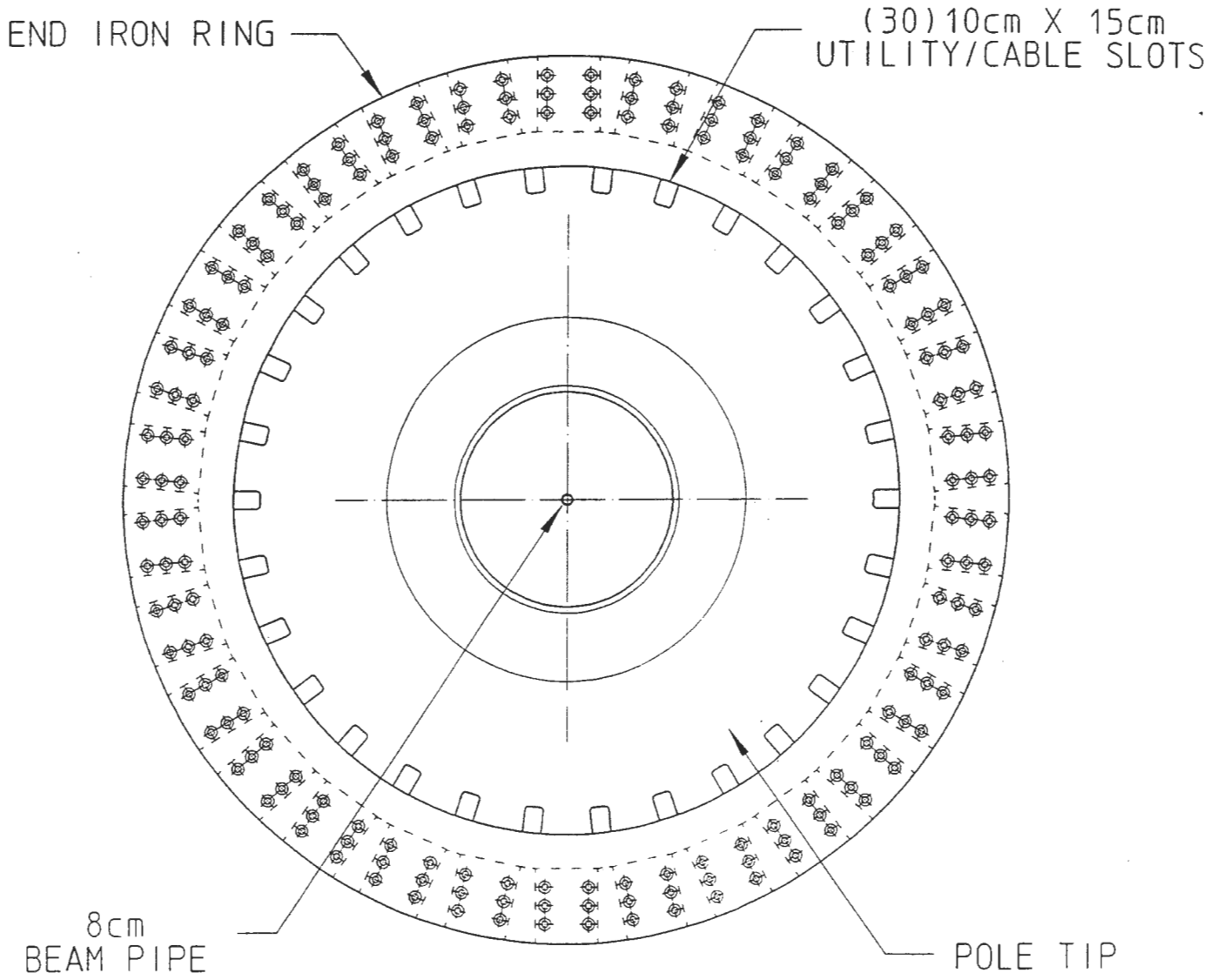


Figure 5-3 STAR Detector in Wide Angle Hall

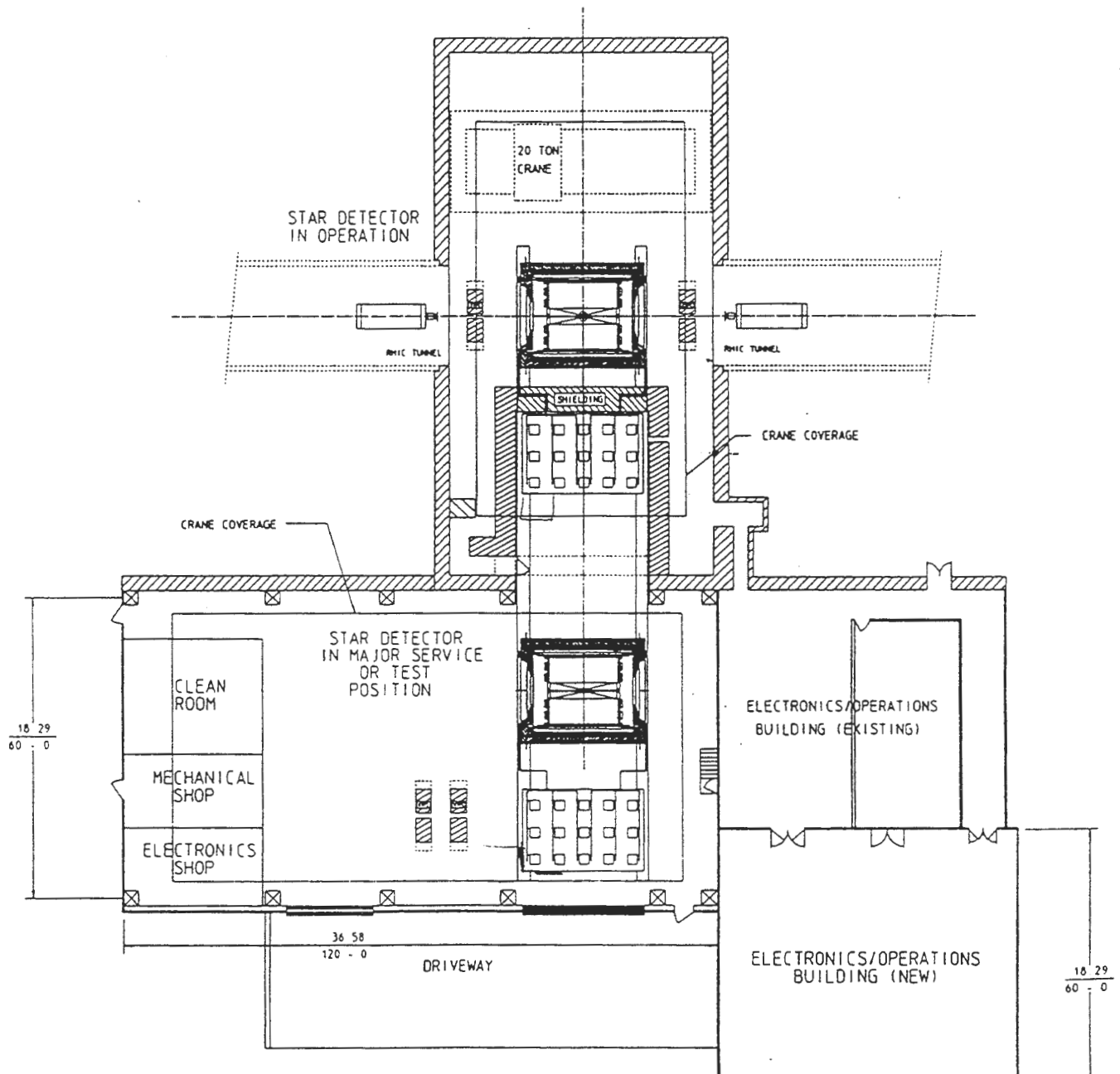
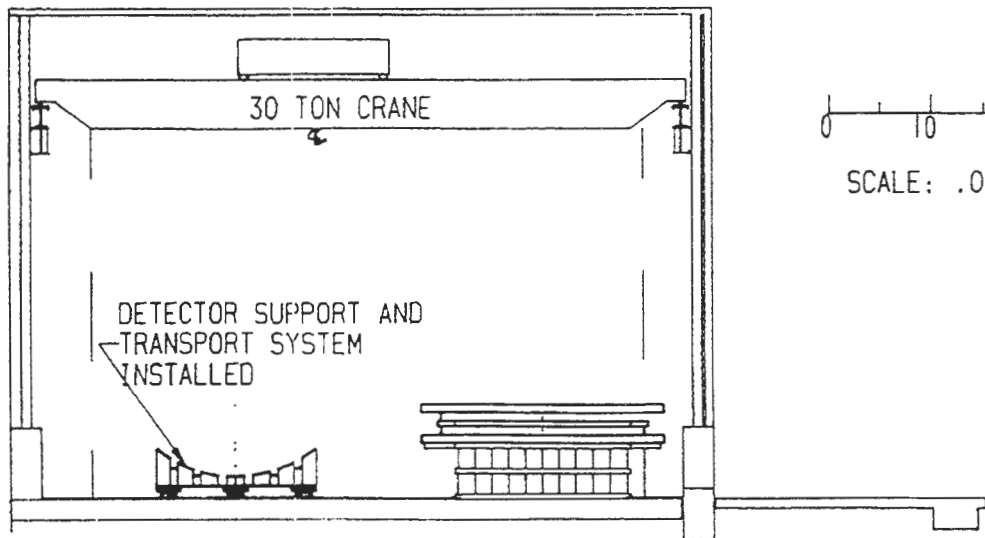
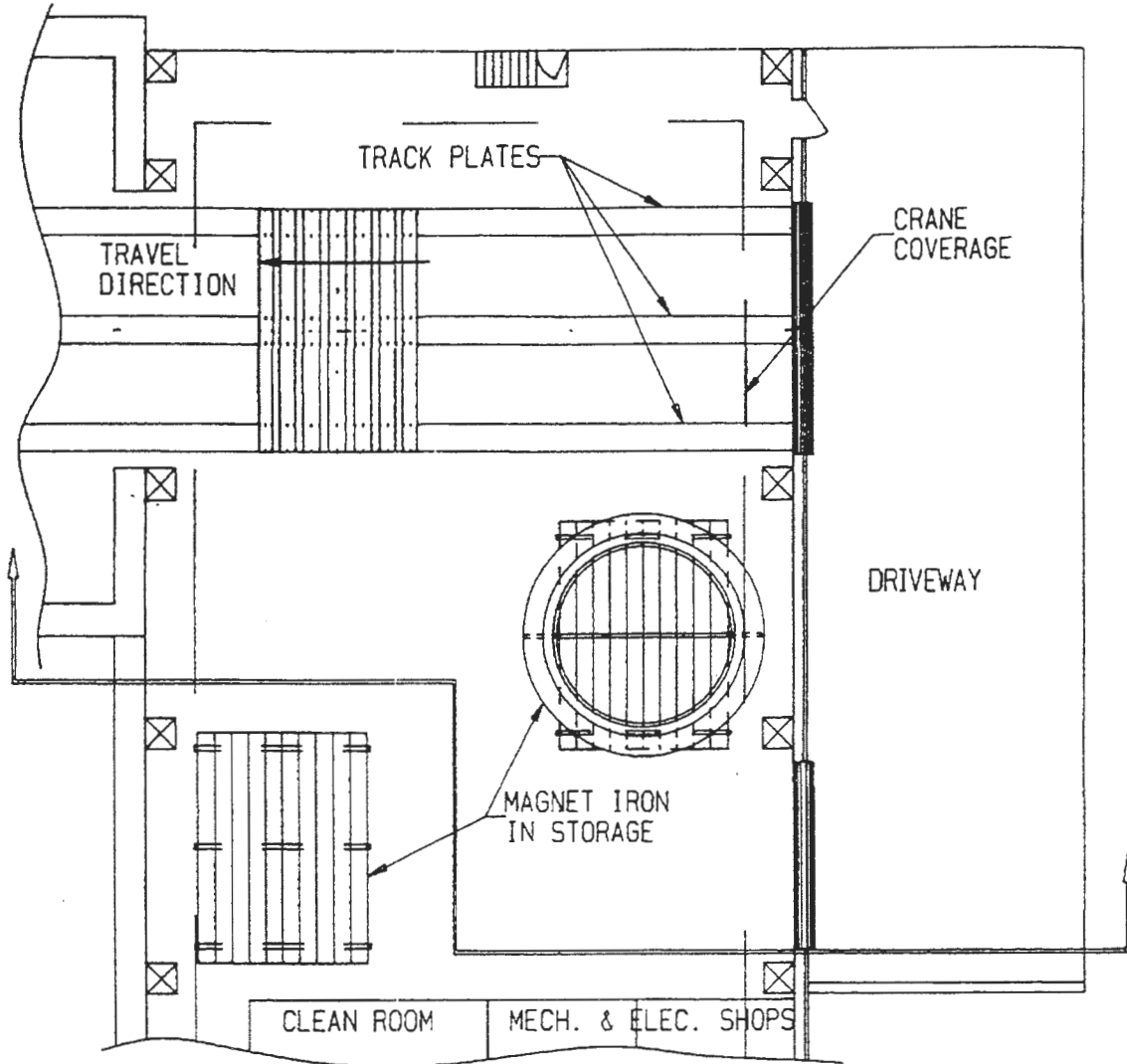


Figure 5-4 Support System Assembly



0 10 20 FT
SCALE: .005

Figure 5-5

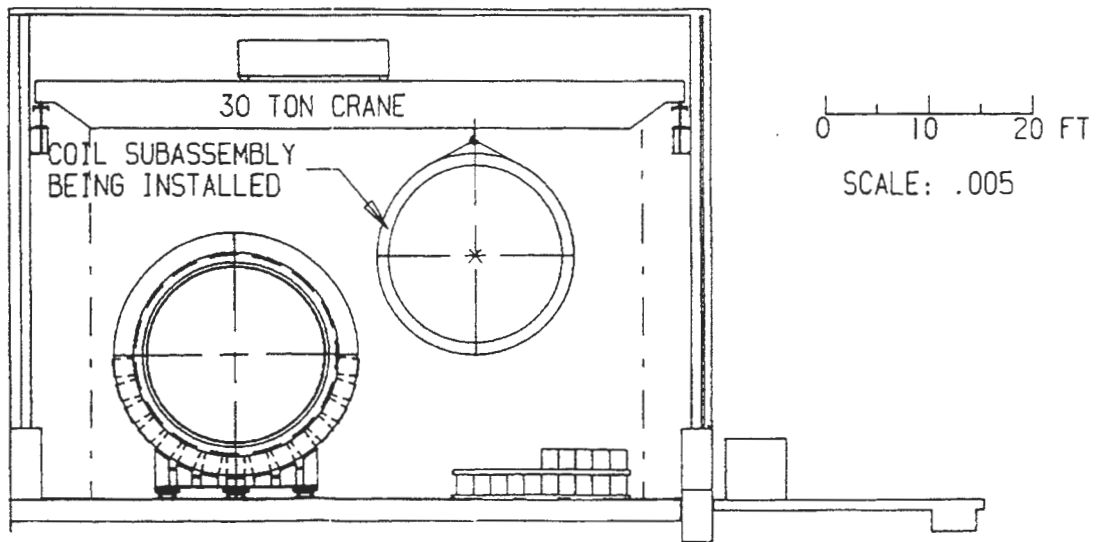
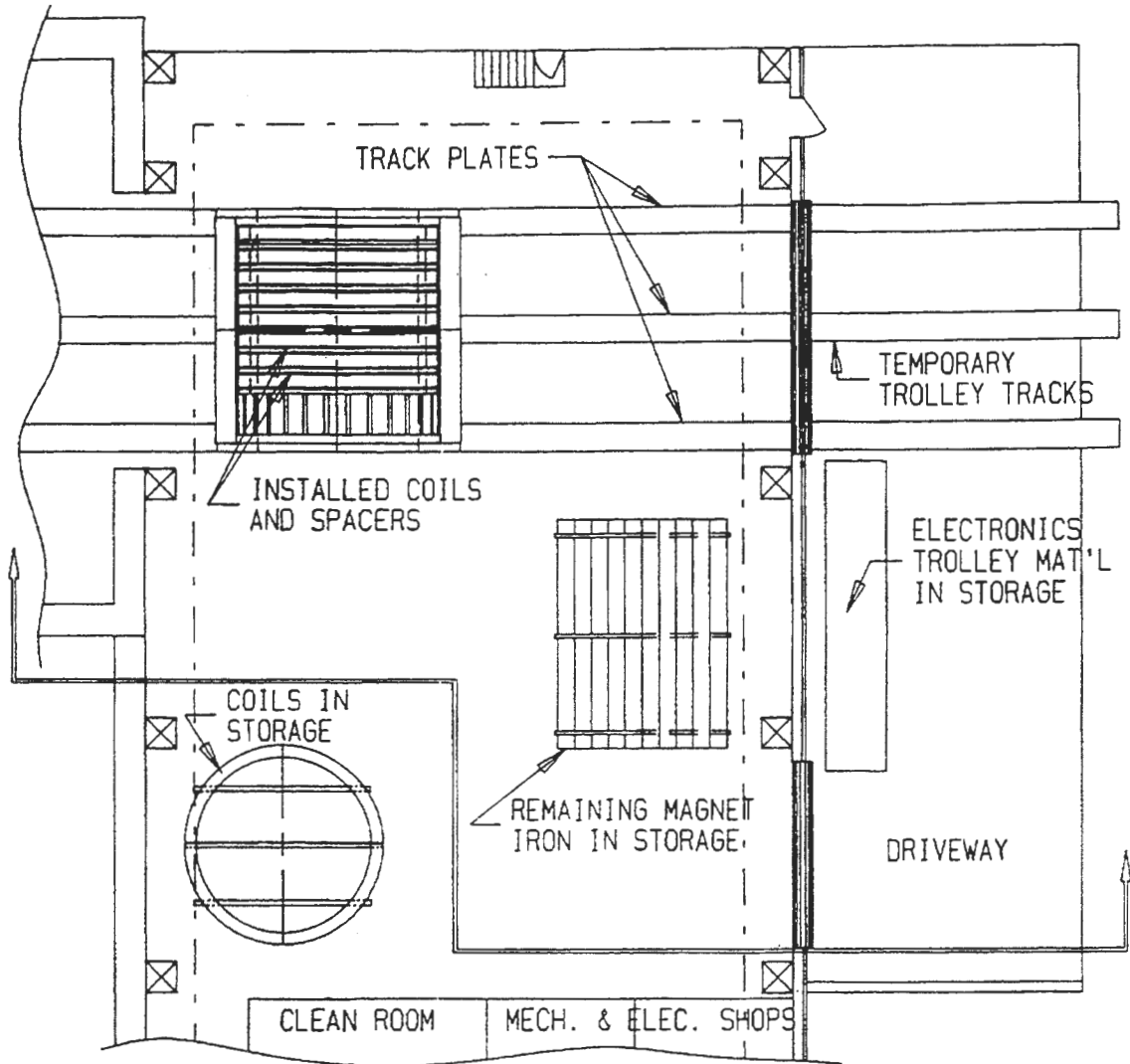


Figure 5-6 Installation of End Return Rings

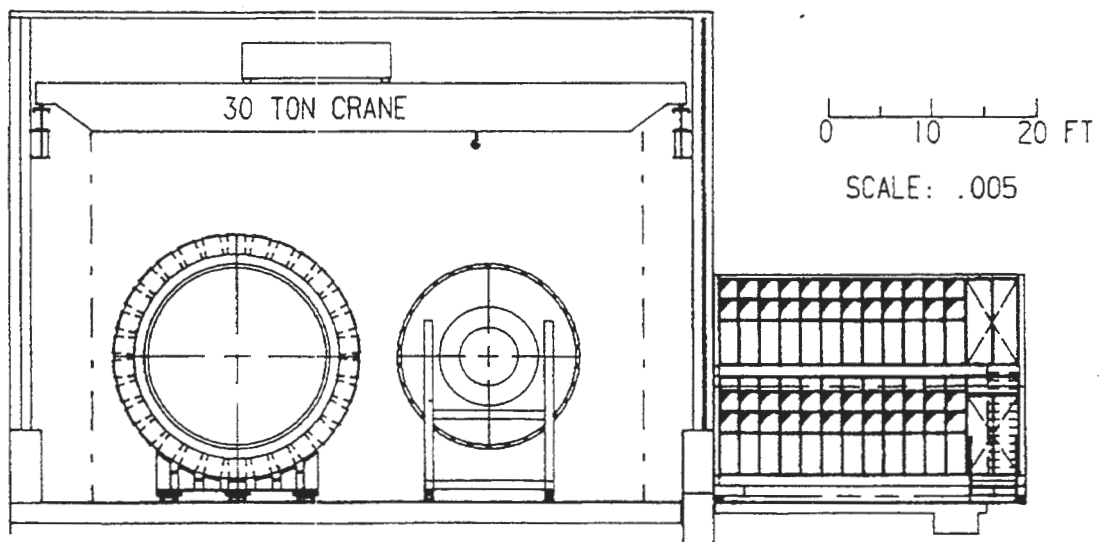
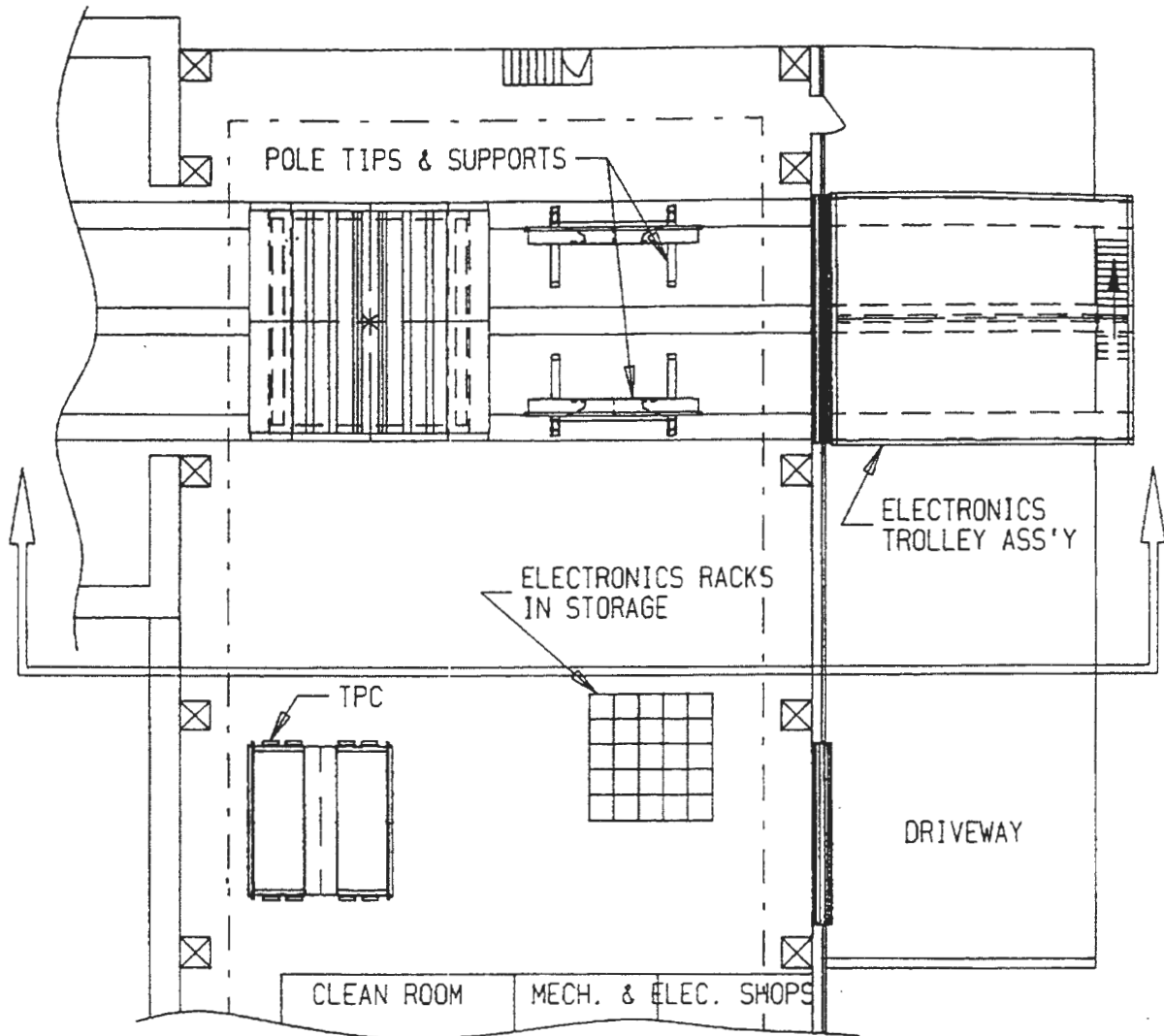


Figure 5-7 Front Elevation with End Rings Installed

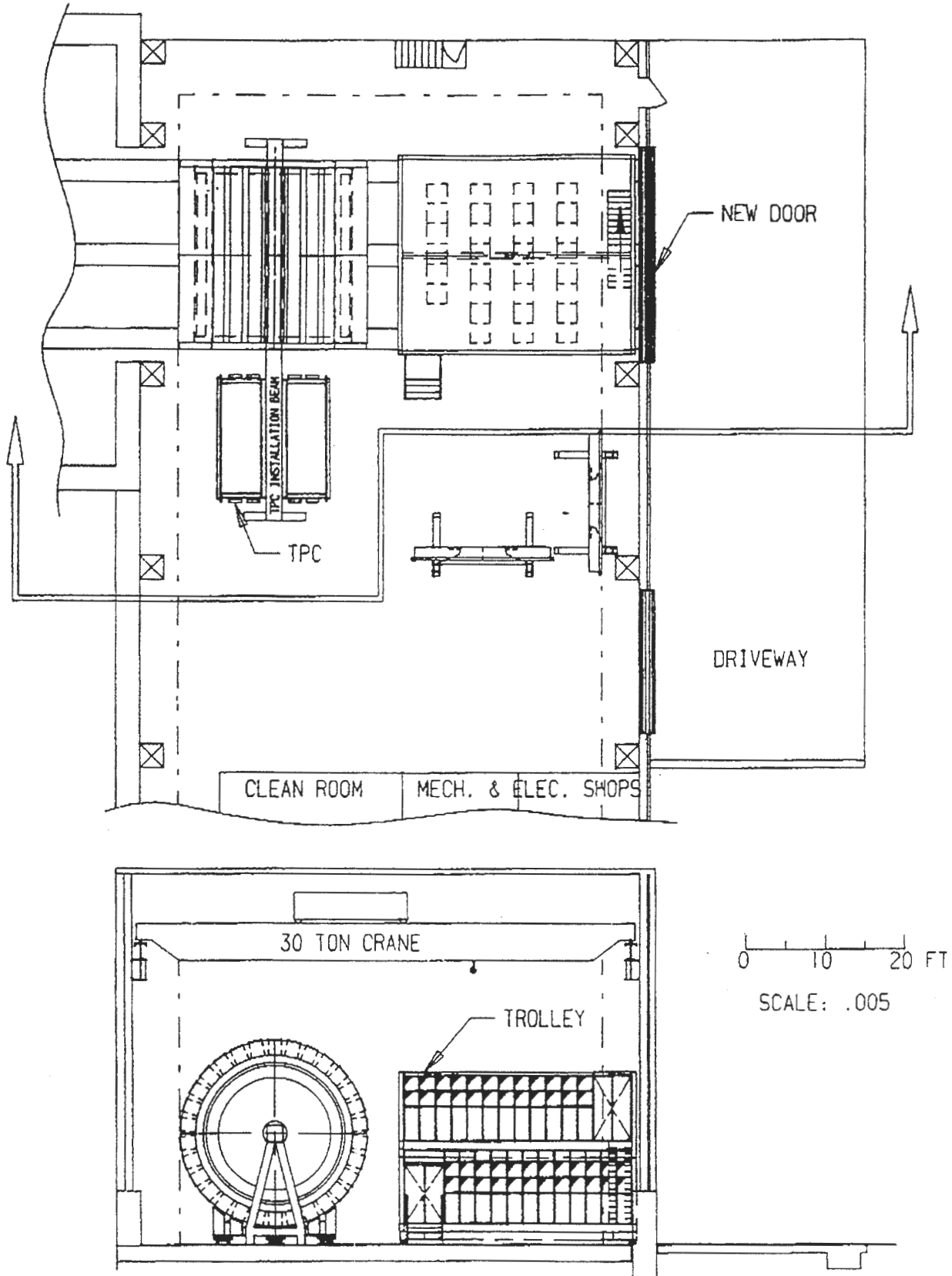


Figure 5-8

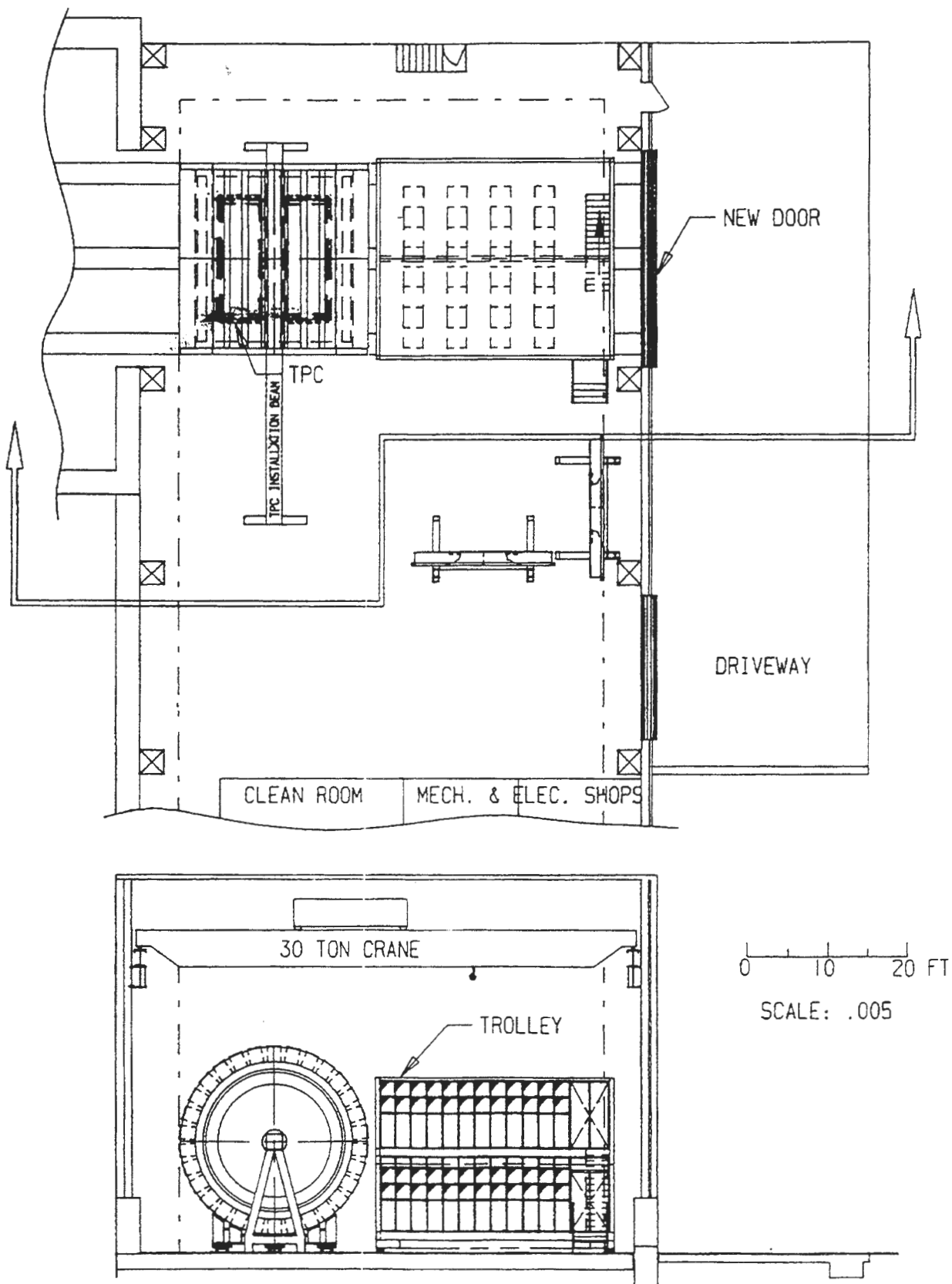


Figure 5-9

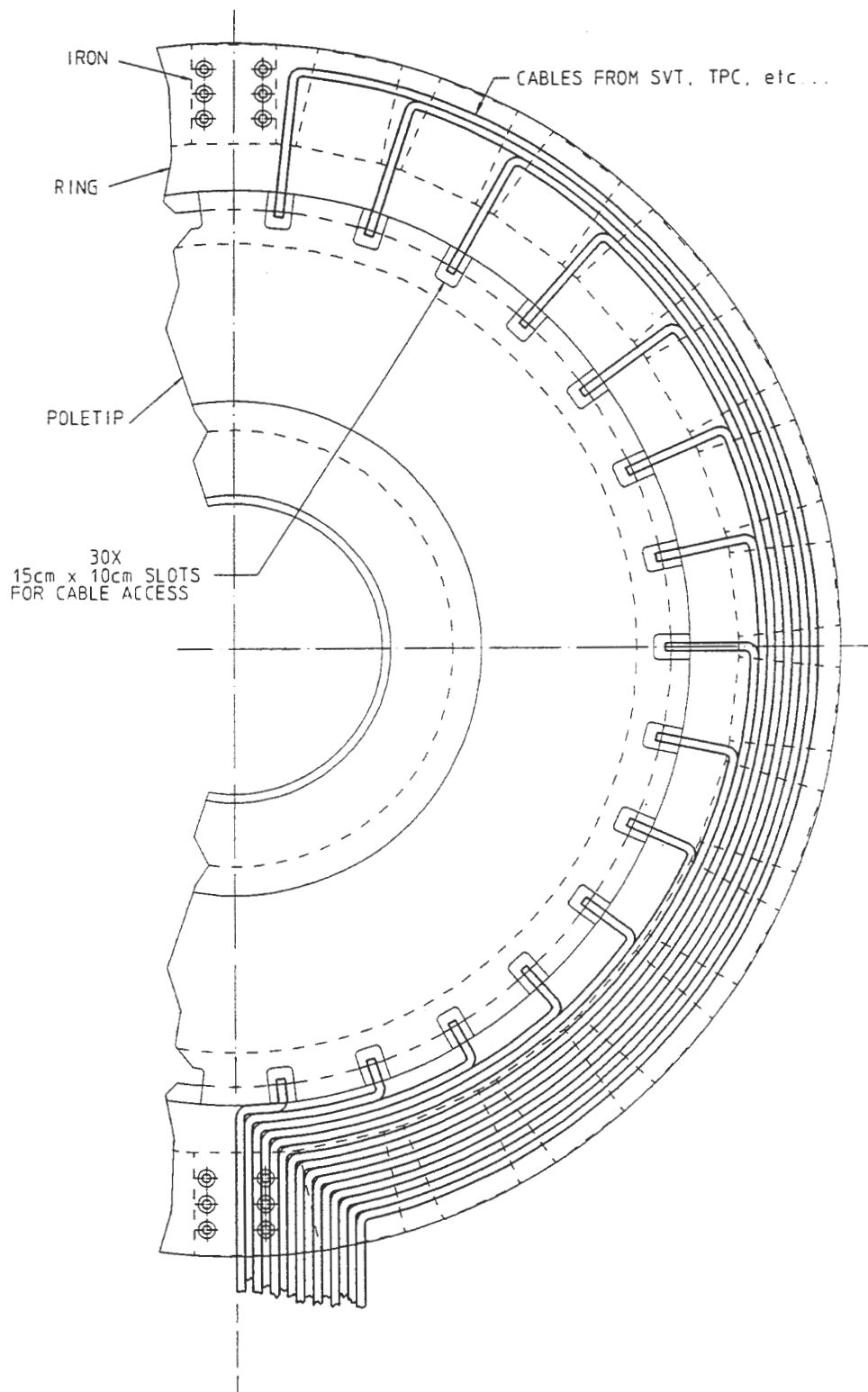


Figure 5-10 Wide Angle Hall, as presently built, plan view.

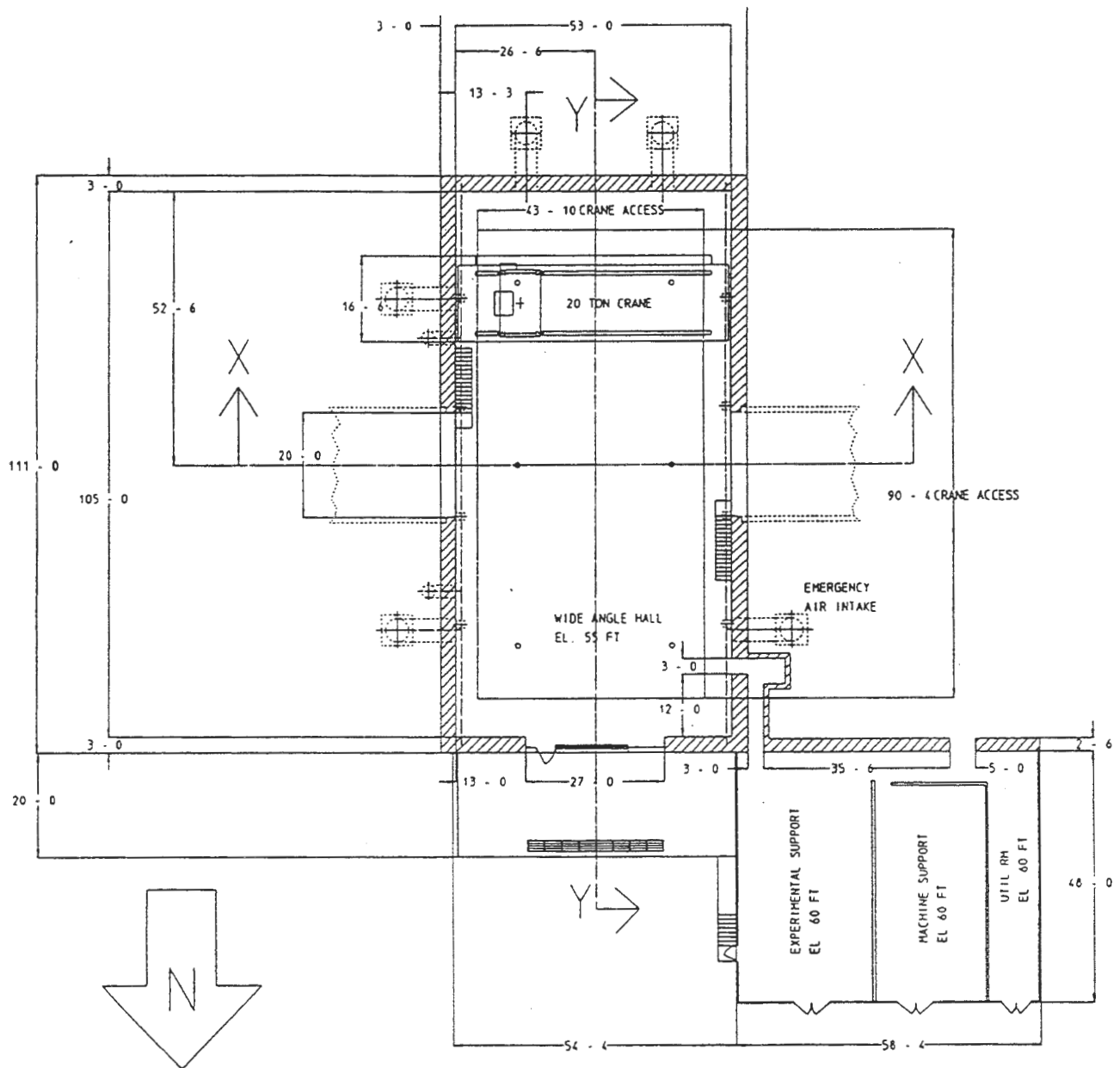


Figure 5-11 Wide Angle Hall, as presently built, elevation view.

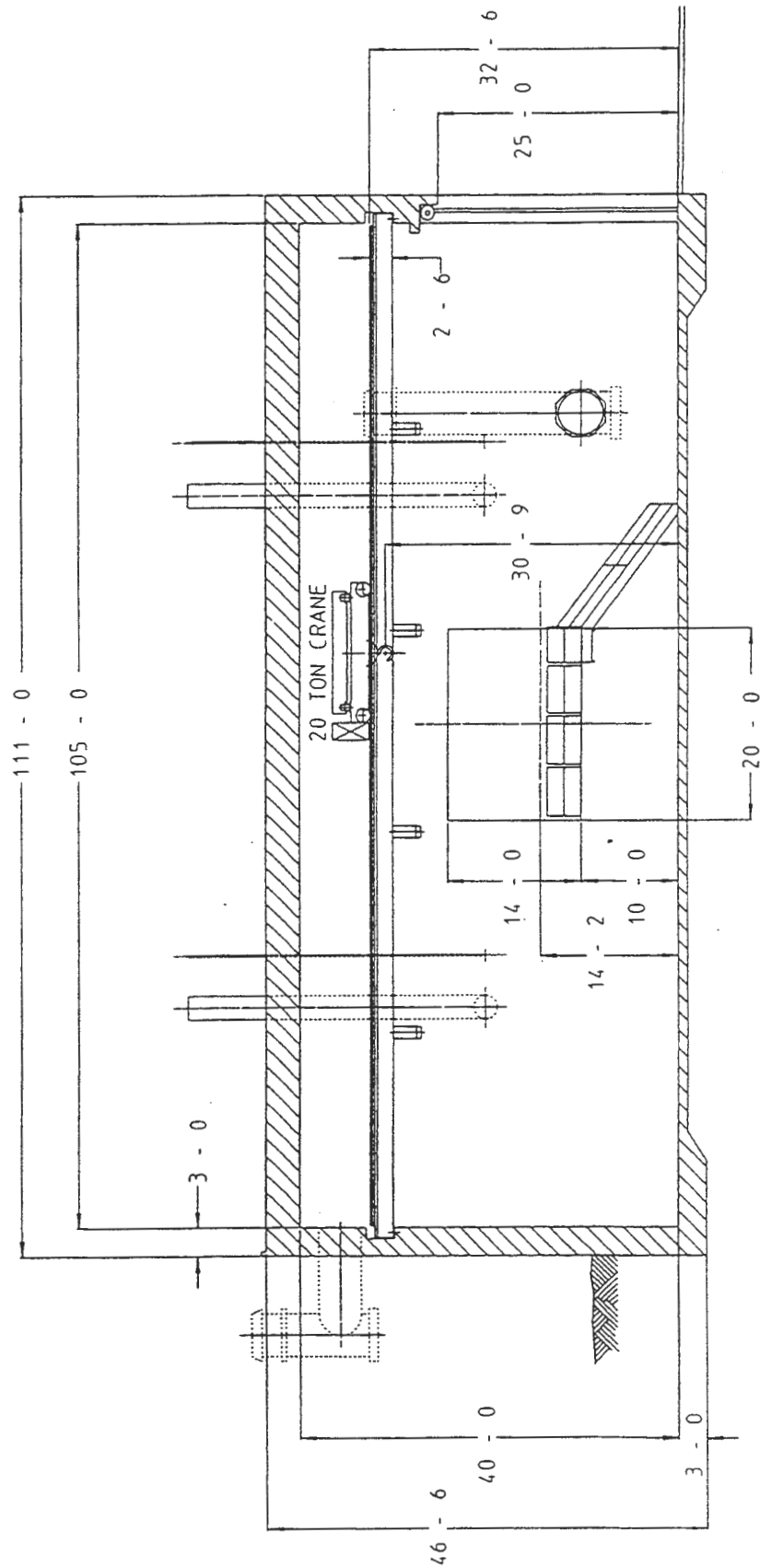


Figure 5-12 Electronics Trolley, front elevation

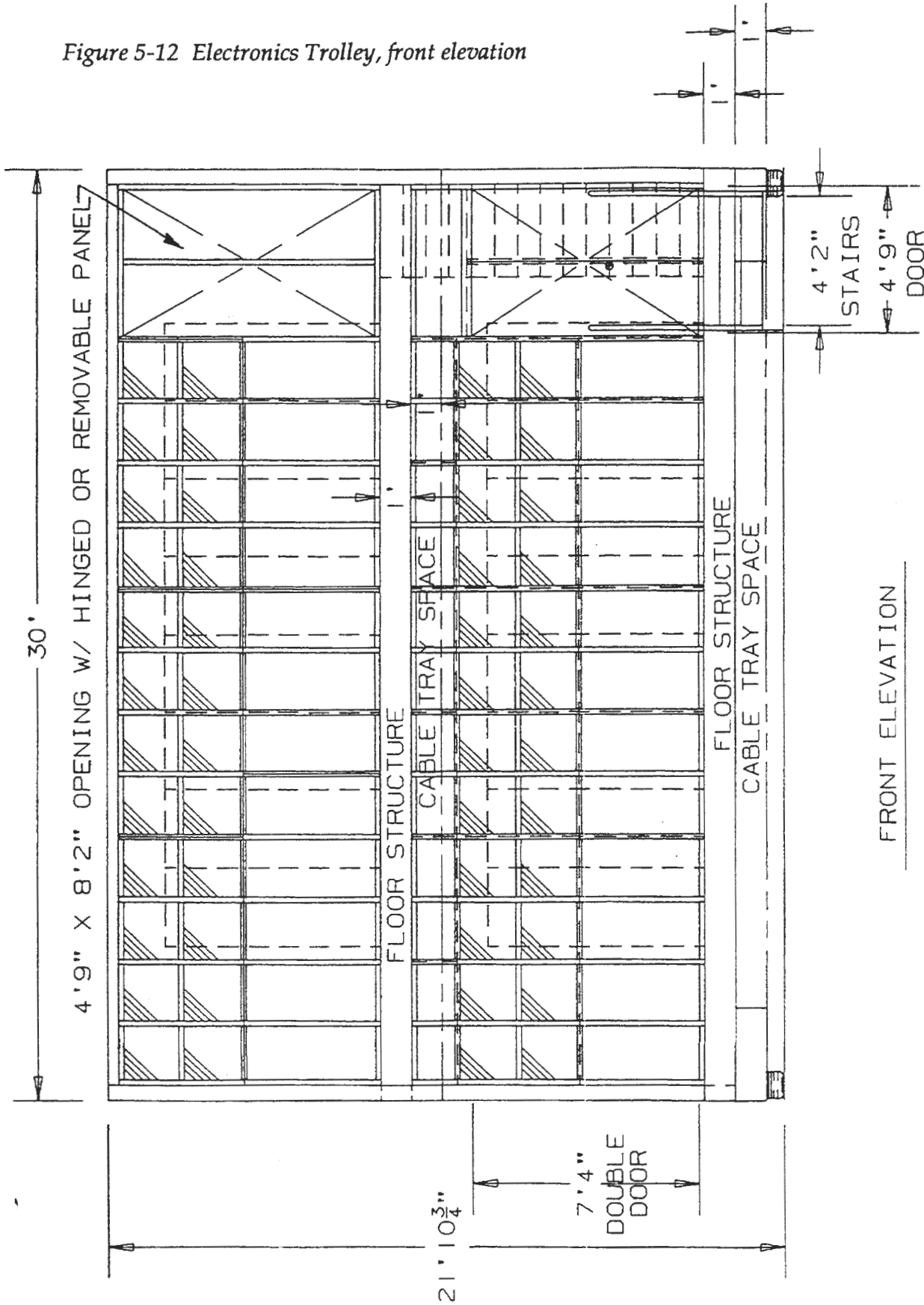
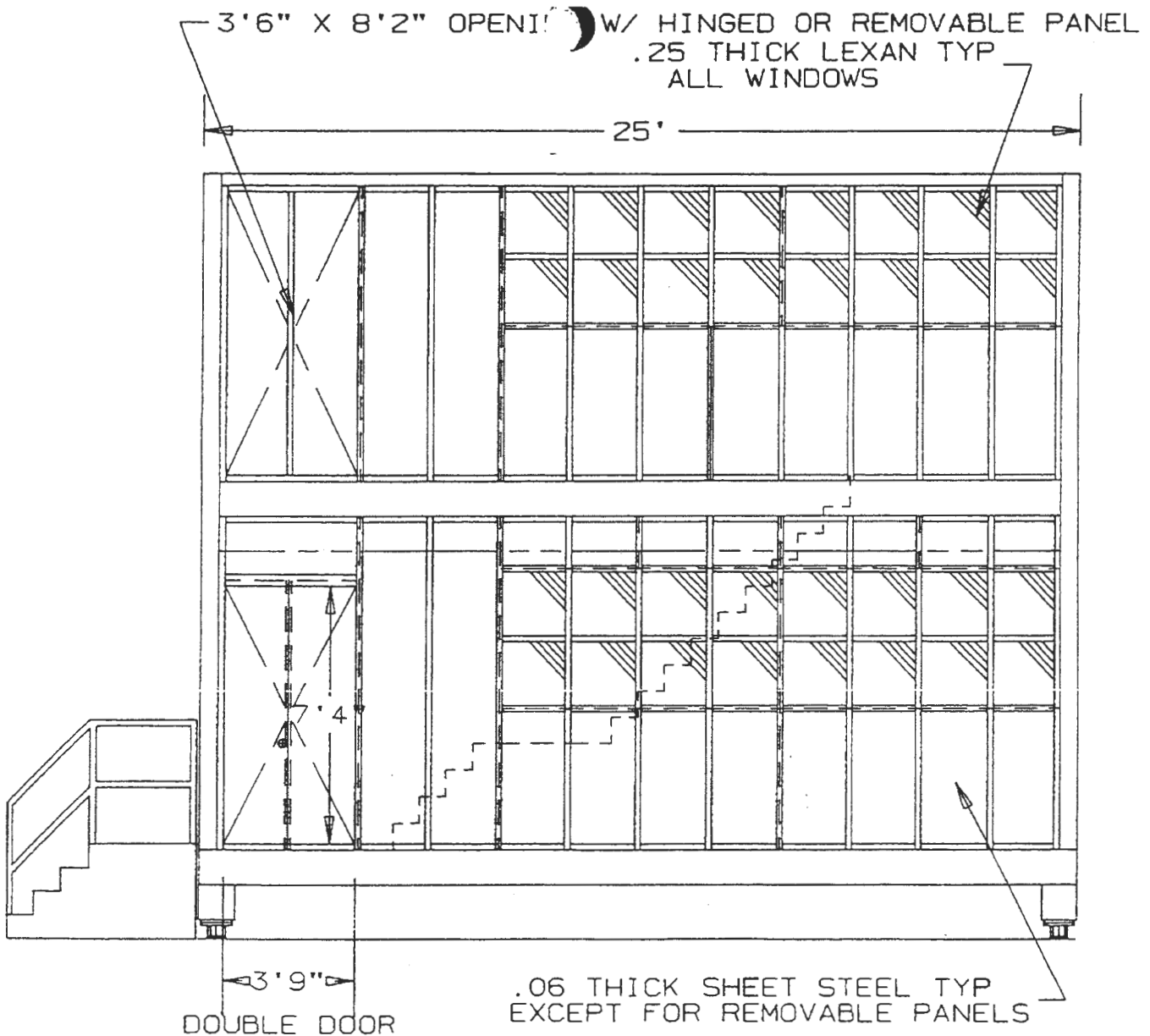
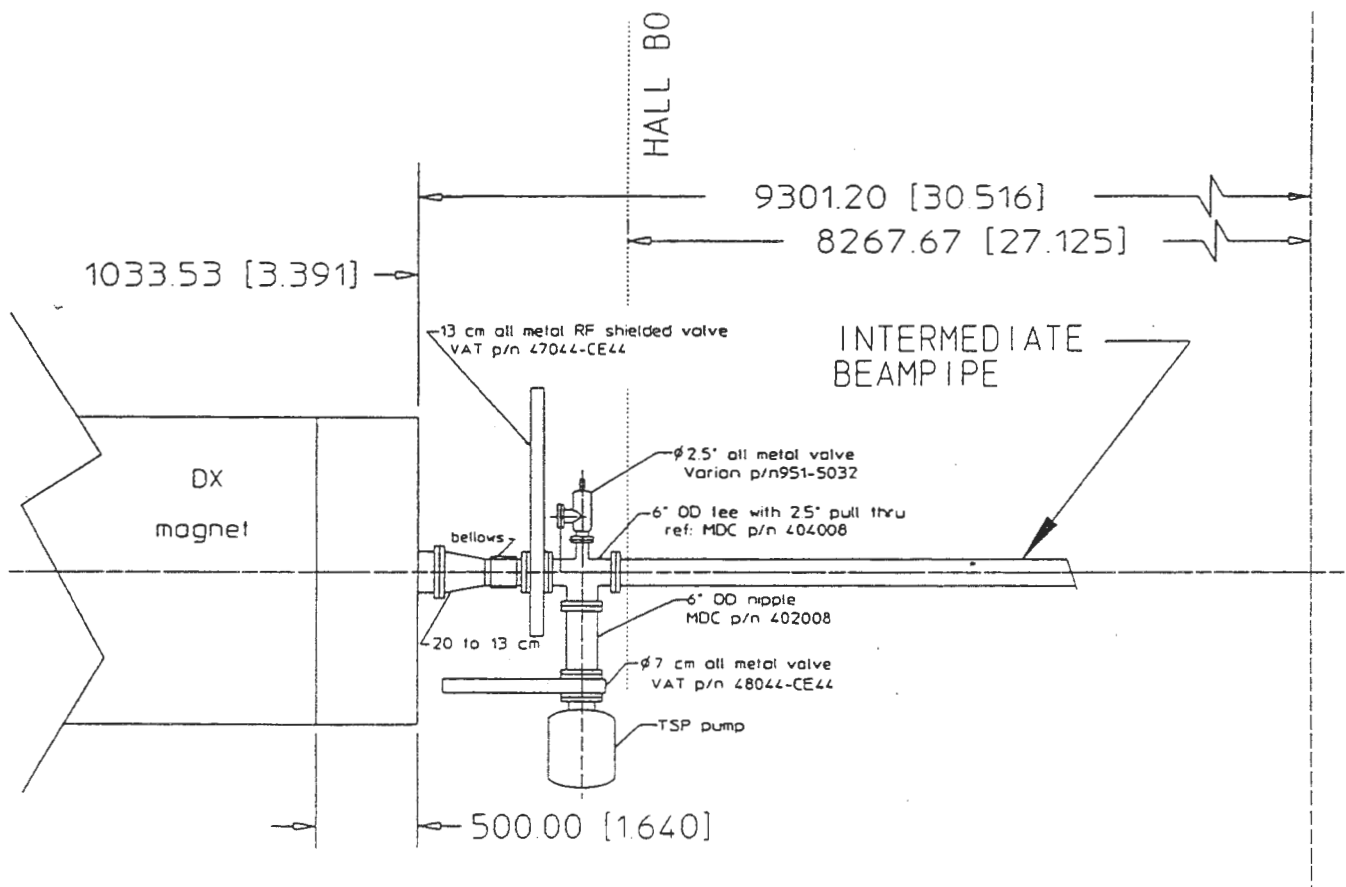


Figure 5-13 Electronics Trolley, right side elevation.



RIGHT SIDE ELEVATION

Figure 5-14 RHIC vacuum equipment, at each end of beampipe.



DIMENSIONS ARE IN MILLIMETERS [FEET]

6. Facility Requirements

The detector facilities requirements are derived from the specific subsystem needs and the overall detector integration conventional requirements. The following is a list of the facility requirements:

- Additional Buildings
- Electrical Utilities
- Computing Facility
- Mechanical Utilities
- Detector Physical Access System
- Area Shops

The interfaces between facilities provided by RHIC and facilities provided by STAR are presented at the end of this chapter.

6.A. Additional Buildings

The STAR experiment has the following building requirements:

- New assembly building
- Upgrades to the existing Wide Angle Hall
- Larger operation/DAQ building
- Gas mixing house and gas bottles shed
- Magnet power supply building
- A movable trolley to house the electronics racks

The proposed assembly building discussed in Chapter 5 needs a usable floor width, in the North/South direction, of at least 60 feet in order to accommodate the detector and its electronics trolley, as shown in Figure 5.3. This allows the detector to be fully cabled and tested inside the assembly hall before moving it into the wide angle hall. The proposed assembly building length of 120 ft is based on the space required to assemble the detector in the sequence described in Chapter 5, keeping in mind the assembly hall will also be used for steel lay-down and assembly, storage of lifting fixtures, pipes, cables, electronics racks, etc. as they arrive. It will also be used for minor subassembly, modification and repair of various items as they are fitted to the detector. The assembly area also includes a clean room for TPC sector and SVT work.

Preliminary crane capacity requirements in the assembly building are as follows: It will be necessary to have two separate bridge cranes, with the main rails for the bridges running along the length of the hall. This allows accurate positioning of long, large, components such as the barrel return iron segments, and TPC installation beam(s), without

building specialized lifting fixtures. This will likely allow lower capacity (30 tons per bridge) cranes to be used.

The existing Wide Angle Hall (WAH) will require some upgrades to facilitate housing the STAR detector. The floor of the WAH must be capable of supporting the 1,200 tons detector, and the doorway may have to be enlarged to its maximum permissible dimensions to insure that the fully cabled detector can pass through it.

The existing DAQ building attached to the WAH is too small for an experiment the size of STAR. As discussed below in the computing facility requirements section, an addition to the building, 50 ft by 50, ft is proposed. Figure 6.1 shows a preliminary layout of the DAQ building interior.

A separate gas mixing house is required to mix the TPC gas. Because one of the components of the gas mixture (methane) is flammable, the gas house needs to have reasonable temperature control, an explosive gas detection system, an emergency ventilation system and wide walk ways. Near the gas house there should be a storage shed for flammable liquids. The shed should have a floor above grade with ramps to the mixing house.

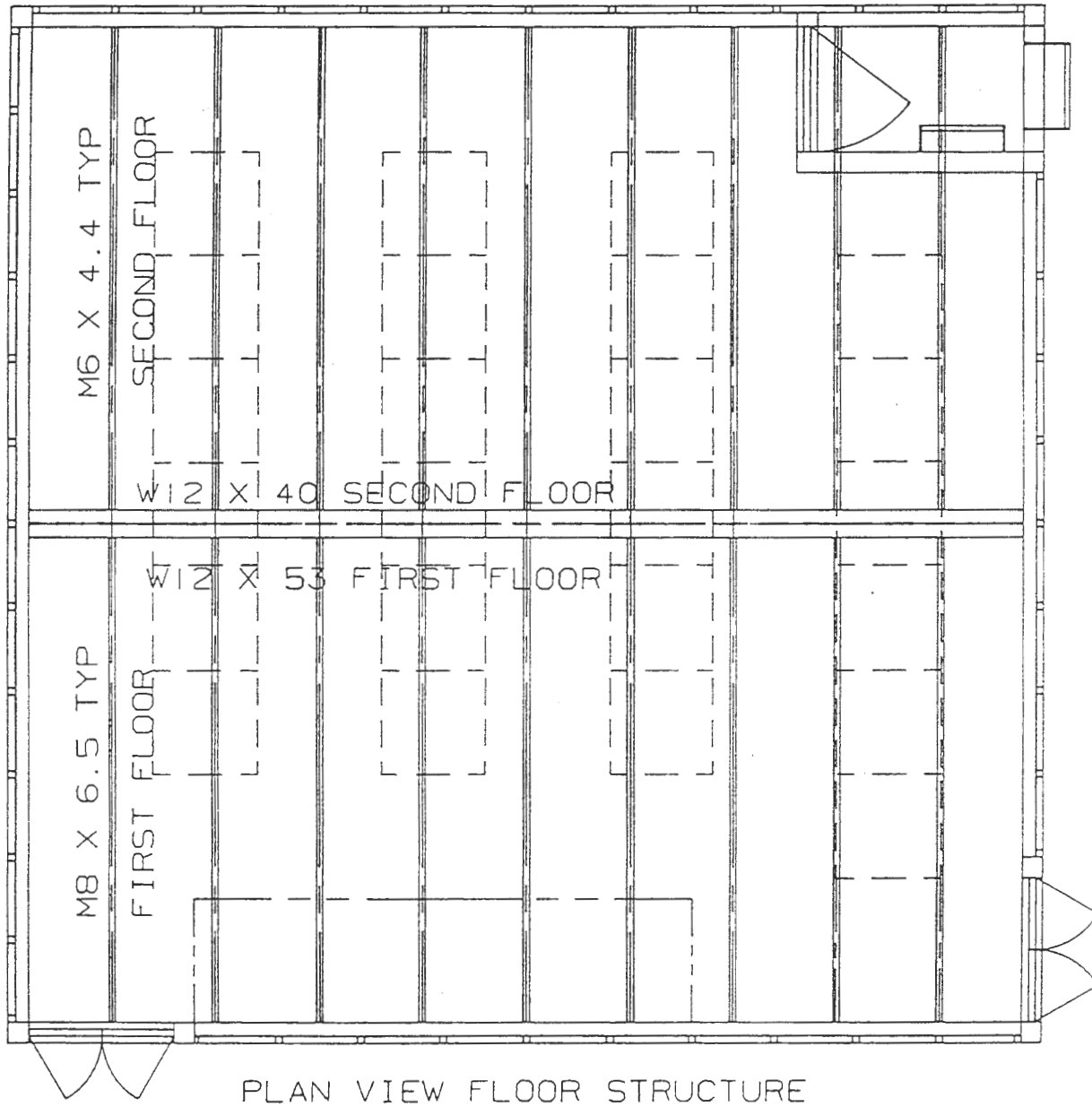
As currently envisioned, the warm solenoid magnet requires 2.2 MW power supply. A building is required to house the power supply and its control system. The building should have fire protection and ventilation systems.

The electronics trolley is required to house electronics racks that must be located near the detector. The trolley is attached to the detector and is placed on rollers to facilitate its movement between the two halls. The trolley is two stories high (the height is limited by the height of the door between the assembly building and WAH) and is sized to house approximately 40 racks, each rack is 24 in W x 30 in D x 7 ft H. Approximately, 3 feet of space will be available in the front and rear of each rack. The top floor of the electronics trolley will also be used for other auxiliary equipment such as the TPC chillers, and electronics test equipment.

Figures 6.1 and 6.2 show plan and side views of the electronics trolley. Access to the first floor is provided at two separate locations. Stairs to the second floor, suitable for personnel and light equipment, are located inside the trolley. There is also a second set of stairs for an emergency exit. The outside panels of the second floor are designed for easy removal to facilitate delivery and installation of large equipment such as racks.

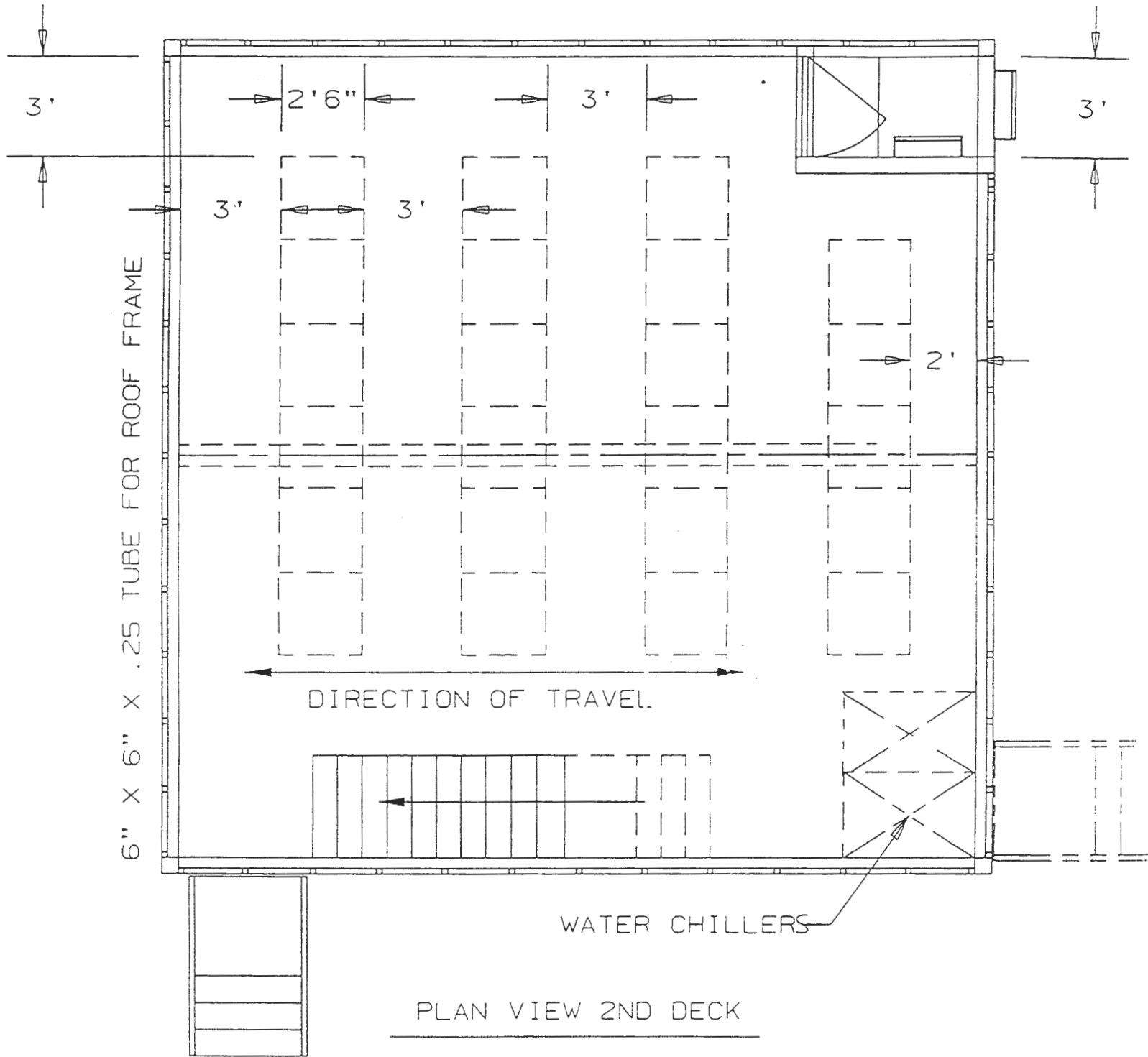
Figure 6.1 Plan and side view of electronics trolley, first floor.

TUBE 12 X 8 X .375 AT BASE AND 12 X 6 X .25 AT 2ND LEVEL



PLAN VIEW FLOOR STRUCTURE
FIRST FLOOR

Figure 6.2 Plan and side view of electronics trolley, second floor.



6.B. Electrical Conventional Systems

As mentioned in Chapter 5, the objectives of Electrical Conventional Systems are as follows:

- To provide the necessary AC power to run the instrumentation for the various detectors and sub-systems of the STAR experiments. This includes the requirements for future upgrades.
- To provide power for the magnet
- To provide a system for carrying signal and DC power cables between the detector and the electronic instrumentation.
- To identify and support issues that are common to the various sub-systems.
- To support the mechanical engineering effort on issues that are relevant to electrical integration.
- To interface with RHIC/BNL on issues common to the various sub-systems.

Power will be provided by RHIC as Facility Electrical Power (FEP), and Experimental Electrical Power (EEP). FEP is defined as the supply network extending from the main feeder lines to main distribution panels and wall outlets. This will be provided by RHIC/BNL. EEP is defined as the supply network extending from the main distribution panels and wall outlets to the electronic instrumentation used by the STAR sub-systems.

The requirements described are for a fully implemented Detector that includes all the future upgrades described in this CDR.

6.B.1. Magnet Electrical Power

The Present copper coil design of the STAR solenoid magnet requires that RHIC provide 2.5 MW of 13.8 KV power at the transformer level. The magnet power should be isolated from the facility power. Power distribution from the transformer to the power supply building and the magnet will be performed by STAR.

6.B.2 Facility Electrical Power

6.B.2.a. General Description

The Facility of the STAR system that will require AC power consist of the following:

- An Assembly room where Detector is assembled.
- The Wide Angle Hall where operations are conducted around the beamline.
- The Operations room. This room houses racks for subsystem

instrumentation, computers, workstations and tape loggers for the DAQ sub-system.

- The computer room. This room houses the computers, workstations, and the tape loggers for On-line Computing. In addition the control and monitoring workstations reside here.
- Electronic and Mechanical shops. These shops are used to perform any day to day calibration, testing and repairs of subsystem components, as necessary.
- A "clean" room. This is a nominally clean area for the repair and testing of the Pad planes used by the TPC subsystem. No special filter system is used to control the size and density of dust particles.

6.B.2.b. Types and Distribution of FEP

Utility power is used for general lighting and power outlets in the facility as described above. In addition power will be used for the following:

- Lighting within the shielded area that contains the trolley.
- Chillers, Fans, and Water pumps for the cooling system used in the detector, and the equipment racks.
- The Air conditioning system
- Hydraulic equipment used to move the Detector and the trolley between the Assembly room and the Wide Angle Hall.
- Cranes used for lifting components of the detector.
- Welding equipment, drill presses and other equipment used in the mechanical shops.
- Emergency power. This power is used to light up exitways and support a fire alarm system. The shielded area will also be illuminated by emergency power.
- Clean power for the Experiment Electrical Power. This power is brought to main breakers in the Assembly room for distribution as EEP.

6.B.3. Experimental Electrical Power

6.B.3.a. General Description

The STAR detector system consists of the following:

- The magnet power and control system
- The detector subsystems with signal processing and control electronics
- Systems for data acquisition, processing, and bulk storage
- A system for data analysis
- A monitoring and interlock system
- Calibration, drift gas control, and cooling systems.

These systems are located in the detector, a trolley that is attached to the detector, and the operations and control rooms. In addition, the detector and the trolley must be operated in two locations viz., the experimental hall and the

assembly area.

Power is required to be routed from the main breaker panels to electronic instrumentation which is situated in racks or desk-tops. It is also required that the signals are carried between the systems described above.

6.B.3.b. Types of AC Power

There are four types of power required to be distributed.

- **Isolated clean power.** This power is used for driving the electronics of the detector sub-systems only. It is isolated from the rest of the power supply system. Aside from the magnet power supply, it uses the bulk of the power used for the STAR system.
- **Filtered Power.** This power is used for computers, workstations and electronic workbenches. It is derived from the clean power by passing it through a filter and surge suppresser.
- **Uninterrupted power.** This power is derived from the clean power. It provides a temporary backup for the few critical areas that exist. This power is generated from a battery back-up UPS unit. An example is the power for generating the High Voltage of the Field Cage, which needs to be allowed to be ramped down in a controlled manner.
- **Emergency power.** This power is used for emergency lighting within the detector during assembly and repairs, and for a few miscellaneous areas.

6.B.4. Power Distribution

6.B.4.a. AC Power

Basic Scheme

The main breakers for each type of power are located in the Assembly room. Power is provided on 208 V , and 120 V, down to a minimum current rating of 20A. The requirements by type are shown in Table 6-1. The requirements by sub-system are shown in Table 6-2. Figures 6-2 and 6-3 show the distribution of Clean and Filtered Power.

Isolated Clean Power

This power is taken from the main breaker for clean power and routed to the trolley and the operations room.

Distribution to trolley

Power to the trolley is switched between two main breakers in the assembly and the experimental halls, so that only one area can receive power at a time. The power switch has three selections: Area 1, OFF, and Area 2. The power from the main breaker to the trolley is disconnected by setting the switch to the OFF position when the trolley has to be moved. The trolley is then moved to its new destination and bolted on to the power cable coming from the other breaker, after which the switch is moved to select the corresponding area.

The responsibility for providing the switched power to the secondary main breakers is with RHIC/BNL. A total of 400 KW of power is provided at 480 VAC. This power allows for a margin of 20% in estimating baseline and upgrade sub-system needs. Another 15% is allocated for future modifications to sub-system design parameters.

Distribution within trolley

Power from the main breaker is connected up to the trolley and taken to a distribution panel in the trolley. Power is then transformed to 120/208 V from 480 VAC. This power is further distributed by internal power panels.

The trolley has two levels, with plans for four rows of eight racks on each level. Each row has its own feeder circuit, and power cables are carried to them on wireways. The power that arrives at a row of racks is then taken to breakers rated at 30 A, 208V, and 20 A, 120 V before being further distributed to each individual rack. The maximum power allowed to be consumed in a rack is 10 KW.

The bulk of the power (225 KVA) is used by supplies and instruments that run on 120 V. Power of 175 KVA is provided at 208V.

Power to the Operations Room

The operations room will have two rows of eight racks which will be supplied with clean power. 40 KW of clean power will be carried in wireways, from the main breaker in the assembly hall. A distribution panel with four feeder circuits rated at 20 A is used to provide power on 208 V and 120 V circuits. Transformers will be used as necessary for 480 V to 120/208 V conversion.

Filtered Power

This power is taken to the operations room, the computer room, the clean room and electronics shop.

Operations and computer rooms

Power from the main breaker in the assembly hall is taken to a surge suppresser and then to a distribution panel in each of the operations and computer rooms. Power is then delivered to 120 V and 208 V outlets, using IMT conduit. The distribution panels each have a 20 KW main breaker with 6 feeder circuits rated at 20 A.

A total of 80 KW of power is provided. This will run 19 workstations, a computer for the on-line system, a DAQ computer, two tape loggers, a FAX, a copying machine, and six 20A circuits for additional needs.

Electronics shop and clean room

Power from the main breaker in the assembly hall is taken to a surge suppresser and then to a distribution panel in each of the operations and computer rooms. Power is delivered to 120 V and 208 V outlets, using IMT conduit.

The 120 V and 208 V outlets in the clean room and the electric shop receive their power from a common filtered distribution point. A total of 10 KVA is provided for each voltage rating.

Uninterrupted Power

This power is provided to any critical electronics that cannot accept any interruption. It is derived from the clean power, and will be accommodated within a rack. 1 KVA for one hour will be provided in the trolley to power to the Field Cage of the TPC in the event clean power is lost. An additional 2.5 KVA for 2 hours is provided for the equipment in the operations room.

Emergency Power

This power is used to provide lighting within the detector during assembly or repair work. The responsibility for a general emergency system is the responsibility of RHIC/BNL.

DC Power

Types & Distribution of DC Power (carried outside the racks)

This power is produced by various types of DC power supplies.

Low Voltage Power

This power is taken from the trolley racks to the detector. It is carried in 6 AWG cables within wireways that are separate from the signal cables. This power is used to run the electronics of the TPC, SVT, and other subsystems. The voltage is less than 10 V.

High voltage power

This power is taken from the trolley racks to the detector to run elements of the TPC and SVT, and the Photomultiplier tubes of the detectors. HV power of up to 4 KV for the PMTs is carried on co-axial cables terminated in SHV connectors. The Field Cage of the TPC requires 30 KV, and is carried on cables suitably rated to carry this High Voltage.

6.B.5. Signal Distribution

6.B.5.a. Types and Distribution of DC Power (carried outside the racks)

Signals are carried between the detector and trolley, the detector and the operations room via the trolley, and between the trolley and the operations room.

Detector to Trolley

Signals are required to be transported between the detector, the trolley racks, the operations and the control rooms, using wireways. The detector with the trolley may be moved between the assembly room and the experimental hall. There will be approximately 4000 copper conductors going between the ends of detector and the trolley. These are round multiconductor shielded cables, or co-axial cables of various voltage types (SHV, UHV, or RG58/U). These conductors will go to the TPC, SVT, and CTB/TOF subsystems.

There will also be 14,000 fiber optic cables from the ends going between the above mentioned sub-systems and trolley. These are also in multifiber cables. The Photomultiplier tube (PMT) of the EMC and the Shower surround the barrel return iron. The signals from the PMTs are carried from there to the trolley on 540 fiber optic cables. Power to these PMTs are carried on 480 copper conductors.

All cables between the trolley and the detector are carried in wireways. Signal cables are routed to the racks from within a sub-floor of each deck of the trolley.

The XTPC requires 4048 copper conductors for power and signals. The number of fiber optic conductors is 448.

Trolley to Operations Room

Signal cables to the operations room will arrive there from either of the two positions of the trolley and detector (namely, the assembly area or the experimental hall). The method for transporting these signals is to use a cable carrier made up of links that permit it to be flexed in a controlled manner. This carrier would be guided in a trough and supported on ladder trays.

The signals are the data and control signals between the sub-systems and the DAQ, and are carried on 2600 fibers.

Racks

Rack locations in the trolley are allocated to the sub-systems in such a way that the high power supply cables are nearest to the detector, so as to minimize cable losses. An effort will be made to keep the racks for each sub-system grouped together.

6.B.6. Safety Grounding

A grounding grid for safety is provided throughout the facility. The trolley will be connected to the ground grid at both locations. This will be accomplished by bolting a cable from the trolley to a rod connected to the ground grid, which would exist at the destination points of the trolley. Grounding will be applied to Equipment and Raceways throughout.

6.B.7. Electrical Interface

6.B.7.a Interface with Sub-systems

The interface between electrical integration and the sub-systems is as follows:

- AC power will be distributed down to a minimum rating of 20A, and 120 V or 208 V. Breakers and power cables used below this rating will be the responsibility of the sub-systems.
- Signals cables will be installed between the detectors to their destinations at the rack level in the trolley or the operations and control rooms. Connections within the racks will be the responsibility of the sub-systems.
- The wireways and supports for transporting the power and signal cables to their destinations will be provided. It is the responsibility of the sub-systems to provide the signal cables and connectors.
- The DC power for the solenoid is not part of the integration effort. It is the responsibility of the Magnet sub-system to carry the power to the magnet.

6.C. Computing Facility Requirements

Table 6-3 Design Parameters for STAR event analysis

Raw Data Size	
TPC (140k X 512 X 10 bits)	90 MB
SVT (72k X 256 X 10 bits)	23 MB
Zero Suppressed Data Size	
TPC (10% occupancy)	15 MB
SVT (1% occupancy)	3 MB
Recording (Tape limited) rate	1 Hz
Estimated Reconstruction CPU time per event	5 Gflop-seconds
# tracks/event	5000
# 4-byte words/track in DST	10
DST event size	0.2 MB
Data set	
running time	2000 hours
# events	7.20E+06
raw data size	108 TB
DST size	1.44 TB
Data access bandwidth	
processing raw data (at record rate)	15 MB/sec
search data set DST in 24 hours	17 MB/sec
search 10^5 DST events/hour	5.56 MB/sec
Storage requirements	
long term, archival for raw data	270 TB/year
rapid access for DST data	3.6 TB/year

The scale of computing required for timely analysis of a 1 Hz central Au-Au event rate is estimated to be 5 Gflops. Since this will involve processing thousands of equivalent events (both real data and Monte Carlo simulations) the computing is efficiently partitioned as a farm of inexpensive RISC processors. At the present time 20 Mflop workstations are common, so that 250 such processors would be needed. These nodes would be networked to three or four event-server machines which would have high speed tape I/O and large disks. The need for computation other than the analysis of raw event data, including especially event simulation, and the needs of other experiments sharing the off-line facility could multiply the size by a factor of five or ten. By 1996, when acquisition of the facility should take place, individual nodes should be substantially more powerful so fewer would be required.

Equally as important as the magnitude of the processor power required is the need to move and manage a few times 10^{14} bytes of raw data per year and to provide the databases and access to manage the processed data and extract the physics results. The raw data recording medium will be determined by the more

critical rate requirements of the DAQ system. The data handling will mean massive amounts of conventional disk storage and 8 mm tape technology as well as newer storage media such as optical disks.

The aggregate data access bandwidth required for off-line physics analysis is greater than the requirement for online recording. The off-line system should be capable of supporting several physicists searching the central DST database at the rate of 10^5 events/hour. This sets the scale of the bandwidth at tens of MB/sec.

It is presently envisioned that a team of approximately 15 people will staff the STAR detector during running periods. These people will be responsible for monitoring the operation of the detector, the control and monitoring of data acquisition, and for quality assurance of the data. To accommodate these functions it is thought that approximately one workstation per person will be required in addition to a small number of electronics racks and communications equipment. Given these assumptions, the amount of space required is estimated to be approximately 3,000 sq. ft. at the detector site. The HVAC requirement to support these operations has not yet been calculated.

Given the experience of CDF and SLD, it will also be necessary to provide workspace for as many as 50 other physicists who travel to RHIC to participate during running periods. A conference room adequate for group meetings required to distribute information, results, and run plans will also be necessary. At present, the space necessary to accommodate these additional people has not been identified and requires additional discussion with RHIC/BNL management.

6.D. Mechanical Utility Requirements

The mechanical utility system for STAR consists of the following subsystems:

- Modified Chilled Water (MCHW)
- Industrial Cooling water (ICW)
- Dry, Conditioned Air.

Low Conductivity Water system (LCW) which is required for the magnet system is discussed in Chapter 4.

6.D.1. Modified Chilled Water System

The MCHW system is required to cool electronics (including upgrades TOC) at the following locations :

1. SVT, TOF and TPC electronics (other than readout cards) inside the

- detector
2. PMT's outside the return iron
 3. XTPC electronics
 4. Electronics racks on the house
 5. Electronics racks in the DAQ/Operation building

The Electronics racks are generally cooled by circulated chilled air which is chilled by the MCHW. TPC electronics on the ROC inside the detector are cooled by water chilled from separate local chillers for better temperature control. The chiller's condensers are cooled by industrial cooling water which is supplied by STAR conventional systems (WBS 2.4.9)

6.D.1.a. MCHW System Performance Specifications

Detailed MCHW requirements by location and subsystem are presented in Table 6.4. The cooling requirements include subsystem upgrades.

Table 6.4

Location	Capacity	T _{in}	T _{out}	Flow, gpm	P max
Detector electronics	56 kW	60°F	70°F	38	100 psi
EMC PMT's	62 KW	60°F	70°F	42	100 psi
External TPC	12 kW	60°F	70°F	8	50 psi
Electronics trolley	166 kW	60°F	70°F	113	100 psi
DAQ building	11 kW	60°F	70°F	7	100 psi
Total	307 KW	60°F	70°F	209 gpm	

The main chilled water will be produced by RHIC/BNL. Supply and return manifolds will be located in the assembly building. STAR conventional systems is responsible for distributing the MCHW to subsystem distribution manifolds and to common distribution headers in the electronics trolley. MCHW distribution within each subsystem is the responsibility of the subsystems, and distribution to individual racks is responsibility of the electronics STAR conventional systems. Figure 6.4 shows the details of the MCHW distribution system.

6.D.2. Special HVAC System

For safety purposes, conditioned air will be circulated inside the detector at a rate of 15 air changes per hour or 150 CFM. This system is not

designed to remove any heat load. Its main purpose is to maintain uniform temperature and low humidity conditions inside the detector.

The conditioned air is introduced to the detector at the detector centerline from both ends. The air will circulate radially inside the detector space then will be exhausted to the hall through gaps between the cable ways. The detector supply vent is easily detachable to facilitate removing the detector end caps for routine service.

6.D.3. Industrial Cooling Water System

Readout TPC electronics inside the detector are cooled by chilled water produced by a local chiller provided by the TPC group. The system integration group provides the condensers of the chillers with cooling water.

ICW system specifications are:

Location	Capacity	T _{in}	T _{out}	Flow, gpm	Max P
TPC Chiller	40 KW	95°F	110°F	18	100 psi

6.E. Detector Physical Access System

An access system to enter the detector to perform routine services will be provided for in STAR conventional systems by the integration group. This system will consist of portable scaffolds, hydraulic or electric man lifts and ladders. A special climbing ladder will be constructed around the barrel return iron to facilitate the assembly and service of the EMC PMTs.

6.F. Shop Requirements

As the detector is built, many components/elements will need to be assembled, modified, repaired, re-fitted, etc. A mechanical shop located near or in the assembly building will be needed for this work. Similarly an electronics shop will be needed for ongoing work on the electronics. These are small shops, geared primarily for low-volume small fabrication/repair work. Each of these shops is estimated to require an area of approximately 400 sq. ft.

6.G. STAR Utility Interfaces with RHIC

The following is a preliminary list of general mechanical and electrical utility interfaces between RHIC's provided equipment and STAR equipment.:

6.G.1. Chilled Water System

RHIC will provide supply and return chilled water manifolds in the assembly building as shown in Figure 6-5. The system capacity is 400 KW at a supply temperature between 45-50 °F . The return temperature is expected to be 15°F higher. This system will exchange heat(via a water-to-water heat exchanger) with the close-loop modified chilled water system.

6.G.2. Industrial Cooling Water System

Supply and return manifolds of industrial cooling water are to be provided by RHIC in both the assembly and Wide Angle buildings as shown in Figure 6.5. The capacity of the system is 50 KW at 80-90°F supply temperature. The return temperature is expected to be 15°F higher.

6.G.3. Low Conductivity Water System

Low conductivity water (LCW) which is required for the solenoid magnet will be supplied by RHIC. LCW supply and return manifolds are required in both the WAH and the assembly building. The detailed specification of LCW production system is presented in a separate document.

6.G.4. HVAC System

RHIC will provide all STAR buildings with conditioned cooled air. The average building temperature should be kept at about 75°F with relative humidity below 55%. The ventilation system should be capable of maintaining a maximum temperature variation within each building of less than 5°F . The heat load of the HVAC system is mostly due to ambient temperature changes. The maximum heat load from STAR related equipment such as motors and machines is about 200 KW.

In addition to general building HVAC requirements, RHIC will provide the electronics trolley with the necessary ventilation supply line. The supply should be located in both the assembly and Wide Angle buildings. The trolley will return the air back to the halls where it is re-circulated by the main circulation fan. The heat load in the trolley is about 70 KW.

6.G.5. Building Safety System

RHIC is to equip all building, including the electronics trolley, with all required fire, gas, and electrical safety equipment needed to detect and mitigate potential hazards occurring inside the buildings.

6.G.6. Electrical System Interface with RHIC/BNL

The responsibilities for the electrical interface between STAR and RHIC/BNL is described as follows:

- STAR integration will specify the required AC power, describing the power rating for each type. It is the responsibility of RHIC/BNL to provide this power up to the main breakers as defined by STAR, and situate them as specified by STAR. STAR has the responsibility for distributing the power past this point.
- Facility Electrical Power including the mechanical and electrical shops, cranes, building lighting, etc. is considered to be the responsibility of the RHIC/BNL group. Emergency power and a building fire alarm system will also be the responsibility of RHIC/BNL.
- BNL will also provide a grounding grid for safety, according to specifications given by STAR.

6.G.6.a. Electric Power Specifications for RHIC/BNL

Experimental Electrical Power (EEP)

This power is provided in the Assembly room, the Operational and Computer rooms, the Clean room and the Electronic shops. The total power for EEP is 550 KVA @ 208 V. A breakdown of power distribution by room is shown in Table 6-5.

The interface for power distribution of Clean Power is shown in Fig. 6-8. RHIC/BNL will provide the 480 V/208 V transformer, the three position switch, and the two main breakers C1 and C 2.

Filtered Power is derived from Clean Power. Refer to Figure 6-6 for the interface. RHIC/BNL will provide power from the 480 V/208 V transformer up to the Surge suppressers in the Operations room, the Computer room and next to the Clean room. The exact locations for the placement of the equipment for AC power will be determined upon inspection, at a suitable time during the design phase.

Facility Electrical Power (FEP)

This power is provided throughout the facility as described below.

Lighting

Lighting requirements will be in accordance with codes used at BNL. However it is recommended that fluorescent lighting is used throughout the facility. An exception can be made for the area within the radiation shield. Incandescent lamps may be used here, if necessary.

A guide for lighting based on good reflectance and clean conditions, is 150 foot-candles per square foot. This would require 5 W per square foot of Utility power.

Emergency power

Lighting of exits, and the fire alarm system will be provided in accordance with safety codes used at BNL. Emergency power outlets should be available in the Assembly room and the Wide Angle hall for use when working in the detector. The fire alarm system should have a visual component for the hearing impaired.

Power for Equipment

Power required for equipment for the cooling system, the hydraulic system, etc. described in the section "Types and distribution of FEP will be determined at a suitable time during the design phase.

Safety Grounding

A ground grid will be provided throughout the facility. This grid will consist of 4/0 cables bolted to the columns of the buildings, and to ground rods. They will also be welded to rebar within the concrete floor. Suitable connection points will be provided for connecting up to this ground plane.

Figure 6-3 Proposed Layout of Operation/DAQ Building

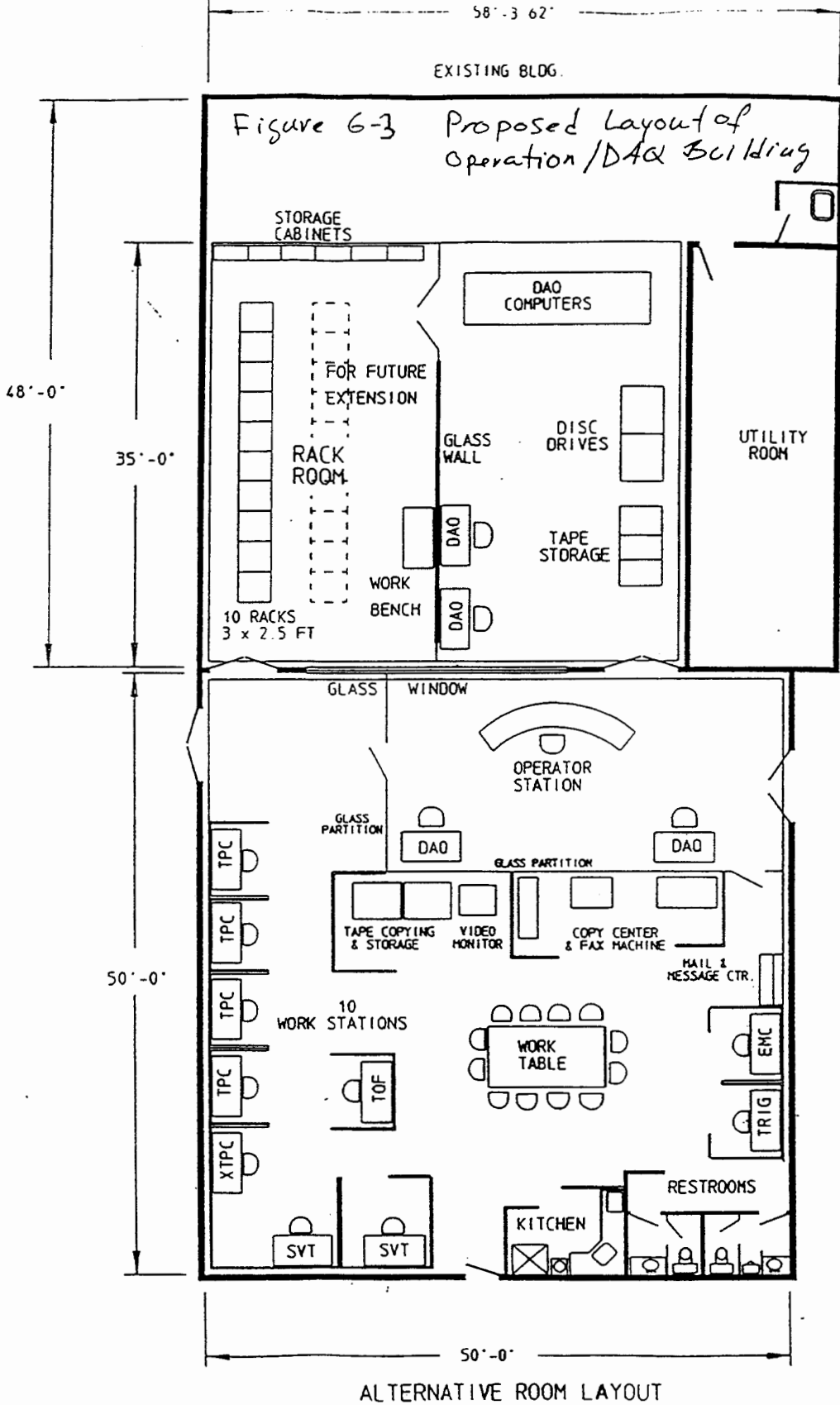
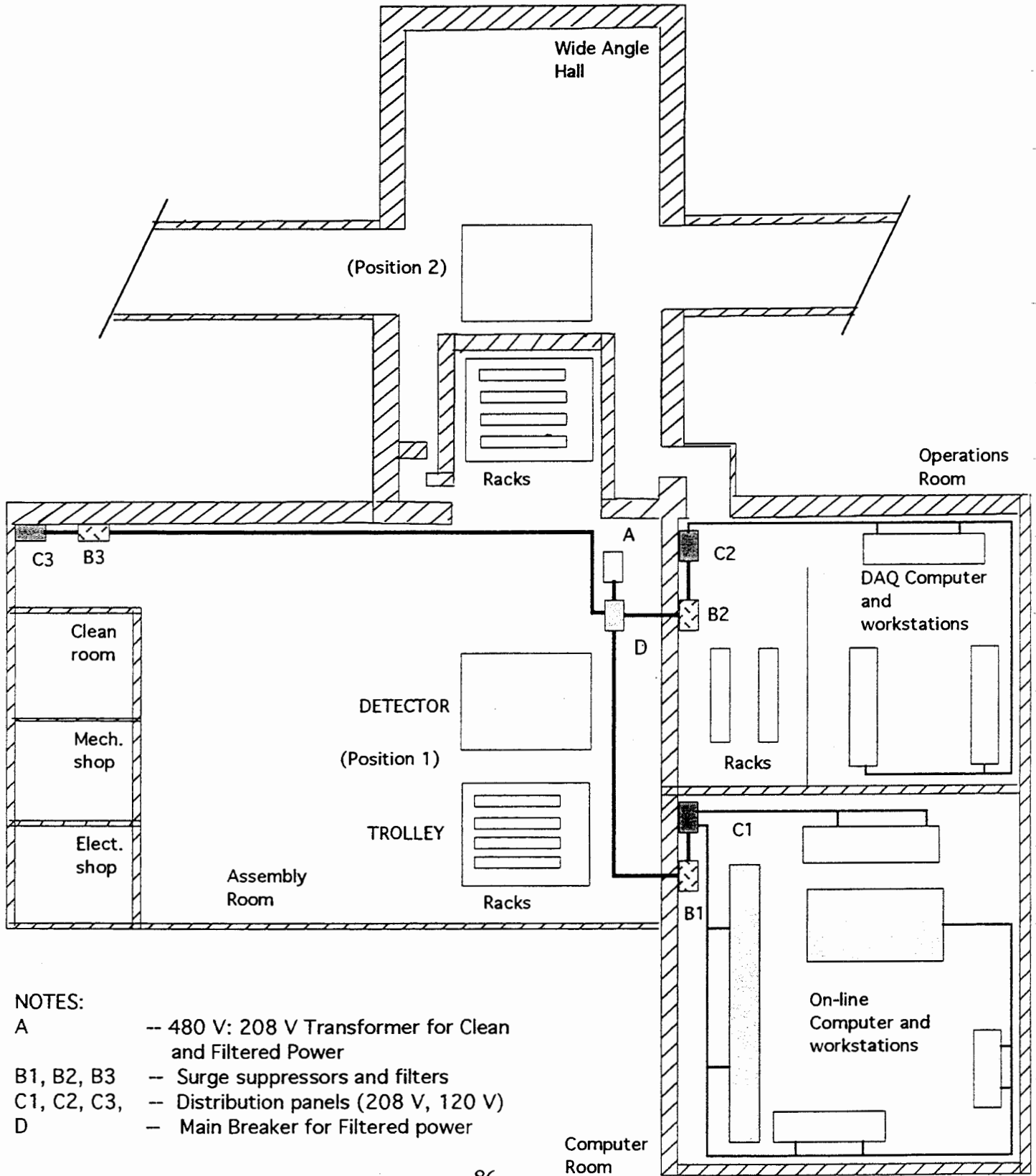


Figure 6-4 Diagram of filtered power distribution

DIMENSIONS ARE NOT TO SCALE

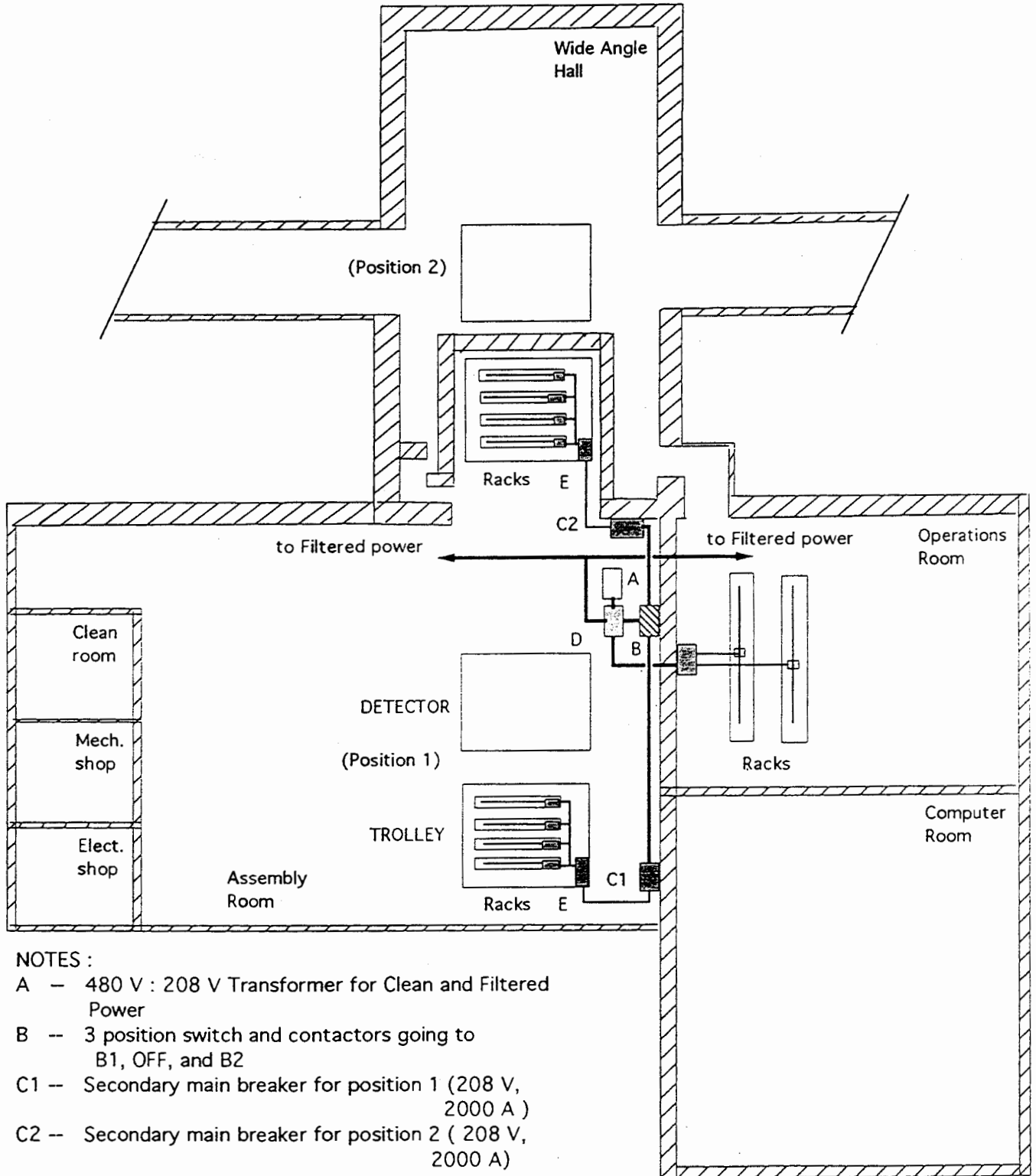


NOTES:

- A -- 480 V: 208 V Transformer for Clean and Filtered Power
- B1, B2, B3 -- Surge suppressors and filters
- C1, C2, C3, -- Distribution panels (208 V, 120 V)
- D -- Main Breaker for Filtered power

Figure 6-5 Diagram of clean power distribution

DIMENSIONS ARE NOT TO SCALE



NOTES :

- A -- 480 V : 208 V Transformer for Clean and Filtered Power
- B -- 3 position switch and contactors going to B1, OFF, and B2
- C1 -- Secondary main breaker for position 1 (208 V, 2000 A)
- C2 -- Secondary main breaker for position 2 (208 V, 2000 A)
- D -- Main Breakers for Clean and Filtered power
- E -- Distribution panel for the Trolley
- -- Distribution panels

Figure 6-4 SCHEMATIC
MODIFIED CHILLED WATER
(MCHW)

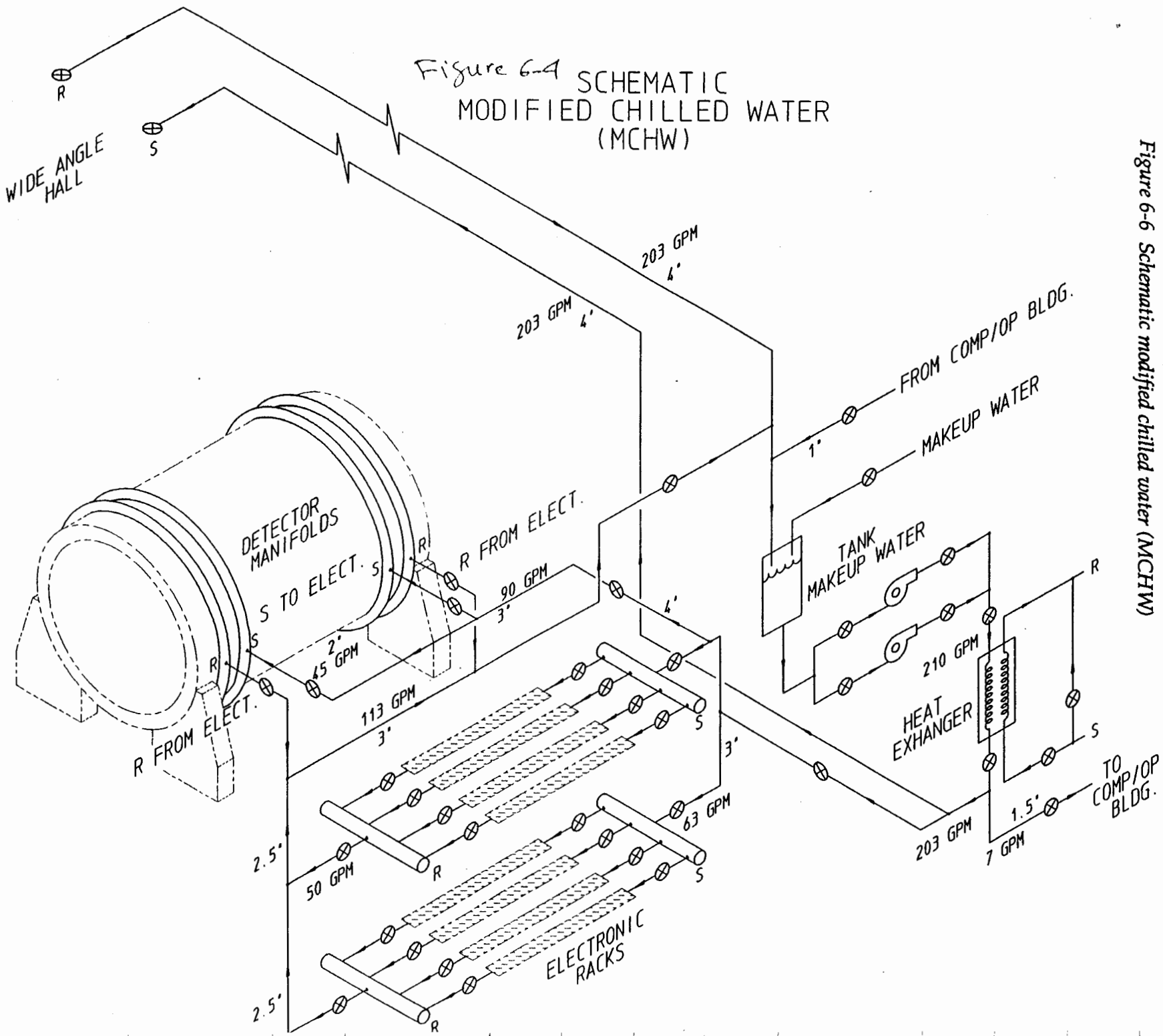
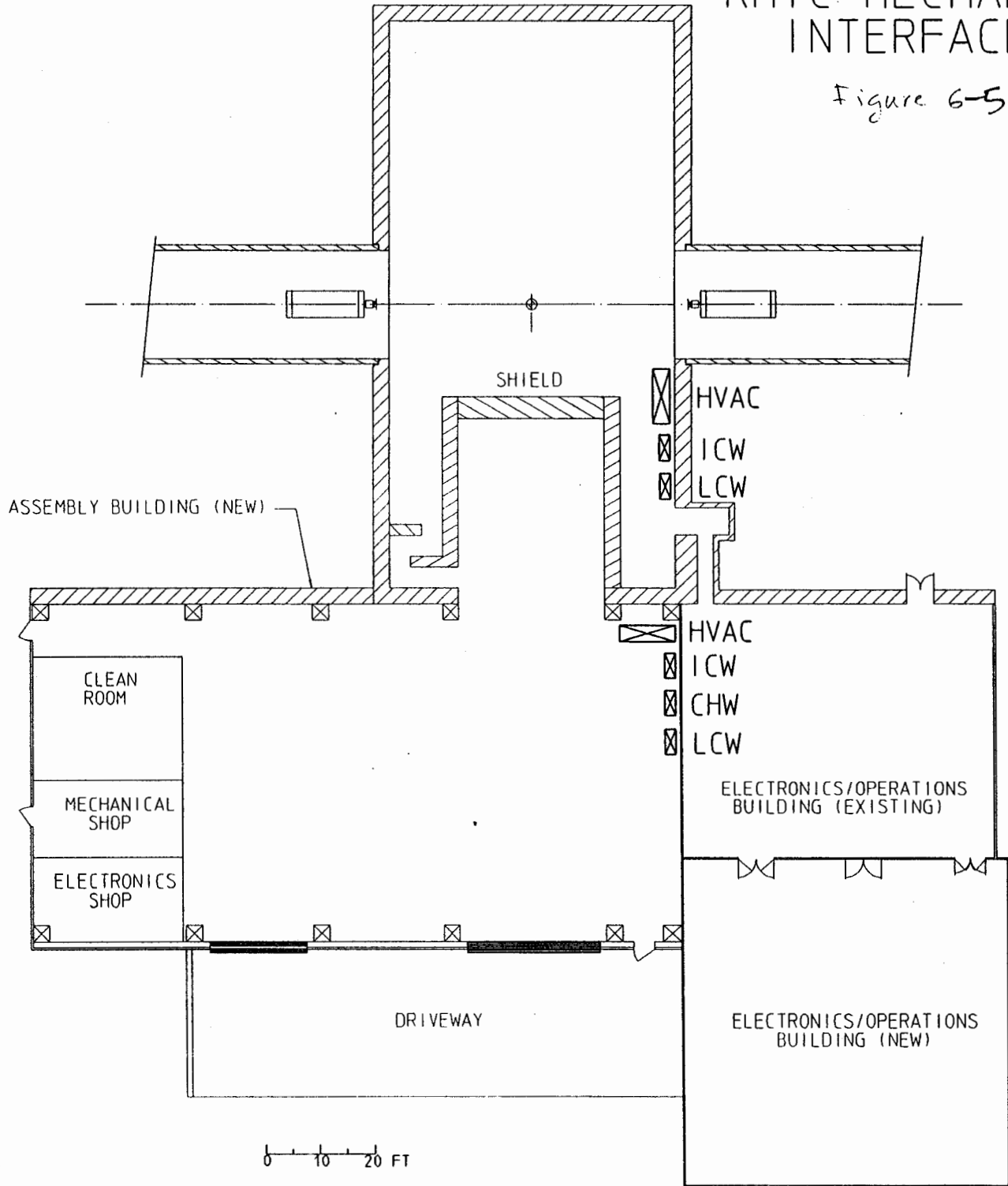


Figure 6-6 Schematic modified chilled water (MCHW)

RHIC MECHANICAL INTERFACES

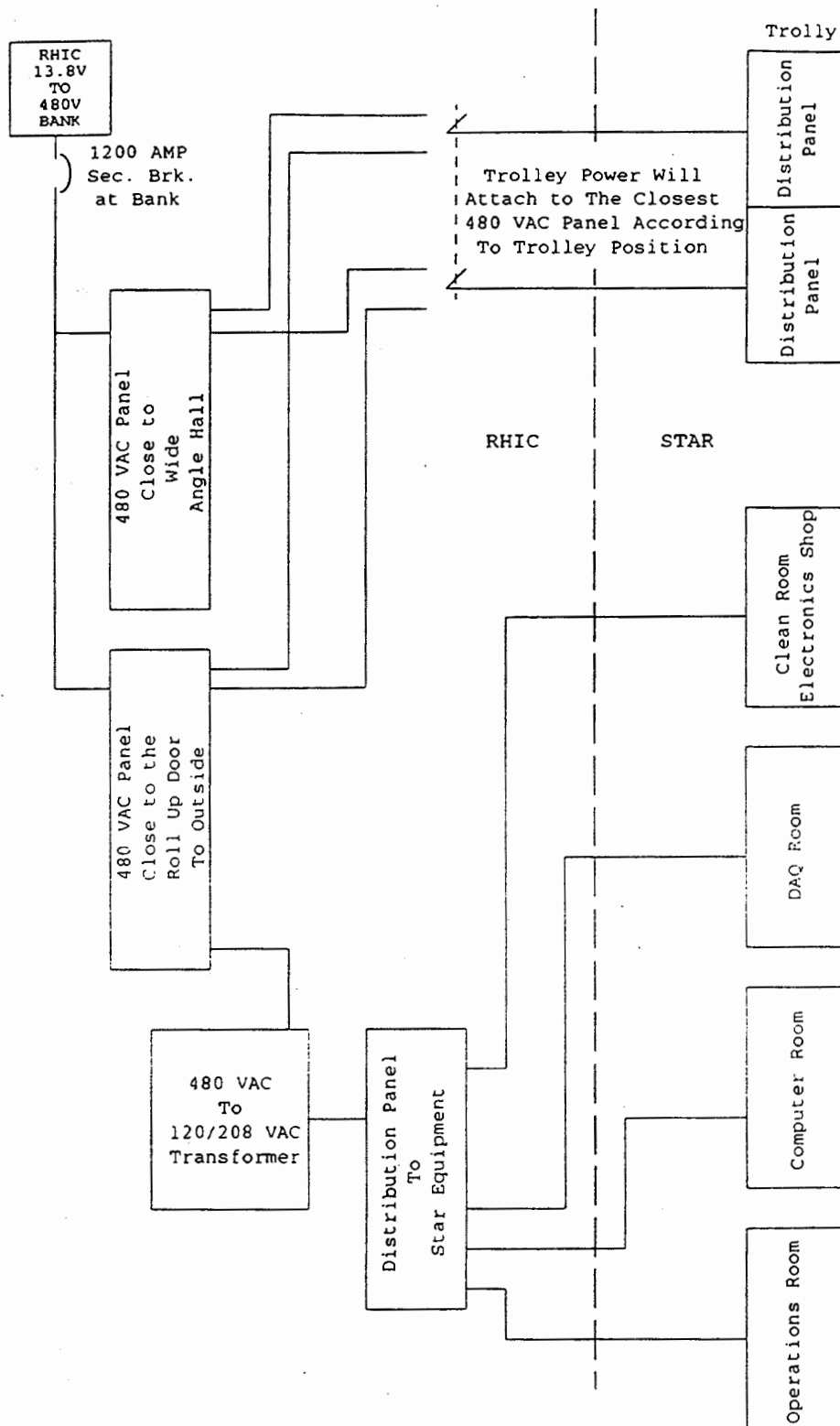
Figure 6-5



0 10 20 FT

Figure 6-7 RHIC mechanical interfaces

Figure 6-8 Power interface between RHIC and STAR



Filters and Surge Suppressors will be used where necessary

Notes:

1. Non-linear loads with high third order harmonic currents due to Switcher P/Ss

9. Cost, Schedule, Manpower and Funding

9.A. Detector Scope

The STAR Phase 1 detector includes the following detector subsystems and other necessary elements: Time Projection Chamber, Solenoid magnet and return iron, TPC front-end electronics, DAQ, trigger, slow controls, and on-line computing, structure and utilities needed to support the detector in the Wide Angle Hall, installation and testing of the detector in the hall, project management, and systems integration. The list of upgrades to Phase 1 include the electromagnetic calorimeter, the silicon vertex tracker, two stages of Time of Flight (TOF) detector (a patch and a full 7776 channel system), and an External TPC (XTP) and their associated incremental electronics, DAQ, computing, and installation. It is the goal of the STAR collaboration to have these upgrades on-line as quickly as possible.

The cost estimate presented in the following section is based on the detector described above. The cost is based on a point design, the scope of which is defined by the STAR CDR, CDR update and Parameters Notebook. The contingency has been developed to take into account the uncertainty in the design and the associated cost estimate and on a reasonable level of problems and unknown situations based on experience with detectors of similar scale and complexity. Construction of the Phase 1 portion of STAR including any new changes in scope brought on by the collaboration, will take place within the cost envelope described in this document.

9.B. Detector Summary Cost and Schedule Estimates

A cost estimating effort for the STAR detector was begun early in calendar year 1992. Formal cost and schedule (C/S) estimating guidelines¹ were published prior to beginning this effort. These guidelines have been reviewed and approved by a subset of RHIC Project Management. The Phase 1 detector cost estimate presented in the original CDR represented the fifth formal iteration of the estimate and thus received a significant amount of internal review. In the CDR Update Cost and Schedule Book², the costs for constructing the Phase 1 detector are summarized by major subsystem (RHIC WBS level 3) and represents the seventh formal iteration. Further details of the cost estimate can be found in this Update C/S Book, where each subsystem is presented to level 5 (6 in some cases). A detailed description of the individual WBS elements can be found in the STAR WBS Dictionary³. Details of estimate basis are found in the STAR Basis of

¹ STAR Cost & Schedule Procedure manual, Rev. 2, August 27, 1992, W.R. Edwards and C.R. Barney

² CDR Update Cost & Schedule Book, December 22, 1992.

³ CDR Update WBS Dictionary, December 22, 1992.

Estimate⁴

The cost estimate for the upgrade detector subsystems did not receive the same amount of review as the Phase 1 detector. The Original CDR Cost and Schedule Book includes discussion of the upgrade detector costs and presents these costs in terms of each subsystem, its front end electronics, and incremental DAQ, computing, and installation. These cost estimates should be viewed as more preliminary than the Phase 1 detector cost estimate.

9.B.1. Level 4 Cost Summary

A cost estimate summary for the STAR Phase 1 detector is presented in Table 9-1a. All estimates are in fiscal year 1992, US dollars, as defined in the C/S Procedure Manual. The total Phase 1 project cost is \$40.1 M, including \$8.4 M which is being held as contingency. This total represents all costs of construction beginning in FY 1993 and continuing through FY 1997 (completion) except certain experimental hall upgrades and utility services for the magnet and other subsystems that are provided by BNL/RHIC. At present an estimate of STAR Collaboration resources which can be credited towards specific costs of the detectors amounts to approximately \$4.3 M. A portion of installation, testing and other relevant activities will be supported by pre-operations funding and by RHIC project support for experimental operations. An additional reduction of \$1 M of STAR's contingency budget is taken by assuming that a portion of the \$2 M RHIC management reserve fund set up for the RHIC experimental program will be available to STAR. This amounts to an effective credit of \$6.7 M including \$1.4 M as part of RHIC project support for experimental operations. The amount of capital funding required for the STAR Phase 1 detector system is \$33.4 M in FY'92 dollars. In addition, an R&D budget of approximately \$4.0 M in FY'93-95 is anticipated from RHIC R&D funds.

The column headings in Table 9-1a require some definition. The material column represents the sum of all costs associated with materials used in fabrication, procured items and expenses. The next column, MFG or manufacturing labor, represents all skilled (technician, machinist, and crafts) and unskilled labor used in the fabrication, assembly, test and installation efforts. The EDIA (Engineering, Design, Inspection and Administration) column represents the costs associated with engineering and design efforts, as well as the management and administrative efforts, for the life of the project. The next column, WBS Base, is the sum of the previous three columns. Contingency % is the weighted average value of contingency, and is presented as a percentage of the base. When the dollar value of contingency is added to the Base column, the result is the Total column.

⁴ CDR Update Basis of Estimate, December 22, 1992.

Table 9-1a STAR Phase 1 Detector cost summary (numbers in \$K unless otherwise noted).

WBS	DESCRIPTION	MATERIAL	MFG LABOR	EDIA	SUBTOTAL	CONT %	TOTAL
4.2	Time Projection Chamber	2853	1988	1450	6291	28.0	8054
4.4	Solenoidal Magnet	6043	139	961	7143	26.0	9005
4.7	Electronics	4701	1060	3881	9642	28.6	12402
4.7.1	Front end electronics FEE	2857	479	1509	4846	28.7	6240
4.7.2	DAQ System	823	57	1636	2515	29.5	3259
4.7.3	Trigger Systems	901	364	446	1711	27.0	2175
4.7.4	Controls	120	160	290	570	27.8	728
4.8	Computing	1024	678	664	2366	31.0	3100
4.9	Detector Conventional Systems	647	48	306	1001	24.2	1244
4.11	Detector Installation & Test	324	1177	626	2127	32.7	2824
4.12	Project Management (PM)	226		1669	1895	10.5	2094
4.13	Systems Integration	207		1034	1240	14.0	1414
	TOTALS	16025	5090	10591	31705	26.5	40137

9.B.2. STAR Schedule Summary

An overall project critical path summary schedule is shown in Figure 9-1. The Magnet system and components of Electronics are on the project critical path, while the TPC is approximately 1-2 months off. Three months off the critical path is the beneficial occupancy date for the assembly building. A more detailed schedule for each subsystem is presented in the STAR Cost/Schedule Book.

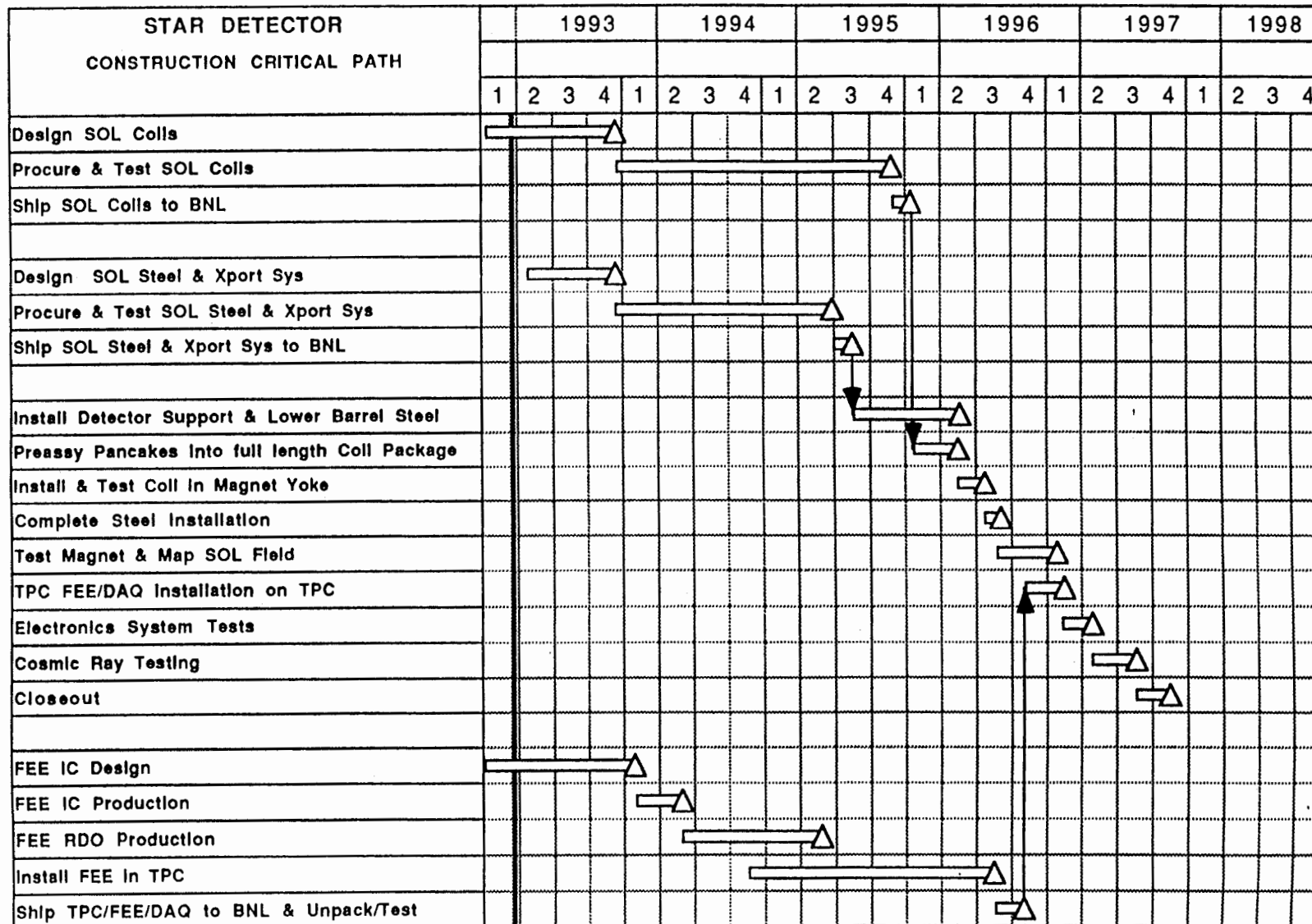
The relatively aggressive schedule for STAR construction is based upon success and the receipt of funding necessary to support R&D, design and construction activities. Given the above assumptions, the schedule is possible but aggressive. It goes almost without saying then that delays in funding will result in a corresponding delay in the completion date for STAR. One bit of schedule contingency does exist however, the 4 month cosmic ray testing task can be reduced or eliminated at the expense of commissioning efficiency.

9.C Project Manpower Resources by Subsystem

Presently there are 30 institutions and 223 physicists and engineers in the STAR Collaboration. From these institutions it is expected some amount of existing resources for constructing and operating the STAR detector will be available. A survey of collaboration resources has shown possible contributions in the areas of engineering, technical support, and computing. A precise accounting of the collaboration resources however, is complicated by the fact that for the resources to be effective they must be carefully matched with the projects outlined in the STAR Work Breakdown Structure (WBS).

The matching of resources and projects is a complete process. Account must be taken of institutional capabilities, time constraints, communications difficulties, and project scope. Additionally, it is necessary to account for the assumptions made in costing a given element of STAR WBS in order to correctly credit resources which may be applied to that element.

Figure 9-1 STAR Detector construction summary schedule.



Wednesday, December 23, 1992

The resources accounted for in the STAR Collaboration thus far sum to approximately \$4.3 M. Areas in which the matching of resources has been possible include:

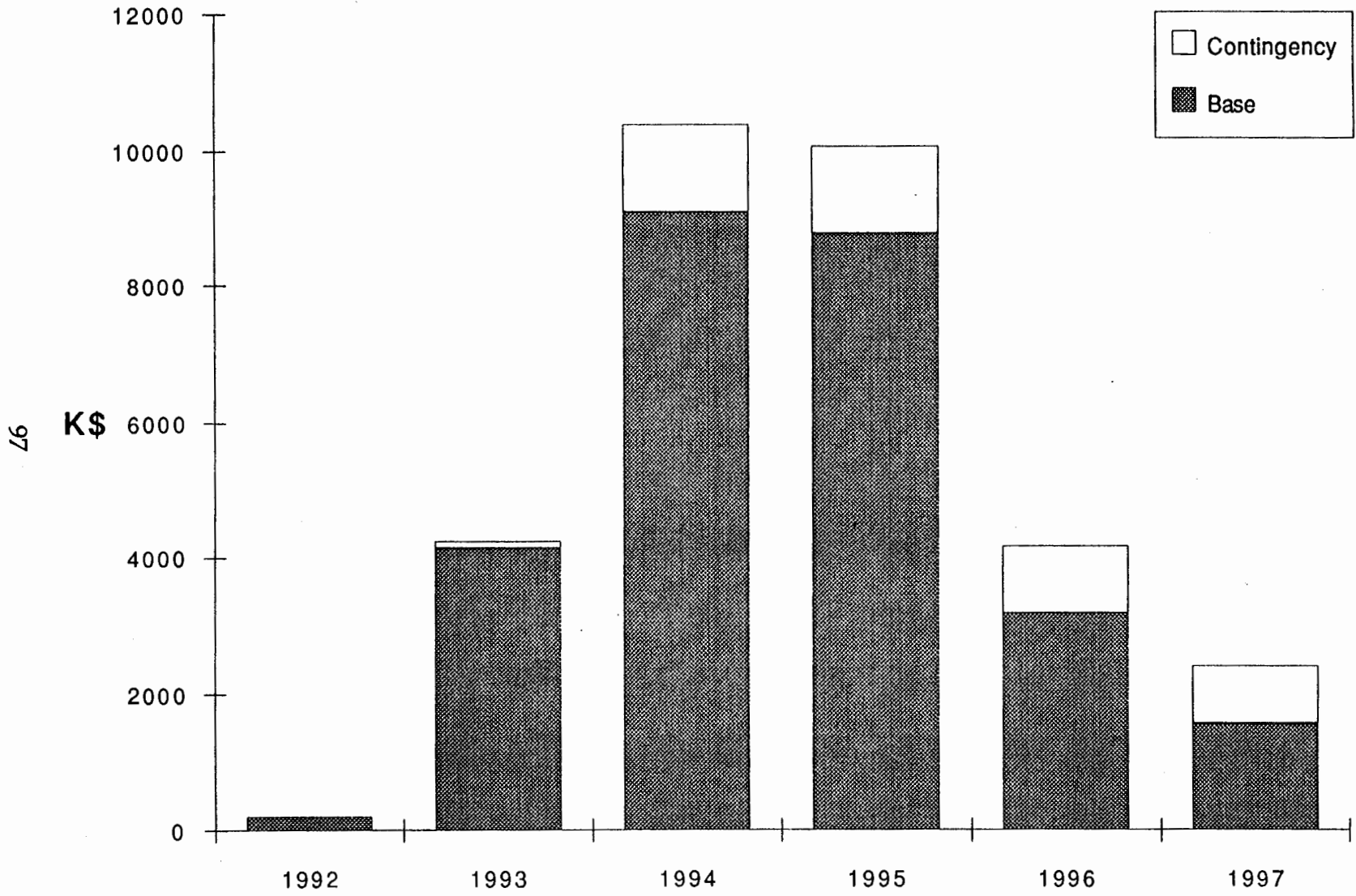
<u>WBS</u>	<u>Element</u>	<u>Institution</u>
2.4.2.10.1	TPC Assem., Test, Fixtures	LBL, UT, UCD, Texas, Wayne St.
2.4.2.4	Sector Mach., Assem., & Test	Wayne St., Purdue, UT, LBL
2.4.2.4.2.4	TPC Anode Bias Circuitry	Kent State
2.4.2.6	TPC Laser System	UCD
2.4.2.9.1	Transport Fixtures	LBL
2.4.4.4	Magnetic Measurements	UCLA
2.4.7.1	Testing TPC Electronics	BNL
2.4.7.2.6	DAQ Software	LBL, Creighton, U. Frankfurt
2.4.7.2	DAQ Design	BNL
2.4.7.3	Trigger Detectors	U. Frankfurt, SSL-UCB/Rice
2.4.7.4.2.2	Slow Control Software	Creighton
2.4.8.2	Professional Software Support	LBL, BNL
2.4.9.6	Mech/Electr. Shop equip	BNL
2.4.11.1.7.4	Slow Control Install. & Test	Creighton
2.4.11.2.4	Magnet Mapping	UCLA

The process of identifying and applying resources will continue throughout the life of the project. It is expected that as details of the Management Plan for STAR are worked out, further areas will be identified where contributions from within the collaboration can be made.

9.D. Funding Profile

The current estimated funding profile for the STAR Detector is shown in Figure 9-2 (*not available at the time of printing, will be included in the final version*). This funding profile assumes that the detector is complete in August of 1997. Assembly of the detector will, for all intents and purposes, be completed in January of 1997, 4 of the months that follow will be spent performing tests at both the subsystem and system level and making last minute repairs. The detector will then be rolled into position on the beamline and closed out, making it ready for commissioning with beam.

Table 9-2 The STAR preferred funding profile (all numbers in \$K).



STAR Funding Requirements by Fiscal Year (\$ 31.5M Total in FY '92\$)

12/22/92

97